UNCLASSIFIED

AD 419023

DEFENSE DOCUMENTATION CENTER

FOR

SCIENTIFIC AND TECHNICAL INFORMATION

CAMERON STATION, ALEXANDRIA, VIRGINIA

UNCLASSIFIED

NOTICE: When government or other drawings, specifications or other data are used for any purpose other than in connection with a definitely related government procurement operation, the U. S. Government thereby incurs no responsibility, nor any obligation whatsoever; and the fact that the Government may have formulated, furnished, or in any way supplied the said drawings, specifications, or other data is not to be regarded by implication or otherwise as in any manner licensing the holder or any other person or corporation, or conveying any rights or permission to manufacture, use or sell any patented invention that may in any way be related thereto.

64-5

CATALOGED BY DDC
AS AD No. 419023

AIR FORCE INSTITUTE OF TECHNOLOGY

AIR UNIVERSITY
UNITED STATES AIR FORCE

419023

SCHOOL OF ENGINEERING

WRIGHT-PATTERSON AIR FORCE BASE, OHIO

DDC
OCT 8 1963
TISIA A

AF-WP-O-OCT 63 1,500

AN EXPERIMENTAL AND THEORETICAL STUDY OF THE WALL-STABILIZED, TRANSPIRATION-COOLED DC ELECTRIC ARC

THESIS

GNE/Phys/63-2

Michael F. Baran
1/Lt USAF

AF-WP-O-SEP 63 30

AN EXPERIMENTAL AND THEORETICAL STUDY OF THE WALL-STABILIZED, TRANSPIRATION-COOLED DC ELECTRIC ARC

THESIS

Presented to the Faculty of the School of Engineering of
the Air Force Institute of Technology
Air University
in Partial Fulfillment of the
Requirements for the Degree of
Master of Science

By

Michael F. Baran, B. S. Phys.
1/Lt USAF

Graduate Nuclear Engineering

August 1963

Preface

This thesis is the culmination of a six month study of a wall-stabilized, transpiration-cooled arc in the Thermomechanics Laboratory of the Aeronautical Research Laboratories (ARL), Wright-Patterson Air Force Base, Ohio, under the supervision of Mr. Erich Soehngen, Branch Chief. The concept is the product of Mr. Soehngen's mind, and the original investigation of the wall-stabilized, transpiration-cooled arc was performed in ARL by Capt. Peter D. Tannen of the Graduate Astronautics Class of 1962 of the Air Force Institute of Technology, Wright-Patterson Air Force Base.

While Capt. Tannen's study of the wall-stabilized, transpiration-cooled arc was primarily one of feasibility, this study was undertaken in the hope of achieving a preliminary theoretical approach to the questions posed by the arc device. A numerical solution to the Elenbaas-Heller equation was obtained for the arc radius as a function of arc power per unit length. Experimental verification to 5% was obtained. In addition, qualitative explanations for some of the phenomena were postulated based on these results and on the literature. Two bibliographies are included. The first contains those references specifically used for ideas, numbers, and comparison. The second contains those references which were consulted, but not used directly in the text of this thesis.

However, I claim credit for only a small part of the work which has gone into this study, and, of course, all the errors which lie therein.

My deepest thanks and appreciation go to Mr. Erich Soehngen for his support and willingness to help. It has been a rare pleasure to work under such a creative person. Also, my sincere gratitude is extended to the personnel of the Thermomechanics Branch of ARL for their invaluable assistance, experience, and encouragement: Maj. D. E. Dye, Capt. T. Andrada, Messrs. Ed Moore, Paul Schrieber, Walt Millhof, Don Linder, Paul Unrue, Ralph Becker, Wallace Inkey, and many others. I must also acknowledge Maj. John V. Armitage and Mrs. Joanne Conniff of the Applied Mathematics Branch of ARL for their aid in the use of the IBM 1620 digital computer for the numerical solution to the Kilenbeas-Heller equation. Others who have contributed so willingly included Dr. G. L. Cann of the California Institute of Technology, who suggested a method for starting the arc device, and my classmate Capt. Benjamin George who patiently helped me run the arc device and take data. And, of course, my thanks to my advisor, Maj. R. C. Wingerson of the Physics Department of the Air Force Institute of Technology, without whose willing, patient help this thesis would never have been written.

Lastly, to my devoted wife who spent many lonely hours waiting for me to come home so she could enjoy an evening typing this work, my deepest and most heartfelt thanks for the patience, and understanding she managed to find. And in a brief departure from the norm, my thanks and appreciation to my late father-in-law for the inspiration he provided me, the skills with machinery he taught me, and the devotion to education for its own sake he exhibited.

Michael F. Baran

Contents

List of Figures

Abstract

The wall-stabilized, transpiration-cooled arc device consisted of a cathode chamber containing a 0.25-in. diameter tungsten cathode, 12 half-inch thick wall segments containing porous graphite segments through which argon at about 1.1 atm was injected into the 0.25-in. diameter arc channel, and a hollow, cylindrical water-cooled copper anode which served as the plasma exhaust. Cooling water to the cathode, the wall sections, and the anode provided information concerning the power losses to the device components. The argon flows to the cathode chamber and each wall segment were individually controlled and monitored by specially built coiled capillary flowmeters. The device proved extremely stable, and after 30 hours of operation, electrode wear was not detectable. For arc powers in the range of 8 to 20 kw DC, and mass flows on the order of 22 to 29 lb/hr, gas enthalpies from 600 to 1,400 Btu/lb were obtained at a device efficiency of 50%. A numerical solution to the Ellenbaas-Heller equation was formulated by assuming a locally linear variation in certain inconvenient functions of temperature. Experimental measurements of arc radius as a function of arc power per unit length agreed with theoretical predictions to 5% for arc radii in the range of 0.220 to 0.300 cm at arc currents of 46 and 50 amps. This agreement supported the assumption of negligible radial mixing and heat loss within the core by convection. The turbulent flow of gas next to the anode prevents formation of an anode spot, thus keeping the power loss to the anode constant at 20% of the arc power. A simple cooling effectiveness model has been proposed to explain

the occurrence of a change in slope from negative to positive of the volt-ampere characteristic at currents of the order of 50 amps and the increase of arc voltage and column gradient with increasing mass flow.

GME/Phys/63-2

AN EXPERIMENTAL AND THEORETICAL STUDY OF THE WALL-STABILIZED, TRANSPIRATION-COOLED DC ELECTRIC ARC

I. Introduction

Background

Electric arcs have been in use for many years, and considerable data has been accumulated concerning their behavior in many gases and under widely varying conditions of pressure and electrode configuration. The advent of high-speed and space flight has stimulated an increased effort in electric arc technology for application in both aerodynamic simulation and in space propulsion. Bade and John of AVCO Research and Advanced Development Division, Wilmington, Massachusetts, performed a rather complete survey of the state of the art of plasma generation and published this in the ARS Journal in January, 1961 (Ref 9:4-17).

While their summary goes into more detail than is desirable at this time, it does indicate that the primary efforts of plasma generation research are tending to three major areas (Ref 9:11). The first of these is an improvement in performance in order to keep the size of the power supply to a reasonable minimum without sacrificing output power and to reduce external cooling requirements (Ref 9:7). Plasma generator performance is defined as maximum production of a high-pressure, high-enthalpy gas for as great a power input as possible, with minimum losses to the device. For wind-tunnel heaters, good performance is a matter of economy; for space propulsion, it is a must.

The secondary area of primary effort is that of reduction of contamination of the exhaust from electrode erosion. This is especially important in hypersonic research where purity of enviroment must be maintained in order to obtain as near true flight conditions as possible (Ref 9:9). Also, electrode erosion has a direct bearing on the third primary area of interest, and that is increasing the lifetime of the arc devices.

This last area is self-evident in importance. Good approximation of re-entry conditions requires operating times of several minutes with equipment lifetimes on the order of hours. The needs of future space travel may necessitate operating times on the order of days or months and equipment lifetimes of, possibly, years. Other requirements must also be met, but they are of secondary importance to these primary factors of performance, electrode erosion, and equipment lifetime.

Approaches which have been taken to meet these criteria include regenerative, transpiration, and radiative cooling techniques to improve performance; vortex flow and magnetic fields normal to the arc axis to reduce anode erosion; and, physical constriction of the arc to produce forced convective cooling in order to boost the enthalpy of the exhaust (Ref 9:7).

While no great progress has been made in any of these areas, one general point of agreement has been found. The electrode configuration has been more or less standardized to a pair of coaxial electrodes separated by an annular gap. This configuration possesses rotational symmetry about a central axis and insures that at least part of the gas flowing through the device will pass through the arc column where heating occurs (Ref 9:7). However, there is not as yet any one type of plasma

generator which has proven completely satisfactory.

The Wall-Stabilized, Transpiration-Cooled Arc

Consideration of these and other problems associated with plasma generation led Mr. Erich Soehngen of the Thermomechanics Branch of the Aeronautical Research Laboratories (ARL), Wright-Patterson Air Force Base, Ohio, to conceive the idea of a wall-stabilized, transpiration-cooled arc early in 1961. The original experimental investigation of this device, shown in Figs. 10 and 11, pp. 24 and 25, was performed in the winter and spring of 1962 by Capt. Peter D. Tannen of the Graduate Astronautics Class of 1962 of the Air Force Institute of Technology (AFIT), at the Thermomechanics Laboratory at ARL (Ref 16). At the conclusion of Capt. Tannen's study, it was decided that the wall-stabilized, transpiration-cooled arc showed great promise for the fields of electric arc research and gas heater development. The device proved to be extremely stable and capable of efficiencies and gas enthalpies comparable to commercial arc units.

In addition, several interesting questions concerning the characteristics of this arc arose during the course of this preliminary study, and Mr. Soehngen elected to continue and extend it, although in a somewhat different vein from Capt. Tannen's investigation.

First, the three primary variables of the device, viz., arc length, power, and rate of mass injection, were to be modified to include only arc power and rate of mass injection. Furthermore, the total length of the arc column was increased to its design limit of about 8-in. (Fig.11) by use of twelve injectors instead of six, which had been the previous

maximum. The increased length allowed higher arc voltages and powers in the same current range as investigated by Capt. Tannen.

Second, the approach to the problem was to include an attempt at a theoretical model which could successfully explain the performance of the device, and, if possible, be subject to laboratory verification by direct measurement. This would be directed first at the electrical characteristics of the arc, and second, at the gas flow and heat exchange between the arc column and the cooler gas.

Third, the remaining parameters of the arc would be subject to a much higher degree of control and variation than was the case in Capt. Tannen's work. This included individual control of the gas flow to each of the twelve wall segments and the cathode chamber and more complete measurements of the power losses to the various components. Also, mass flows and arc powers were to be greated than those used previously.

The Problem and Objectives

In summary, the problem to be investigated is the mass and enthalpy flow in a radially constricted arc discharge with transpiration-cooled walls. The primary objectives of this study include establishment of a preliminary theoretical prediction of the electrical characteristics of the arc, confirmation of the model used by experiment, and analysis of the overall performance of the device in light of the available theory and data.

II. Theory

A great deal of time and effort has been spent studying the characteristics of the wall-stabilised, DC arc (Ref 3:1). Similarly, much work has been done in the field of transpiration, or sweat cooling and its effects on the fluid and heat flows in a pipe (Ref 10:460-485). In either of the above cases, many questions have yet to be solved analytically to the point where theory and experiment are in good agreement.

Also, difficulties in obtaining experimental measurements add to the problem. For instance, the high temperatures and electrical phenomena associated with the arc core have made direct measurements of temperature, pressure, and other important factors very difficult, if not impossible, until recently. Progress has been made in this area, and a probe for measurement of the enthalpy and pressure in the arc core is now in use in the Thermomechanics Branch of ARL at Wright-Patterson Air Force Base, Ohio.

Another problem common to the arc and to the pipe-flow studies is that of disturbing steady-state conditions when taking or attempting to take measurements. This phenomenon tends to distort the experimental data obtained, usually in unpredictable ways.

Moreover, the combination of the two, i.e., the wall-stabilised, transpiration-cooled, DC arc, compounds the experimental and analytical difficulties. An exact solution for the energy balance in the arc core becomes almost impossible (Ref 4:171). Similarly, the gas flow is complicated since the gas channel is no longer a pipe, but an annular volume with the hot core concentric on its axis and the porous walls at its outer periphery. Hence, an approach similar to that of Cann and Emmons was

selected, and the wall-stabilized, transpiration-cooled arc was broken down into a two-part discontinuous model (Refs 3:49; 6:8). Although important, the gas flow through and the heat exchange within the porous wall segments were not considered except for the effects they had on the mass and heat flows within the arc channel. Also, the entrance effects in the cathode region are being examined by Capt. Benjamin George of the 1963 Graduate Nuclear Engineering Class (GNE-63), AFIT, at the Thermo-mechanics Branch of ARL, Wright-Patterson Air Force Base, Ohio as a separate topic.

The Arc Region

From K. S. W. Champion, the differential equation for the energy balance in a high pressure arc column is

$$\rho v \cdot \nabla (S T) - \nabla \cdot (k \nabla T) + B n_e e^{-\frac{V_{ion}}{kT}} = q n_e K E^2 \qquad (1)$$

where:

ρ = density of gas

v = velocity of gas

S = specific heat of gas

T = temperature

k = coefficient of thermal conductivity

B = empirical constant, dependent on gas and conditions

n_e = electron density

K = Boltzmann's Constant

K = total electron and ion mobility

q = electron charge

E = positive column gradient

V_{ex} = excitation potential given by Koch, Lessmann, and Walther.

The first and second terms of Eq (1) are, respectively, the rigorous expressions for the convection and conduction losses from the arc. The third term represents the radiation loss and is only a good approximation. The right-hand term is the power generation per unit volume within the arc column. Many difficulties are inherent in Eq (1), and only for the greatly simplified case of a vertical, axisymmetric arc, with constant gas flow velocity independent of axial position, may an exact solution to Eq (1) be obtained (Ref 4:170). Moreover, since B may vary with the gas and other conditions, it is not really a constant; and, no values of B were found in the literature for various gases and conditions.

However, a theoretical approach using some simplifications was desirable. Examination of the available data for the viscosity of argon shows that the viscosity increases with temperature to a maximum, and then decreases somewhat with further temperature rise as shown in Fig. 1, p. 8. Thus, for the purposes of the discontinuous model chosen, the arc core may be considered so viscous as to approach a very hot rod with a temperature-dependent, volume power density given by:

$$P_v = \sigma E^2 \tag{2}$$

where: P_v = power density, watts/cm^3

σ = electrical conductivity, mhos/cm (Temperature dependent)

E = electric field strength, volts/cm.

The high viscosity of the core region then eliminates the need for the

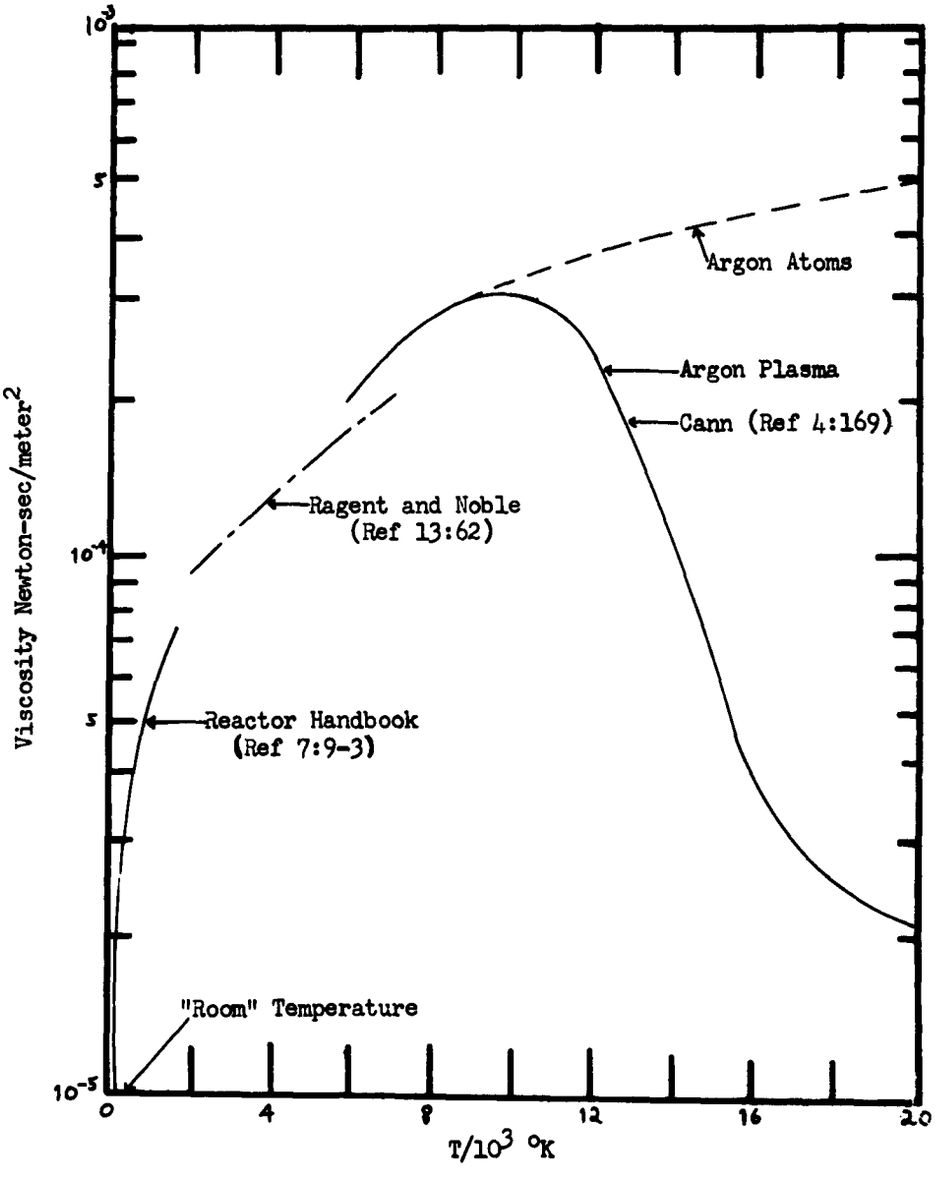

Fig. 1

Viscosity Coefficient of Argon
One Atmosphere Pressure

first or convection, term in Eq (1). The remaining terms are:

$$-\nabla(k\nabla T) + B n_e e^{-\frac{V_{ex}}{kT}} = q n_e K E^2 \tag{3}$$

If we let the radiation term become

$$U(T) = B n_e e^{-\frac{V_{ex}}{kT}} \tag{4}$$

and the power generation

$$\sigma E^2 = q n_e K E^2 \tag{5}$$

then Eq (3) becomes for the steady-state DC arc, with some minor rearrangement:

$$-\nabla\cdot(k\nabla T) + U(T) = \sigma E^2 \tag{6}$$

For the cylindrically symmetric case, Eq (6) becomes:

$$-\frac{1}{r}\frac{d}{dr}\left(r k \frac{dT}{dr}\right) + U(T) = \sigma E^2 \tag{7}$$

This is the reknowed Kllenbaas-Heller Equation for the steady-state, optically thin, DC arc (Ref 14:1-2).

While exact solutions to Eq (7) are possible, their complexity and length place them beyond the scope of this study. (The interested reader is invited to check Ref 14.)

Instead, a form of numerical solution suggested by Maj. R. C. Wingerson of the Physics Department of AFIT, Wright-Patterson Air Force Base, Ohio, in a personal communication was employed. This method was based on the assumption of a locally linear variation with radius of the inconvenient variables in Eq (7). Details of the solution are given in Appendix A, p. 84, as is the Fortran computer program for the IBM 1620 used in obtaining solutions for various parameters, namely, centerline temperature and temperature gradient, and electric field strength.

Since experimental data for the thermal and electrical conductivities of argon at high temperatures was not available, analytic values were used in the above program. These were obtained by Cann and AVCO from a statistical mechanics analysis of the high-temperature transport properties of argon, using an IBM 7090 digital computer (Refs 3:154-155; 17).

However, Cann gives no data for the radiation loss per unit volume within the core. AVCO does have such a set of data, and this was used with the other AVCO data. Also, while the two sets of values for electrical conductivity were in close agreement, the thermal conductivities were widely separated at temperatures above 11,000°K. The above sets of data are presented in Figs. 2, 3, and 4, pp. 11-13, showing electrical and thermal conductivities and volumetric radiation power loss, respectively, versus temperature.

While the method of solution employed is not exact, i.e., analytical, the results are consistent. A Simpson's rule numerical integration was included in the program to find the power per unit length in watts/cm. The results of this integration,

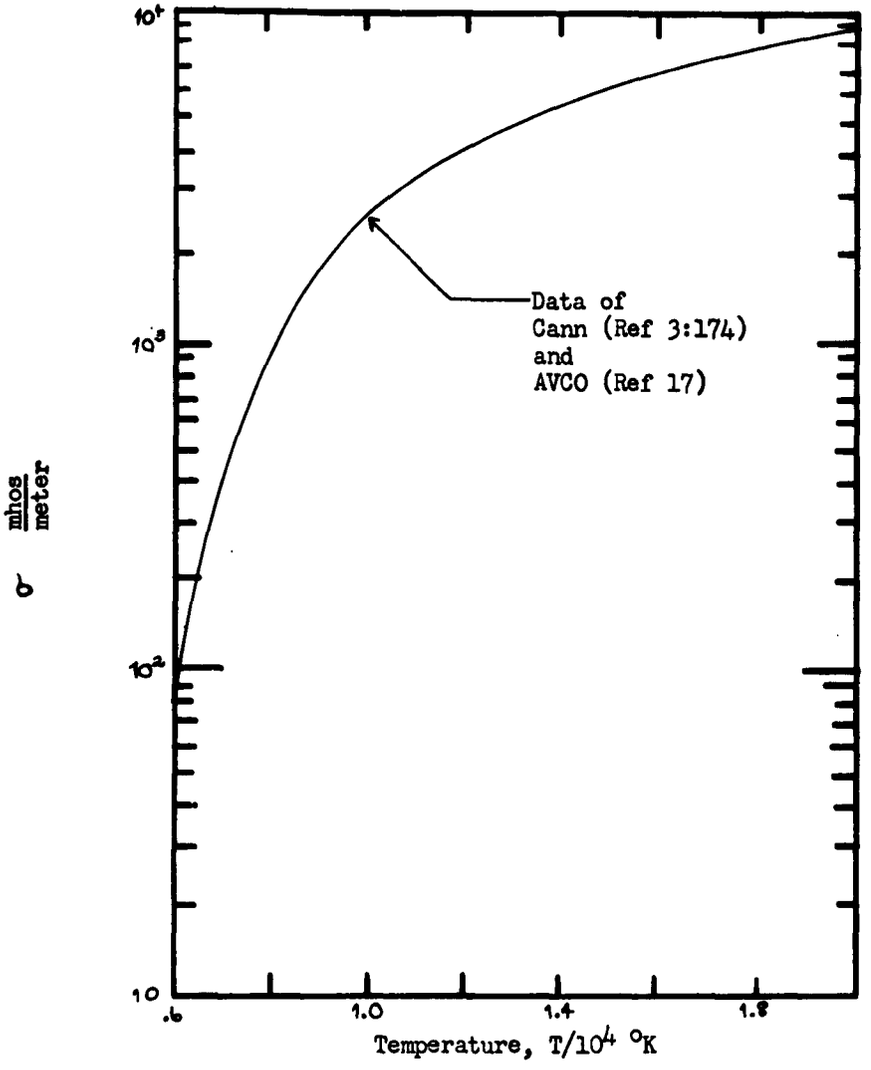

Fig. 2

Electrical Conductivity of an Argon Plasma at One Atmosphere Pressure

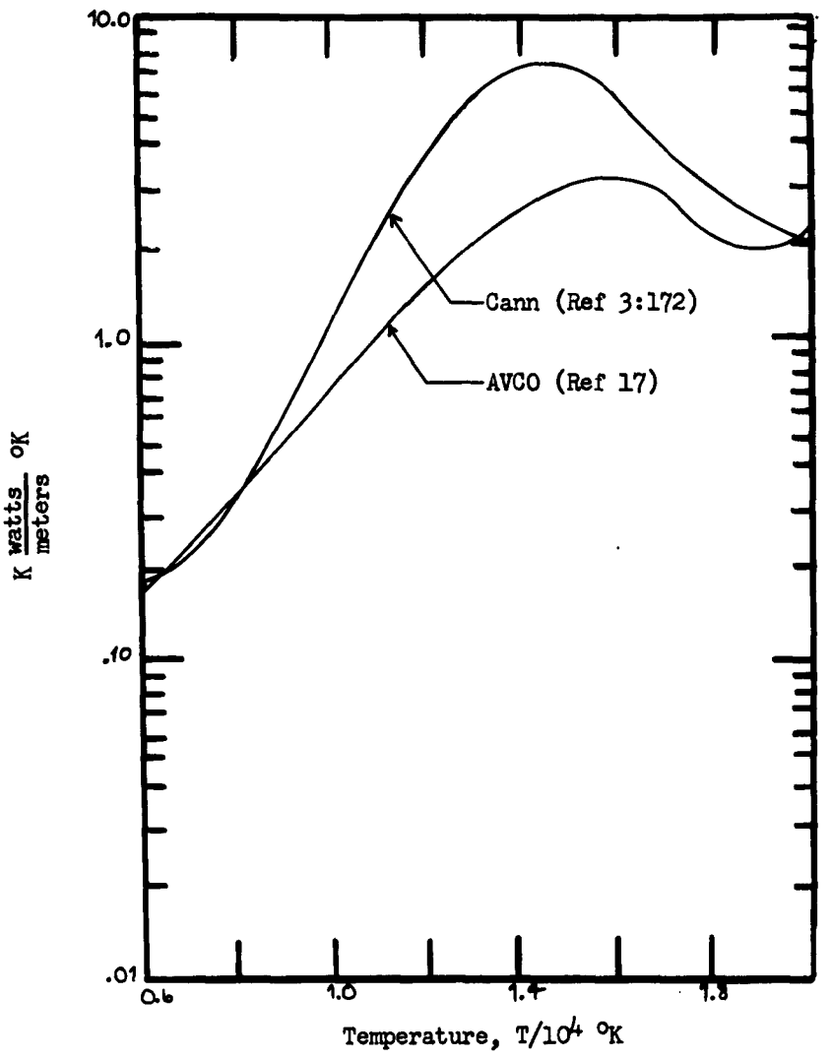

Fig. 3

Thermal Conductivity of an Argon Plasma at One Atmosphere Pressure

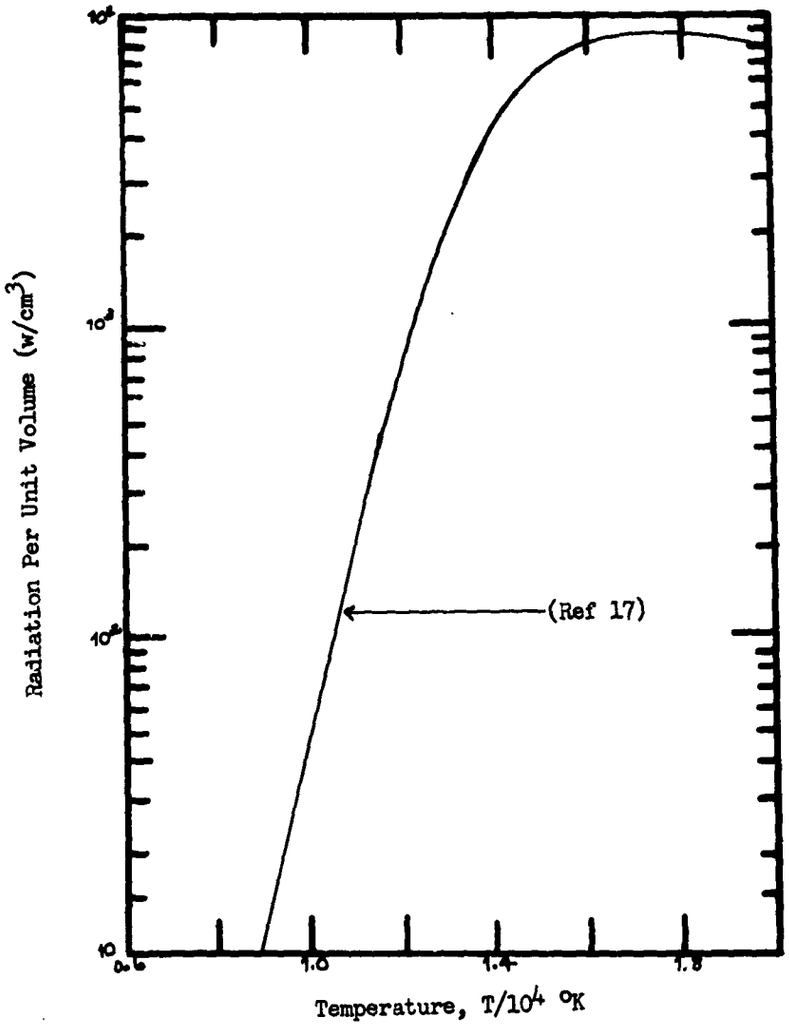

Fig. 4

Radiation Per Unit Volume of an Argon Plasma at One Atmosphere Pressure

$$P_L = \int_0^{RA} 2\pi r \sigma E^2 dr \qquad (7a)$$

where P_L = power/length, watts/cm

E = electrical field strength, volts/cm

σ = electrical conductivity, ohm^{-1} cm^{-1}

r = radius at which σ occurs, cm

RA = arc radius, cm

show that P_L is sensibly dependent only on centerline temperature in the range considered, 13,000°K to 6,000°K. This result is shown in Fig. 5, p. 15. This is supported by additional data from AVCO. At higher centerline temperatures, P_L does show a more pronounced dependence on electric field strength, but this region was beyond that of this study.

The core radius is defined as being in the region where the electrical conductivity becomes (sensibly) zero, namely, in the region of 6,000°K (Ref 3:67). Fig. 6, p. 16, is a dimensionless profile of the arc column showing the variation of temperature, temperature gradient, and thermal and electrical conductivities as functions of the dimensionless radial distance from the arc core center. Figs. 7 and 8a, pp. 17 and 18a, present the variation of arc power per unit length as a function of arc radius, with electric field strength as a parameter for the data of Cann and AVCO, respectively. Fig. 8b, p. 18b, shows the dependence of arc power per unit length on the product of field strength and arc radius.

The results of the above are for an arc at one atmosphere. The data from AVCO indicate a decrease in both thermal and electrical

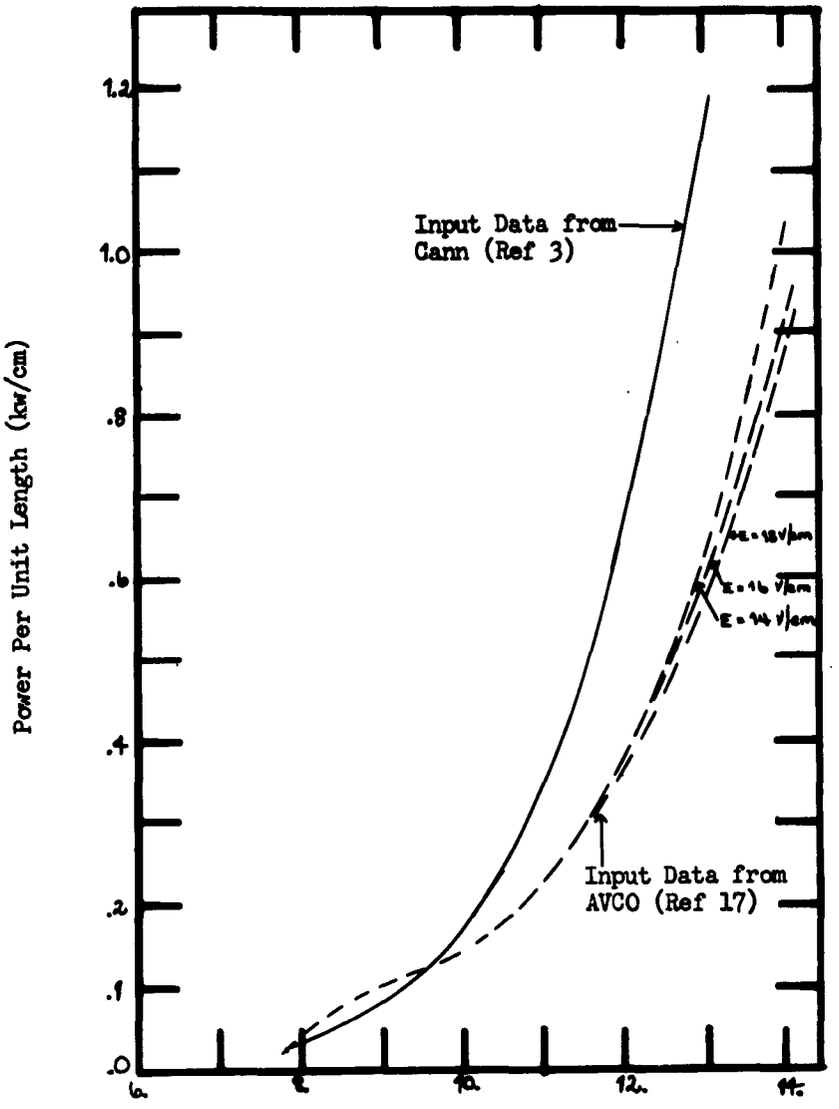

Fig. 5

Arc Power Per Unit Length
vs Arc Centerline Temperature

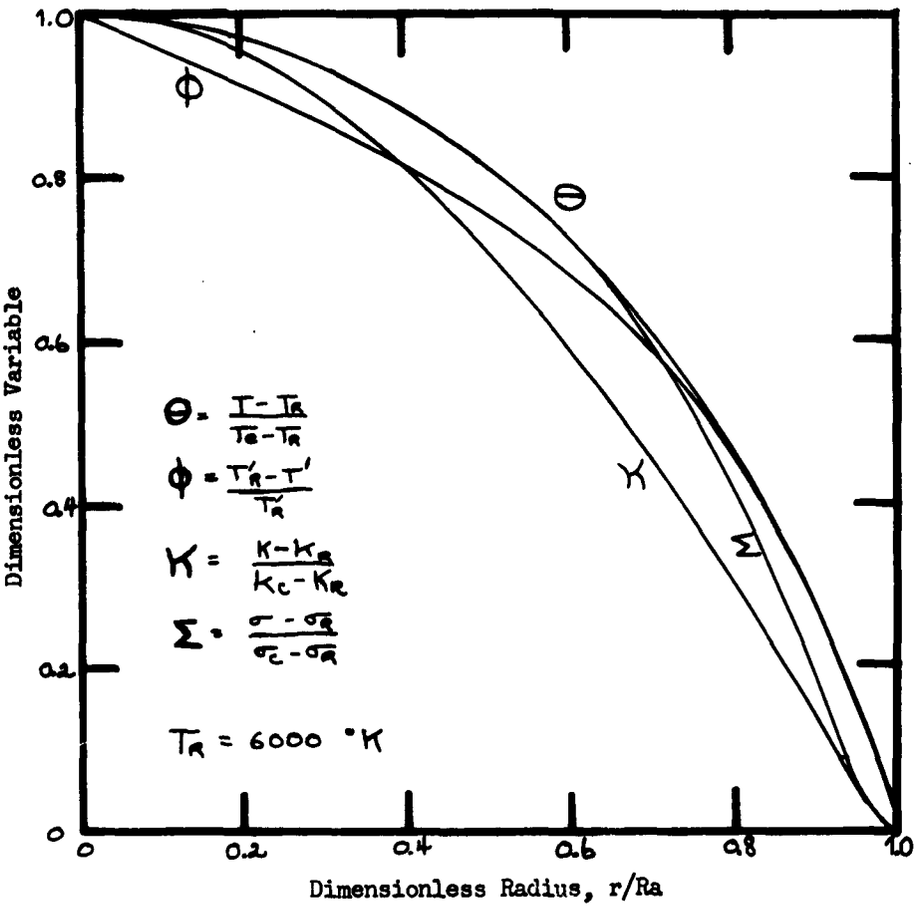

Fig. 6

Dimensionless Radial Arc Profile

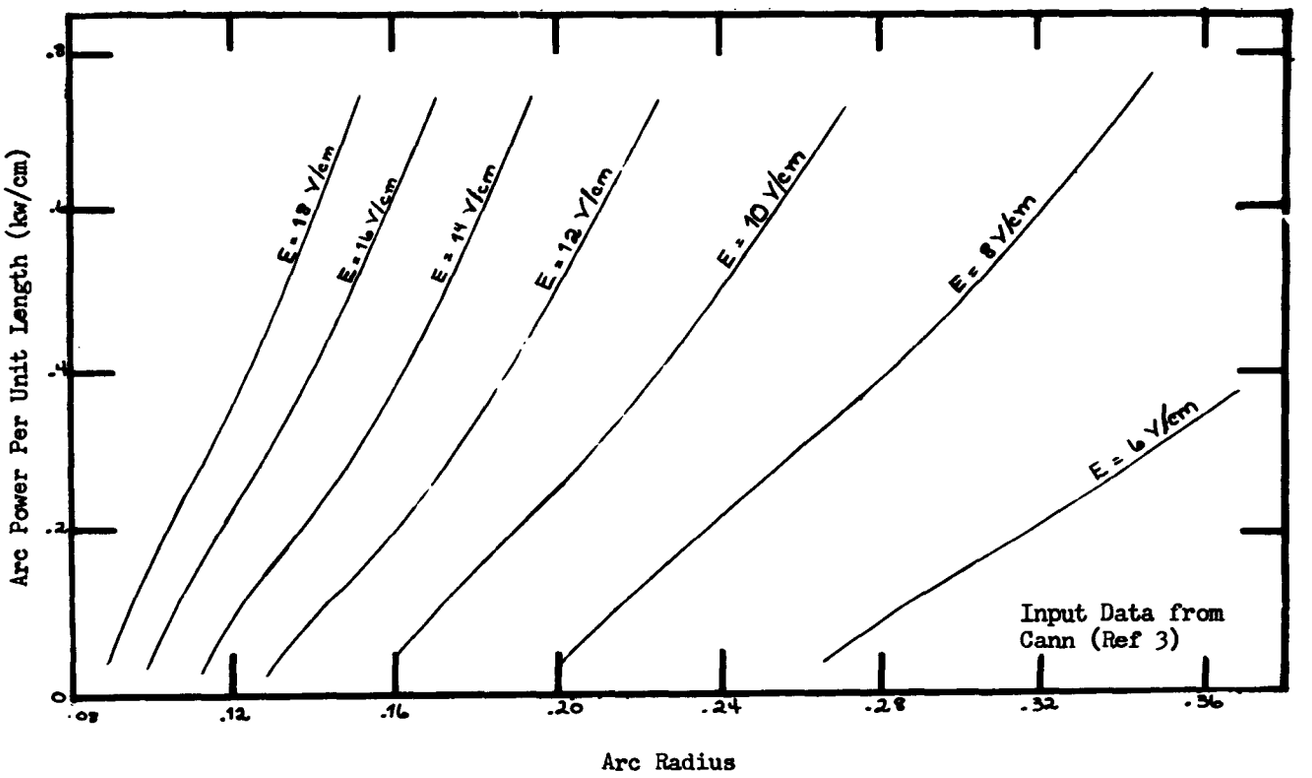

Fig. 7

Arc Power Per Unit Length vs Arc Radius at Constant Electric Field Strength (Data of Cann, Ref 3)

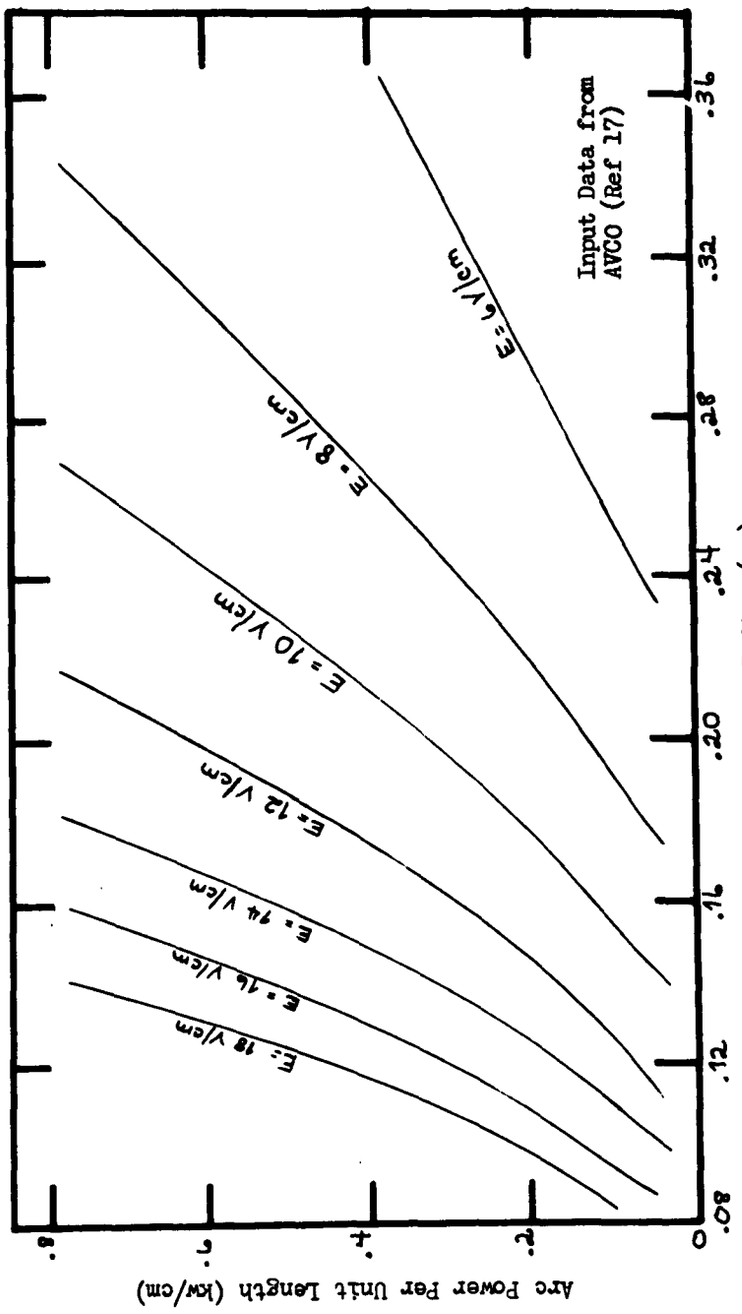

Fig. 8a

Arc Power Per Unit Length vs Arc Radius at Constant
Electric Field Strength (Data of AVCO, Ref 17)

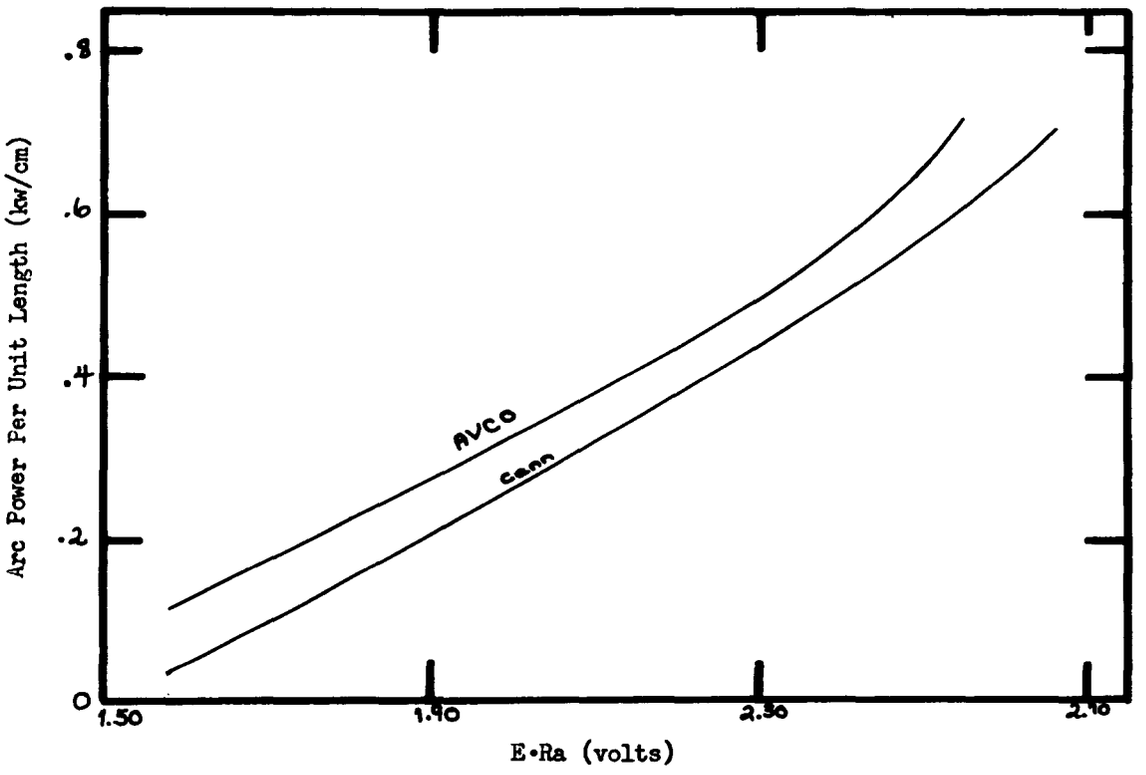

Fig. 8b

Arc Power Per Unit Length vs E•Ra
for Data of Cann and AVCO

conductivities, and an increase in radiation loss per unit volume with increasing pressure, below 15,000°K. The net result of these effects will be a decrease in arc radius and power per unit length for a given field strength and centerline temperature.

The Gas Sheath

Because of the wide range of variables and conditions in gas dynamics, there are at present many mathematical models to describe some of the more simple types of flows. Each of these models entails certain simplifying assumptions in order to make possible a solution or set of solutions to a particular problem or class thereof. It is this very aspect of the mathematics involved which makes the problem of the annular sheath of gas in the wall-stabilized, transpiration-cooled arc so difficult. Several models were carefully examined on the bases of applicability and feasibility. In each case, a primary assumption which was not physically acceptable was found.

One of the first models considered was that of Rayleigh flow. However, one of the six basic assumptions was that the flow occurs in a duct with constant cross-sectional area (Ref 2:8-43). Since transpiration cooling involves constant mass addition through the walls, the mass flow increases with duct length, and the net effect is the same as for a converging duct. Also, the flow is assumed frictionless, but cold-flow pressure measurements showed this not to be the case for the arc channel.

Fanno flow offered another possibility but this, too, required constant duct area, as well as adiabatic flow (Ref 2:8-53). Since the arc is a heat source, the latter assumption is inapplicable.

It was then hoped that transpiration flow theory might yield some means of approach to the gas sheath problem. However, here too, certain assumptions basic to the development and application of the theory were not consistent with the physical problem. The transpiration-cooled, flat-plate model was no good since it could not account for increasing mass flow in a constant channel. The model of transpiration-cooled pipe flow rested on the assumption that the gas temperature and velocity were maxima at the centerline of the pipe (Ref 10:461). While the former condition is true, the latter is complicated by the effect of the high viscosity of the core on the radial velocity profile. Also, these approaches did not use a continuous heat source, but rather a heated gas which received no thermal energy while in the pipe (Ref 10:461, 470).

Furthermore, the transpiration theory for pipe flow accurately predicts ratios of transpiration to longitudinal mass flow on the order of 0.01 or less as being effective in reducing the convective heat transfer from a hot gas to the pipe by as much as 90% (Ref 19:17, 18). This was not found experimentally by Tannen for the wall-stabilized, transpiration-cooled arc (Ref 16:75).

But, the failure of the above approaches to solve the gas-sheath around the wall-stabilized, transpiration-cooled arc by no means renders the problem insoluble. Many different methods have yet to be tried, but unfortunately, lack of time places this beyond the scope of this study. Specific references which may provide the basis for a successful analytic approach include the work of J. T. Howe, who used a numerical approach of a transpiration-cooled flat plate with a laminar boundary layer, as well as the work of Cassie, and Sherman and Yos for electric arcs in nozzles

under forced convection (Ref 8). Further references are included in the General Bibliography, p. 78.

III. Equipment

The wall-stabilized, transpiration-cooled, DC arc required a great deal of support equipment. Except for a brief description of the actual arc device and the support equipment, only the list which appears below will be presented here. For further information, the interested reader is invited to check Appendix B, p. 94, where the instrumentation is presented in detail with the associated schematics.

The block diagram in Fig. 9, p. 23, is numbered to correspond with the following list of equipment:

1. The arc device (Figs. 10 and 11, pp. 24-25)
2. Electrical equipment, including recifiers, load resistance, starting equipment, voltmeters and ammeter (Fig. 35, p. 95)
3. Thermocouples and read-outs (Fig. 36, p. 97)
4. Water flow, monitoring and control (Fig. 37, p. 99)
5. Argon flow, monitoring and control (Fig. 38, p. 100).

The figure referenced with each item is that showing the schematic of that equipment.

As shown in Figs. 10 and 11, pp. 24-25, the arc device consisted basically of a 0.25-in. diameter water-cooled tungsten cathode; a transpiration-cooled channel (transpiration column) 8-in. long, and 0.25-in. diameter for the arc; and a hollow, water-cooled, cylindrical copper anode (Fig. 12, p. 26). All components were designed and built at ARL, and engineering details are available from Maj. Donald E. Dye, Thermomechanics Branch, ARL, Wright-Patterson Air Force Base, Ohio.

Fig. 13, p. 27, is a photograph of a pair of wall segments. The

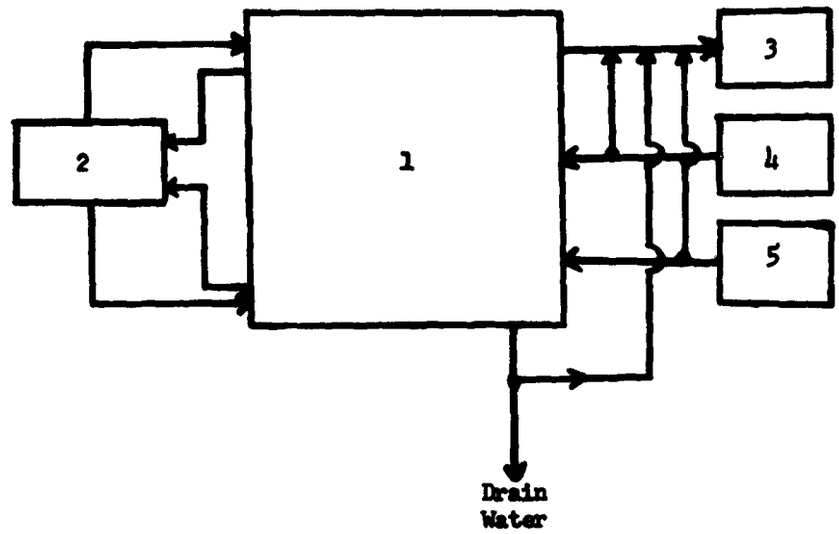

KEY:

1. Arc Device
2. Electrical equipment: rectifiers, load resistance, starting equipment, voltmeters, ammeter
3. Thermocouples and read-outs
4. Water flow, monitoring and control
5. Argon flow, monitoring and control

Fig. 9

Overall Equipment Schematic for
Wall-Stabilised, Transpiration-Cooled Arc

Fig. 10

Photograph of Arc Device

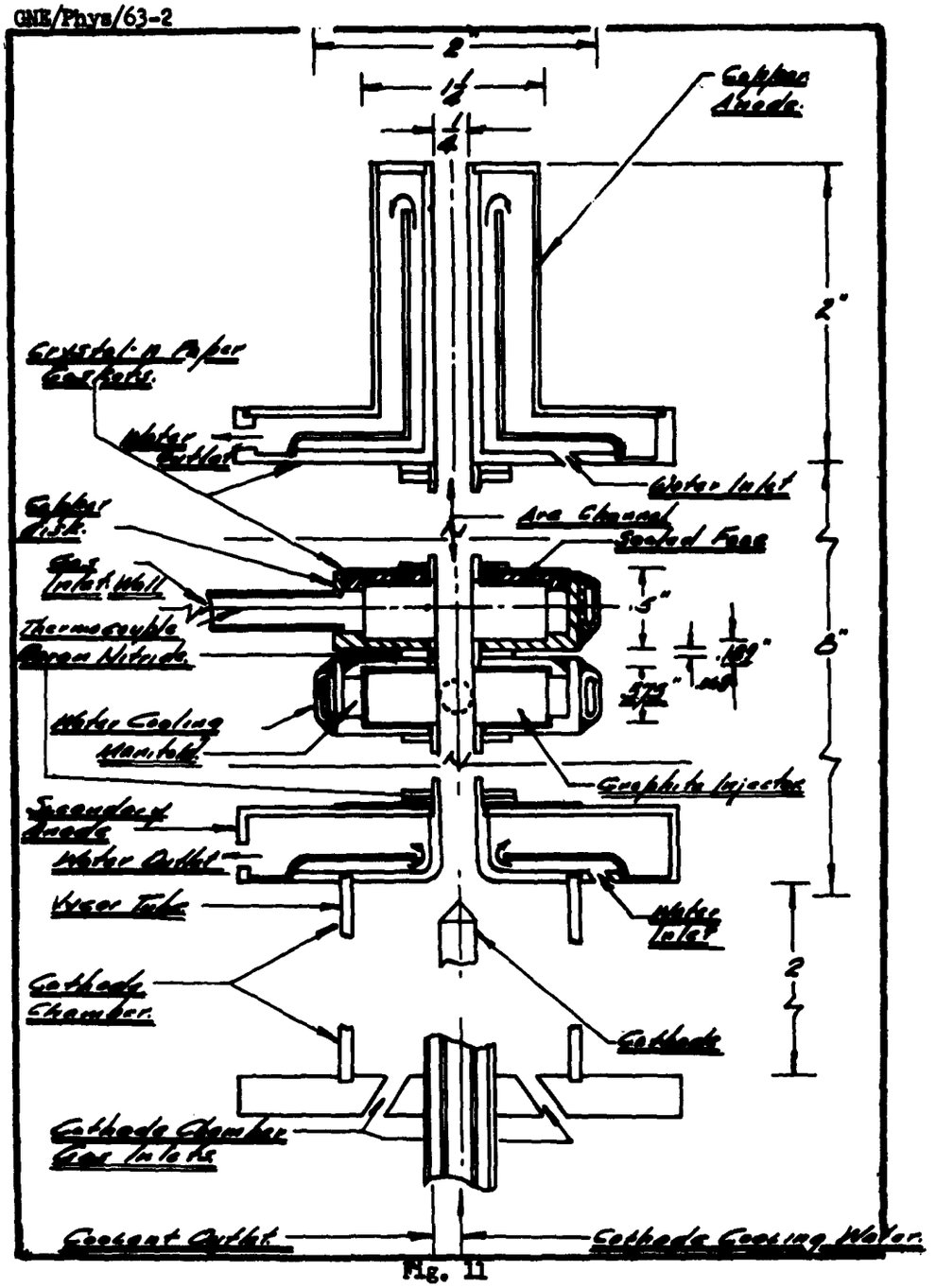

Fig. 11

Cut-Away Sketch of Arc Device

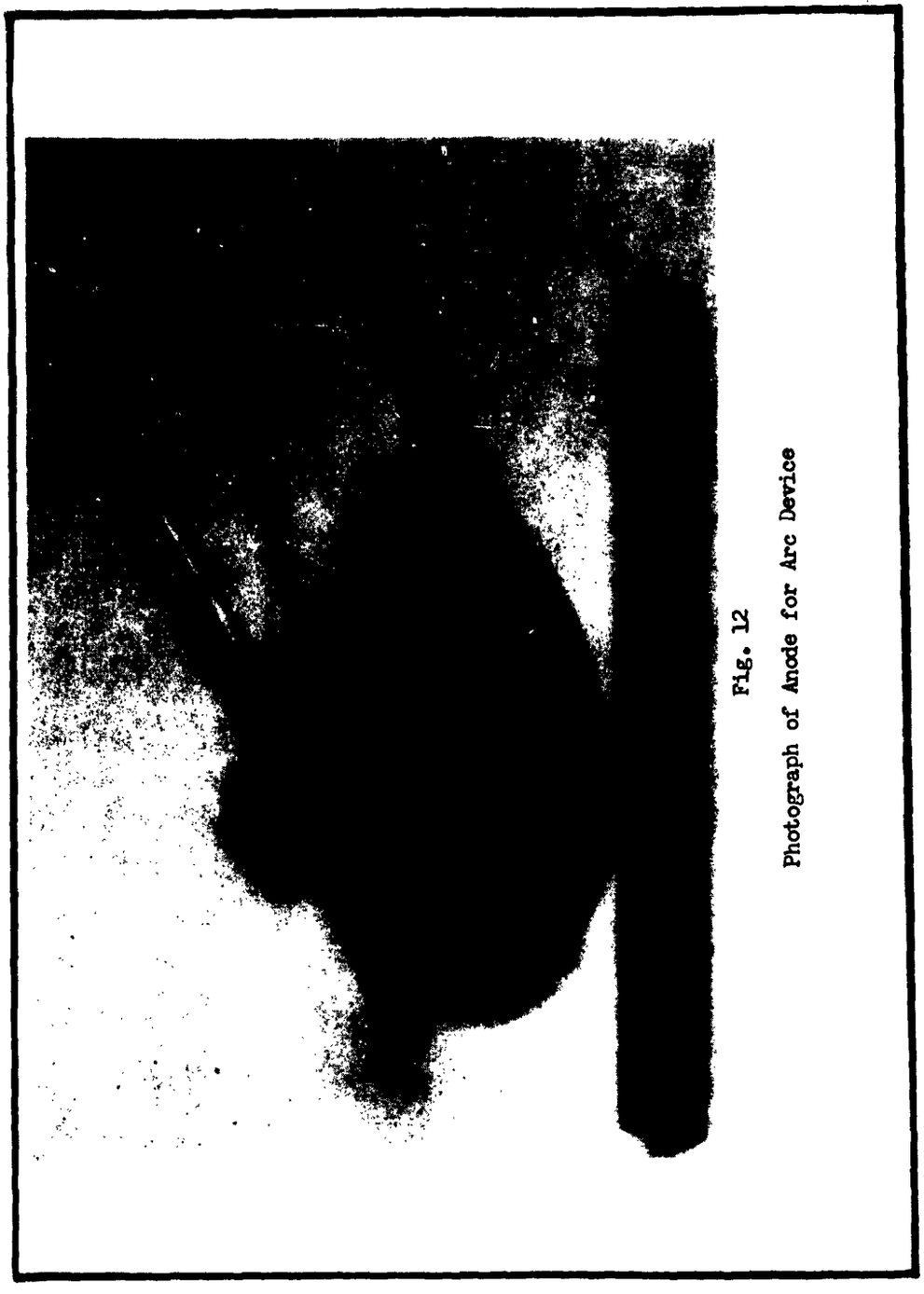

Fig. 12

Photograph of Anode for Arc Device

Fig. 13

Photograph of Disassembled
and Assembled Wall Segment

one on the left is shown with its components; the one on the right is assembled. The transpiration column consisted of twelve of these hollow copper segments, 0.5-in. thick, and 2.0-in. in diameter. Each of these segments contained a porous gradphite insert through which argon gas at about 1.1-atmosphere pressure was passed into the column. The amount of gas to each disk was controlled and monitored individually. Surrounding each segment was a copper cooling line used to measure the net heat loss to the wall of the arc channel. Thermocouples were inserted to within 0.0625-in. of the inside wall of the channel in four of the disks in order to monitor the temperature and thus prevent overheating of the injectors.

Insulation between the wall segments consisted of boron nitride separators, with Crystal-M paper providing a gas-tight seal between the disks and these separators. The inside wall surface alternated between porous graphite and boron nitride liners. The latter were inserted in the column wall between segments to keep the channel diameter uniform.

The electrical equipment included a bank of stainless steel tube which served as a water-cooled resistor, as well as two water resistors, which were cooled by immersed coils. Power was supplied by two A.O. Smith rectifiers, one for starting, and the other for normal operation. The starting spark was supplied by a 30,000 volt spark generator powered by an aircraft lead-acid battery. Simplytrol meters were used for arc voltage and current measurements, and an RCA vacuum-tube voltmeter was used to measure potential differences between arc components as well as the rectifier output ripple voltage.

Iron-constantan thermocouples of various manufacture and sizes were

used to make temperature measurements on the cooling water to and from the various arc components, the interior wall of the arc channel, and the inlet gas. Read-outs for the thermocouples were a Brown pyrometer and four Simplytrols.

The flow rates of water to the various arc components were monitored with Fischer-Porter Flowrators with a maximum flow rating of 1.87 gpm. Coiled capillary flowmeters were used to determine the individual argon mass flows to the different sections of the arc device.

Additional equipment for the arc radius measurements included a brass window holder which replaced one of the center disks, a quartz window, a camera and optical bench, and a densitometer for determining the arc radius from the negatives. The window in the arc device is shown in Fig. 14, p. 30.

As mentioned previously in this chapter, the details of the above support equipment may be found in Appendix B, p. 94, with the associated schematic diagrams.

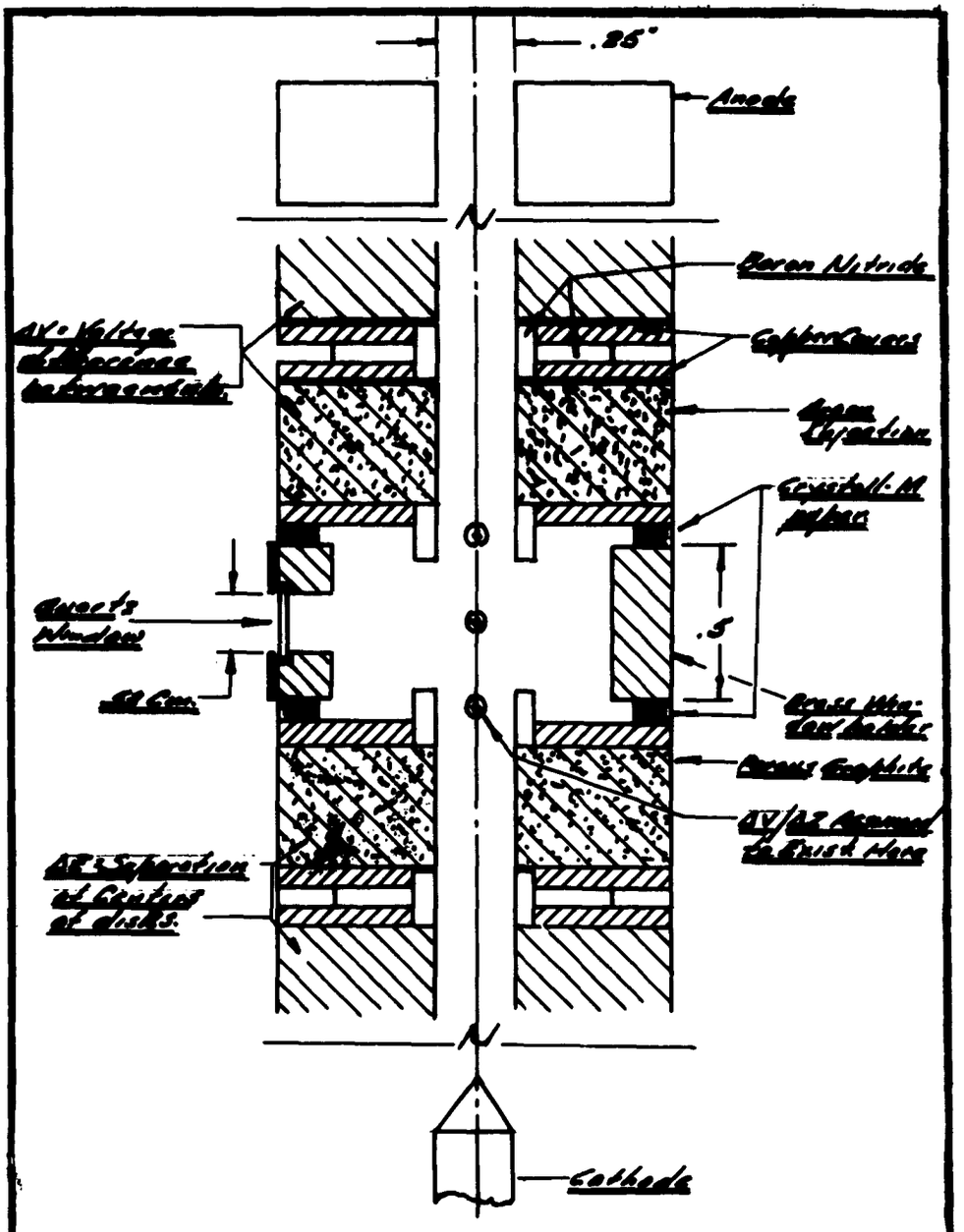

Fig. 14

Sketch of Arc Device with Window
Installed in Place of One Wall Segment

IV. Procedure

General Procedure

Since this experiment involved high voltages and currents, a fixed routine was established to reduce the risks to personnel and equipment. The first step was to ensure that the proper amount of water was in each of the water-resistors. The water flow to the resistor-cooling coils was then checked, and the water flows to the various components of the arc device were established. The gas to the cathode chamber and to each of the porous disks was then turned on. The high voltage was turned on momentarily to check for short circuits and to see if all equipment was functioning properly.

Starting Procedure

The starting procedure for the wall-stabilized, transpiration-cooled arc was based on a method suggested by G. L. Cann of the Guggenheim Aeronautical Laboratory, California Institute of Technology, in a personal communication at ARL, Wright-Patterson Air Force Base. This method involved the use of two independent rectifiers, and a radio-frequency-spark generator. The tip of the tungsten cathode was fixed at about 1.0 centimeter from the bottom of the lower support plate, which became the secondary anode, of the transpiration column. Both rectifiers were turned on, producing a 1,000 v/cm field from the cathode to the secondary anode. The spark generator was connected to a 24-volt aircraft battery, and a spark was initiated across the gap.

This produced a short, low-voltage, high-current arc across the gap between the cathode and the secondary anode. The other rectifier was still

at open circuit potential of 1,000 volts, DC, thus producing a field on the order of 40 V/cm from the secondary anode to the primary anode. When the gas flow to the cathode chamber was about 3.0 lb/hr, and that to each disk about 1.7 lb/hr, the arc would transfer automatically from the secondary to the primary anode. The rectifier to the secondary anode would then be shut off and final adjustments made in the gas flows and total arc power before taking data. The circuitry for this procedure is presented schematically in Fig. 35, p. 95.

Data

The data recorded for each run included total arc voltage and current; water temperature changes and flow rates for the cathode, secondary anode, each of the 3 groups of four disks, and the primary anode; inlet gas temperature; wall temperatures at 4 stations in the transpiration column; gas flows to the cathode chamber and all disks; and voltage gradient along the length of the column. The voltage gradient was obtained by measuring the voltage across each pair of disks and dividing by the separation of the centers of the disks. The result was assumed to exist midway between the disks (see Fig. 14, p. 30). This is a common assumption, and appears reasonably good (Ref 6:4). The sum of the potential differences between components agreed to within 5% of the observed total column voltage. A sample of raw data is presented in Table I, p. 81.

With the window in the arc column, the necessary data included the total arc current and voltage, and the voltage gradient at, above, and below the window to determine arc power per unit length. Also, the negatives of the arc photographs and the densitometer traces of these

negatives would be considered data. These are not shown here but are available on request from the author.

Measurement of Arc Radius

The method of obtaining the arc radii from photographs of the arc column was suggested by Mr. Paul Schrieber of the Thermomechanics Branch of ARL, in a personal communication. This method involved taking a series of still photographs of the arc at 1/200 of a second over a range of stop openings. Then, by looking at the negatives, one could determine the proper exposure for use in the densitometer. Underexposure resulted in a light negative, without much density and contrast, and considerable noise when traced by the densitometer. Overexposure resulted in a large, blurred, heavily contrasted negative which indicated a greatly oversized arc when traced by the densitometer. From each group, as many as two or three negatives were usuable, and the values of arc radius were found to agree to ±10%, the experimental limit of error. (See Fig. 15, p. 34.)

The recorder chart was calibrated by passing the negative through the densitometer and obtaining the trace across the vertical dimension of the window. A sketch of this plot is shown in Fig. 16, p. 35. This dimension of the window was measured with a cathetometer and the longitudinal scale value of the densitometer trace was obtained. The vertical scale of the trace was in units of relative intensity.

To obtain the arc radius, the negative was scanned by the densitometer across the long, or horizontal, dimension of the window. This resulted in a plot of the intensity of the arc across its full diameter. The radius was extrapolated linearly from that portion of the curve where the trace

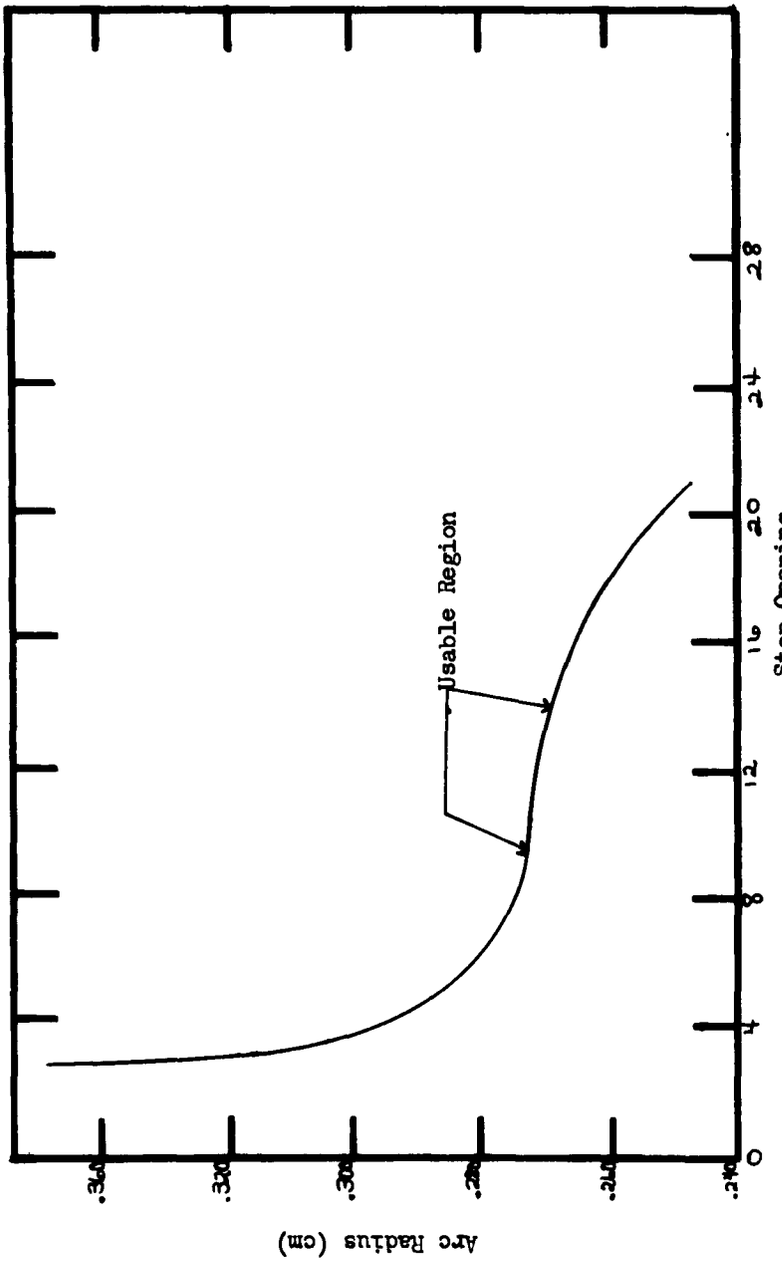

Fig. 15

Variation of Apparent Arc Radius with Stop Opening of Camera at 1/200 second

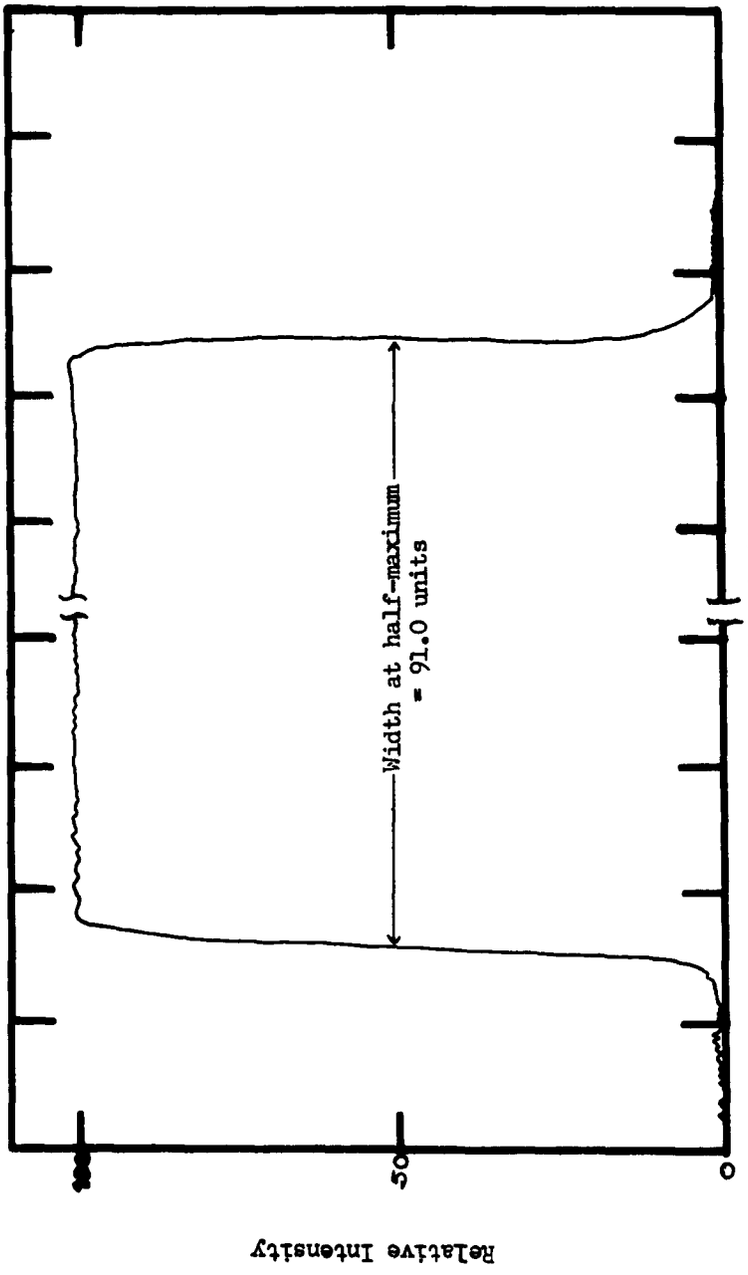

Fig. 16

Calibration of Densitometer
Chart with Arc Window Width

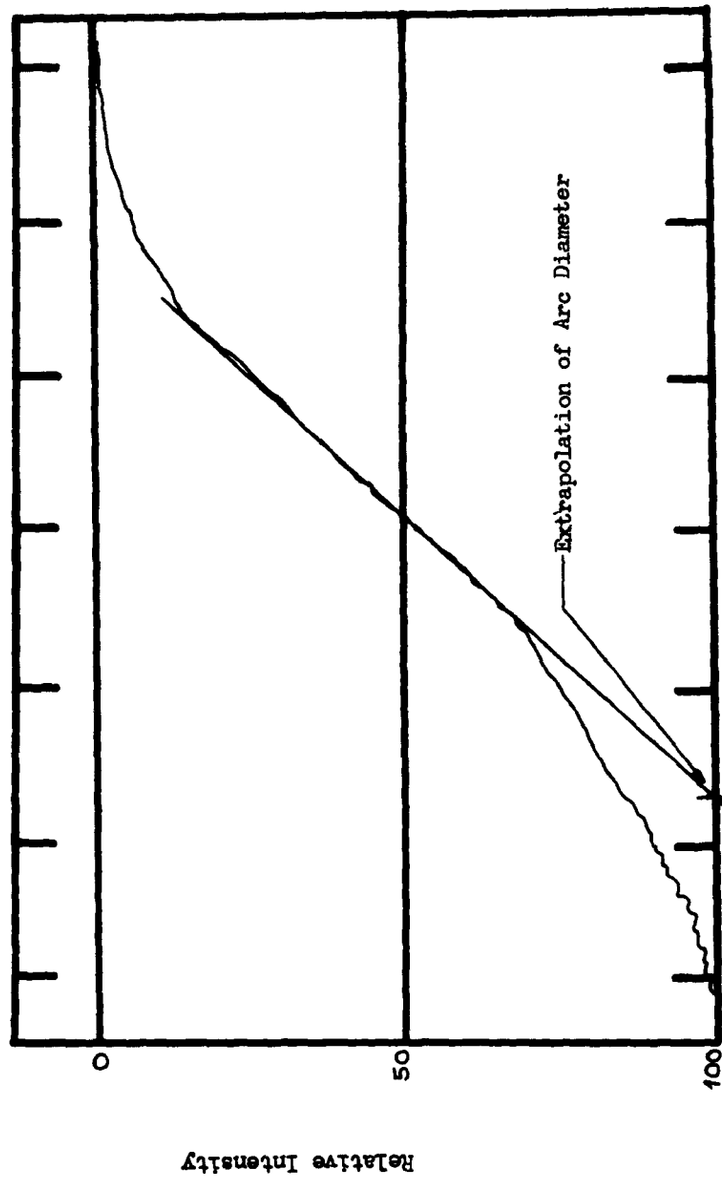

Fig. 17

Extrapolation of Arc Diameter

has a practically constant slope. This is shown schematically in Fig. 17, p. 36. Extrapolation was necessitated by the fact that there was some background in the negative from reflection from the back of the brass window holder and from the luminous, turbulent fringe which surrounded the outer periphery of the core. This appeared in the densitometer output as noise and decreased the definition of the core edge. A check of the result was made by folding the trace in half at the computed center and examining the symmetry of the plot.

Range of Variables

The wall-stabilized, transpiration-cooled arc offered many possible choices of variables. These included total arc power, or voltage and current, arc length, total mass flow, mass flow to individual components, and operating pressure in the arc channel. In order to reduce the scope of the experiment, it was decided to keep the length constant. For the twelve-disk configuration, this meant a transpiration column about 6-in. long and a total arc length of about 8-in.

In addition, the mass flow to each individual component was held equal to that to any other component; i.e., only the total mass flow was varied. Also, the gas pressure in the arc channel was maintained as near atmospheric pressure as possible with the powers and mass flows under consideration. For high flow rates and arc powers, the pressure in the cathode chamber may have been on the order of 2 atm, but no pressure measurements were made.

The current was varied from about 35 to 75 amps DC; the voltage, from 220 to 275 volts DC. Three total mass flows were used: 22.13 lb/hr,

25.72 lb/hr, and 29.20 lb/hr. Table II, p. 82, shows the relationship between the total mass flow and the injection rate to each component in lb/hr.

The range of arc power was 7.9 to 19.4 kw. The observed increases in the specific enthalpy of the argon varied from 600 to 1400 Btu/lb.

Arc radius measurements were made at current of 46 and 50 amps, with power per unit length in the range of 301 to 665 w/cm in the vicinity of the window. The argon flow for these measurements was 22.13 lb/hr. The variation in arc radius was 0.200 cm to 0.286 cm. Arc powers were 9.66 kw and 10.5 kw.

V. Discussion of Results

The wall-stabilized, transpiration-cooled arc device was found to be very stable and relatively easy to operate. The arc characteristics were readily obtained within the range of parameters selected. The choice of gas flows was limited by the pressure at the low pressure manifold, since as heat is added to a fluid moving in a pipe, a greater pressure drop in the pipe is necessary to maintain constant mass flow. The flowmeters for the argon were calibrated to an upstream pressure of 30 psi, and higher pressures were required for mass flows beyond those finally used. Arc radius measurements were made under relatively low flow and low power conditions to maintain atmospheric pressure in the arc channel. No other serious problems such as insulation failure or component overheating occurred, and the device showed no visible signs of wear after 30 hours of operation.

Volt-Ampere Characteristics

Fig. 18, p. 40, shows the volt-ampere characteristics of the arc device over the range of power and mass flows investigated. Table II, p. 82, shows the relationship between total mass flow and the injection rate to each component in lb/hr.

As is readily seen in Fig. 18, p. 40, the total arc voltage is sensitive to the mass flow in the discharge channel and tends to increase with increasing mass flow at constant current. This has been found experimentally by several investigators, including Cann, McGinn, and Schoeck, and seems to be equivalent to an increasing resistance with increasing mass flow (Refs 3:101; 11:971; 15:103). The above have not considered an

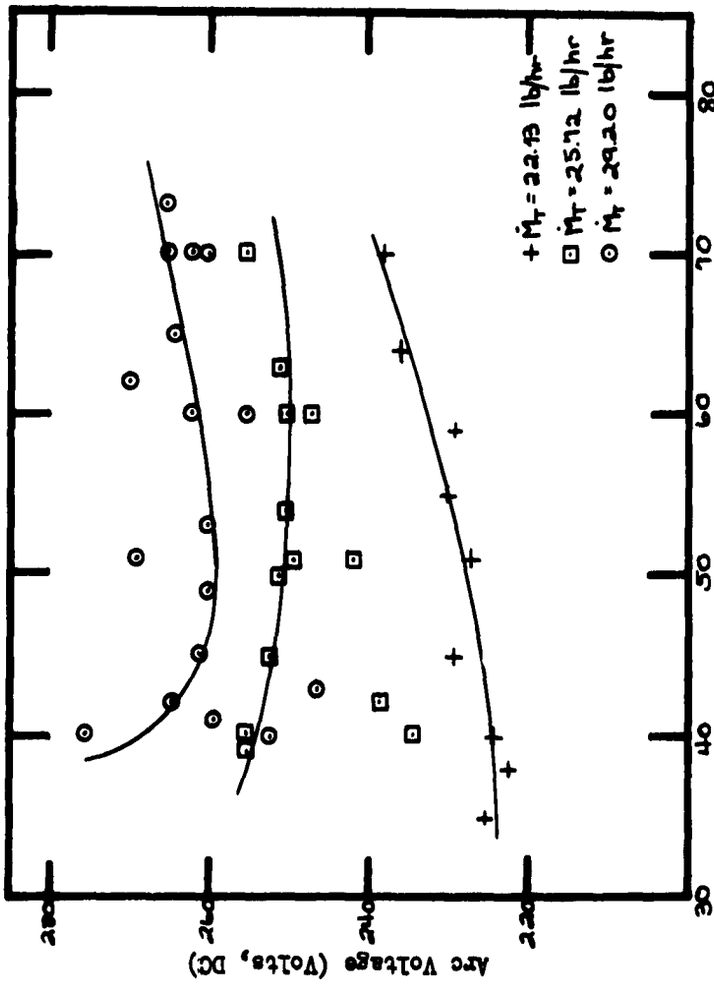

Fig. 18

Arc Voltage-Current Characteristics

arc in a channel with constantly increasing mass flow, but rather they have dealt with constant mass flow through the entire channel. Nevertheless, the effect appears to be the same.

This apparent increase in resistance with increasing mass flow at constant current may be explained qualitatively in terms of a simple model based on the cooling of the arc by the surrounding gas. This model has as its only assumption the physical law that energy and mass must be conserved, and that the arc device obeys this principle. If the gas in the annular sheath removes a given quantity of heat by convection from the surface of the arc core, then that amount of heat must be supplied to the surface by power generation and conduction within the core. Since the convection losses in the core are small, and the cooler argon is sensibly transparent to any radiation from the core, the rpimary means by which heat generated internally reaches the surface of the arc is conduction. If the cooling of the arc were increased and the current held constant, then one would indeed expect the total voltage to increase in order to increase the power generation and maintain the energy balance between the core and the surrounding gas sheath (Ref 5:332). The initial increase in cooling could be easily obtained by increasing the mass flow in the arc channel.

Another way of explaining this behavior is to consider the effect the cooling has on the mean arc temperature. Lowering this temperature would decrease the electrical conductivity, and hence, arc voltage would increase with an increase in mass flow at constant current.

The concept of cooling the arc may also explain the change in the slope of the voltage-current characteristic from negative to positive for

the wall-stabilized, transpiration-cooled arc in the range of relatively low currents, i.e., at about 50 amps. This phenomenon was previously observed near 40 amps by Tannen in the preliminary investigation of this arc device at ARL (Ref 16:17). Emmons reports this change from a negative to positive slope to occur in the range of 80 to 120 amps for gas flows on the order of 0.106 lb/hr and an arc length of 13.6 and 5.6 cm, respectively, for a non-transpiration-cooled arc (Ref 6:13a). Other sources report even higher currents at higher mass flows for the minimum in the curve (Ref 9:9).

If the hypothesis is made that the cooling effectiveness of the annular gas sheath surrounding the core remains nearly constant with increasing arc power at constant mass flow, then the early occurrence of the minimum in the voltage-current characteristic may be explained. That is, as the arc power is increased at constant mass flow, the gas carries the extra power away from the surface of the core and maintains the energy balance. The heat transfer data which is presented graphically in Figs. 27, 28, 29, and 30, pp. 58-61, seems to support this particular hypothesis of constant cooling effectiveness at constant mass flow. Indeed, the heat loss to any particular component of the device is seen to remain an approximately constant fraction of the total power, irrespective of mass flow or power. This is also seen for the overall efficiency of the device which appears to be nearly constant at 50% for all powers and gas flows (Fig. 30).

Arc Column Voltage Gradient

Figs. 19, 20, and 21, pp. 43-45, present some of the typical values

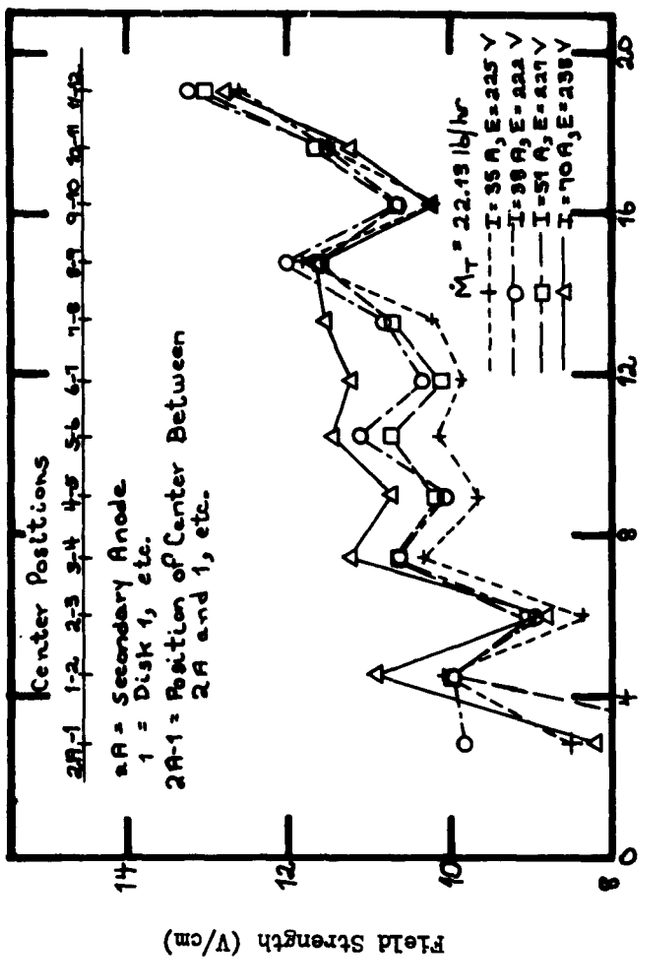

Fig. 19
Axial Electric Field Strength vs Axial Distance from Cathode for $\dot{M}_t$ = 22.13 lb/hr

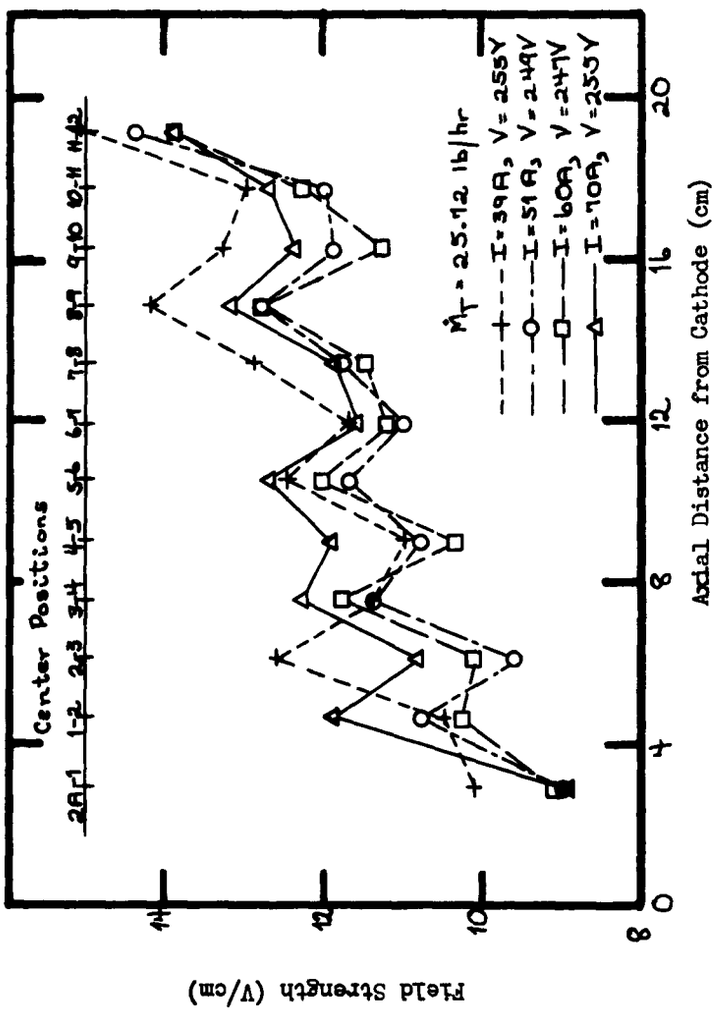

Fig. 20

Axial Electric Field Strength vs Axial Distance from Cathode for $\dot{M}_t$ = 25.72 lb/hr

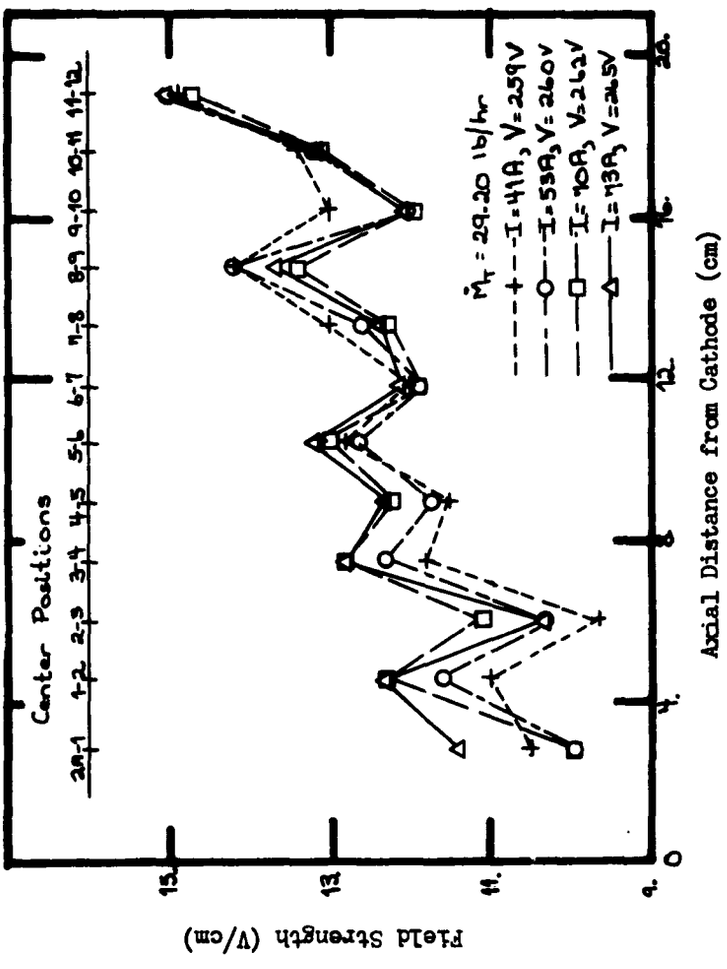

Fig. 21

Axial Electric Field Strength vs Axial Distance from Cathode for $\dot{M}_t$ = 29.20 lb/hr

of the voltage gradient as a function of axial distance from the cathode over the experimental power range for each of the three mass flows. The cathode and anode falls are not shown, but will be presented and discussed later in this chapter. While the voltage gradient data looks erratic, Fig. 22, p. 47, shows the averages of the voltage gradients over all arc powers observed at each point for each mass flow. It is readily seen that the gradients tend to increase with increasing distance from the cathode and with increasing mass flow. Also, the resemblance in the saw-tooth shapes of the four graphs is apparent. The connecting lines are only for purposes of presentation and are not intended to represent the true variations in field strength between the observed points.

The cooling-effectiveness model can also be used to explain the trend for the gradient to increase with increasing axial distance from the cathode. As the arc proceeds up the channel toward the anode, the mass flow in the arc channel increases. The result is that, in order for an energy balance to be maintained between the core and gas sheath, the power per unit length generated by the arc must increase as the surrounding gas removes more heat from the arc surface. Since the arc is a "series" circuit, the current remains constant along its length, and the column gradient must increase as the power increases. In addition, any decrease in pressure from the cathode to the anode in the arc channel will add to this effect because of the changes in the electrical and thermal conductivities with pressure.

The peculiar saw-tooth shape of the voltage gradient as a function of axial distance from the cathode was not expected, and is not understood at this time. While distortions in the field strength are known to occur

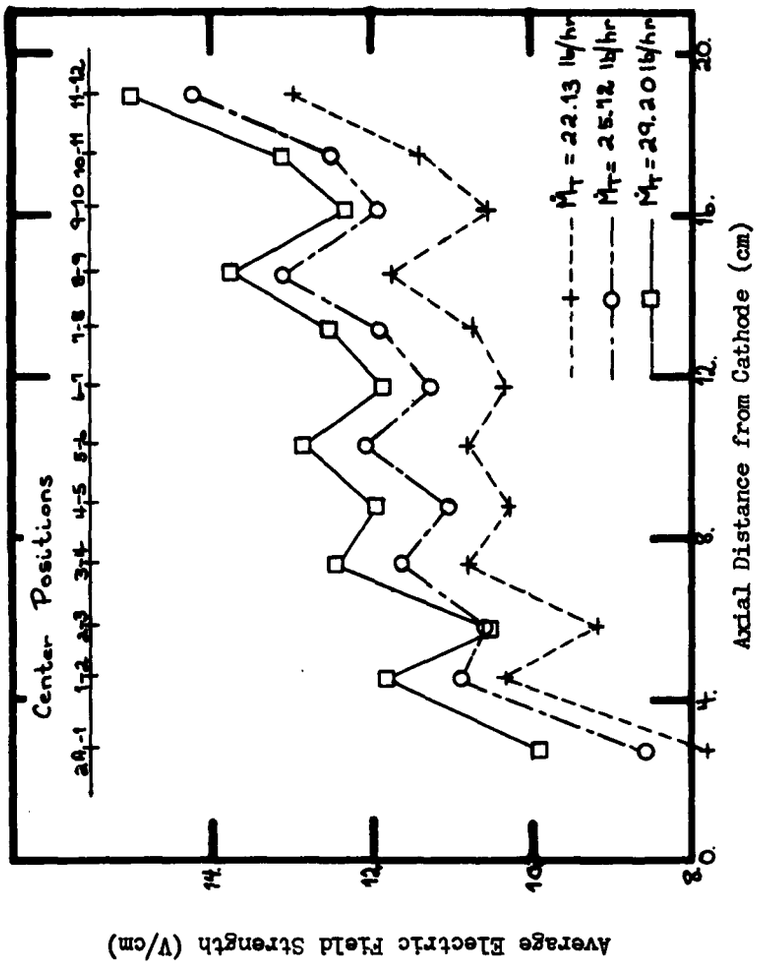

Fig. 22

Average Axial Electric Field Strength vs Axial Distance from Cathode for Each Mass Flow

near the ends of arc channels, these effects are not of sufficient magnitude to produce the saw-tooth behavior found in the wall-stabilized, transpiration-cooled arc (Ref 6:4). Three phenomena may be responsible for this behavior, but further experiments are necessary to obtain the data needed to verify them.

The first of these phenomena is the previously hypothesized cooling effectiveness. This can be used successfully to account for the initial peak in voltage gradient which occurs between the first and second disks, as seen in Fig. 22, p. 47. The flow of gas around the arc in the cathode chamber is longitudinal, but as one proceeds up the arc channel from the cathode, the flow becomes more complicated from the injection of gas at the first wall segment. This produces an increase in the cooling of the arc, resulting in a rise in the voltage gradient as the power generation increases. This possibility can be checked by reducing the flow from the first injector to as near zero as possible and observing the resultant behavior of the voltage gradient in this vicinity. If the peak is caused by the cooling of the arc, this procedure should shift the peak away from the cathode or further up the channel.

However, the cooling effectiveness is closely related to the gas flow around the arc, and this latter is the second phenomenon which will be considered. Since an analytic solution to the gas flow in the annular ring about the arc core was not achieved, many quantitative questions were left unanswered. A possibility does exist that there is a periodic growth and decay of the boundary layer around the core, and that the "wavelength" of this layer does not coincide with the "wavelength" of the gas injection. Thus, a "beat" could be produced in the cooling of the arc

and the shape of the voltage gradient, and the appearance of the second sharp rise in voltage gradient between disks 8 and 9 may be explained. This can also be checked by varying the flow to individual disks and observing the behavior of the voltage gradient.

Also, the existence of a sonic shock or flow transition from laminar to turbulent flow may be responsible for this second peak. Static wall pressure measurements are necessary to determine if either one or both of these two possibilities do indeed exist in the channel. Again, a theoretical analysis of the gas flow in the arc channel may yield the answer to these questions.

The third phenomenon is one which has a direct relationship to the equipment. An unevenness in the column diameter caused by erosion of the graphite injectors may be the cause of the saw-tooth behavior of the gradient. Early attempts at start-up resulted in several short, high-power runs in the vicinity of 30 to 40 kw, well beyond the capacity of the arc device in its present configuration. While no damage was visible in the column, lack of time prevented dismantling of the device and inspection of the injectors to determine the full nature of possible damage to them. Since erosion could produce a distortion in the gradient, the apparent oscillatory nature of the voltage gradient would then be a coincidence of no real physical significance. New injectors of either carbon or some other high-temperature, porous material, such as zirconia or cercor porous glass, would have to be installed, and the behavior of the voltage gradient observed to see if the voltage gradient were sensitive to variations in the channel diameter.

One additional possibility which was considered was that there was

a significant leakage current which distorted the potential gradient through the connecting water lines in the three groups of 4 disks. Since segments 8 and 9 were not in the same cooling current, this leakage current could not occur. However, if this were the case, a similar peak would be expected between segments 4 and 5 since these were not in any way connected electrically. It is readily seen in Fig. 22, p. 47, that the voltage gradient does just the opposite at this position and decreases.

Also, Emmons states that serious distortion of potential differences between wall segments may occur if the insulation between segments is less than 1,000 ohms (Ref 6:4). A check with a vacuum-tube voltmeter showed several thousand ohms resistance between those segments connected with tygon cooling lines, and an essentially infinite resistance between those segments not so connected. Thus, the possibility of leakage currents between segments sufficient to produce distortions in the voltage gradient is eliminated.

Cathode-Secondary Anode Voltage Gradient

Fig. 23, p. 51, presents the values of the voltage gradient between the cathode and secondary anode over the full range of arc powers and mass flows investigated. While there does appear to be a tendency for this voltage gradient to increase with either increasing mass flow or increasing arc voltage, no regular pattern is apparent in the data, and no explanation can be offered at this time. The plot of this gradient vs power shows even less coherency than that in Fig. 23. The phenomena and effects in the cathode region of an arc discharge were investigated by Capt. B. W. George of GNE-63 at AFIT, in the Thermomechanics Laboratory of ARL.

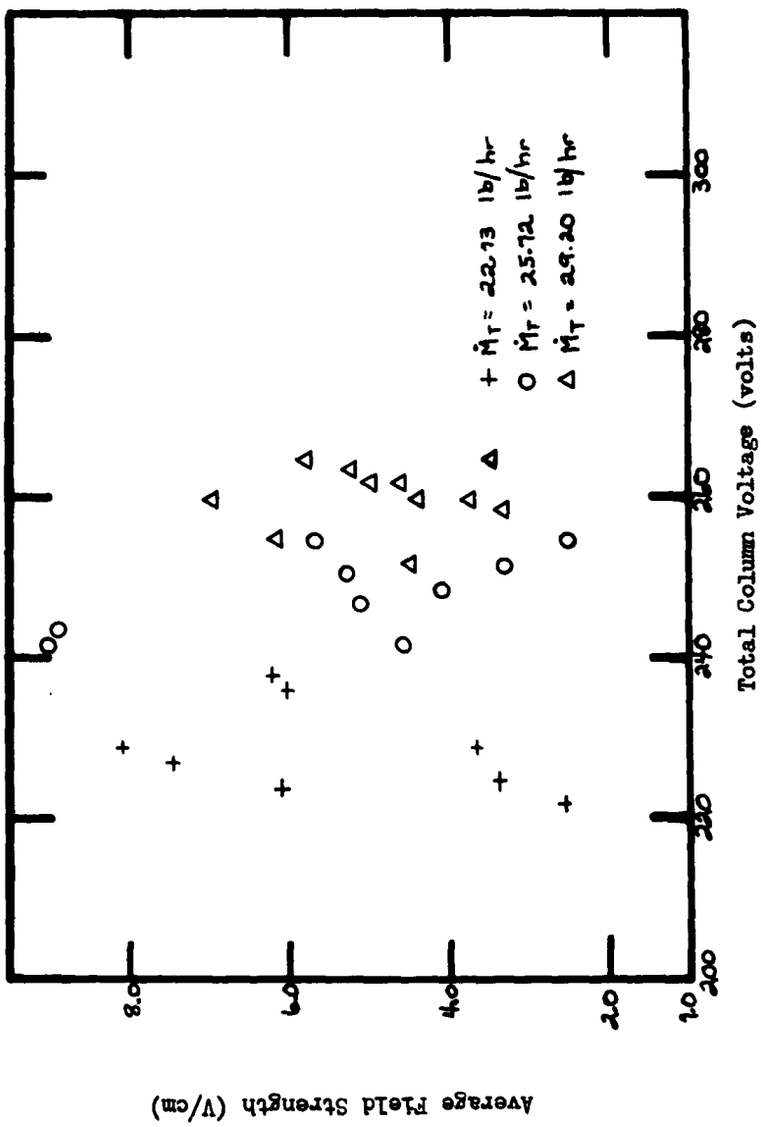

Fig. 23

Average Field Strength, Cathode to Secondary Anode, as a Function of Arc Voltage and Mass Flow

Segment 12-Anode Voltage Gradient

Fig. 24, p. 53, shows the behavior of the electric field between segment 12 (the last wall segment) and the anode. The distance used for computation was taken as that between the center of this last segment and the bottom of the anode. While this is not rigorously correct, it does serve to give an idea of the field strength in this region. In addition, the effective length of the anode is not known. The data is presented as a function of arc power with total mass flow as a parameter. There is a significant amount of scatter, but the observed points do seem to indicate a relatively constant value of field strength for constant mass flow. The broken lines are the numerical averages of the gradient for each mass flow over all powers. The solid lines represent an "eye-ball" estimate based on the grouping of the observed points.

Fig. 25, p. 54, presents a plot of the average values of the gradient between the last injector and the anode as a function of total mass flow. although the data is insufficient to prove the apparent linear relation-ship, there is an indication that this may be case. Schoeck reports that, for a transpiration-cooled anode, the total arc voltage increases nearly linearly with mass flow through the anode in such a manner as to be almost insensitive to arc currents on the order of 100 amps (Ref 15:103). His data was presented for an arc with operating voltages on the order of 30 volts, a maximum length of 1.5-in., and a minimum length of 0.25-in. Thus, if one considers the arc in the region of the last wall segment and the anode to behave similarly to Schoeck's arc, the results of the data for the transpiration-cooled arc appear reasonable. It must be noted here that, for the wall-stabilized, transpiration-cooled arc, arc power varies

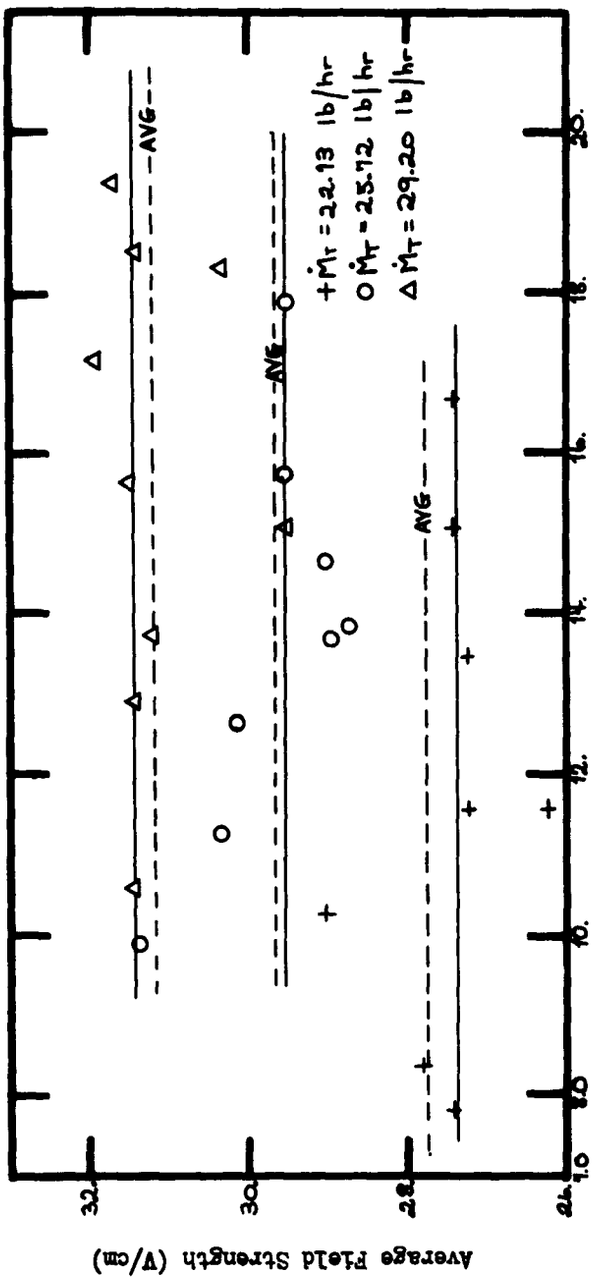

Fig. 24

Electric Field Strength, Segment 12 to Anode, as a Function of Arc Power and Mass Flow

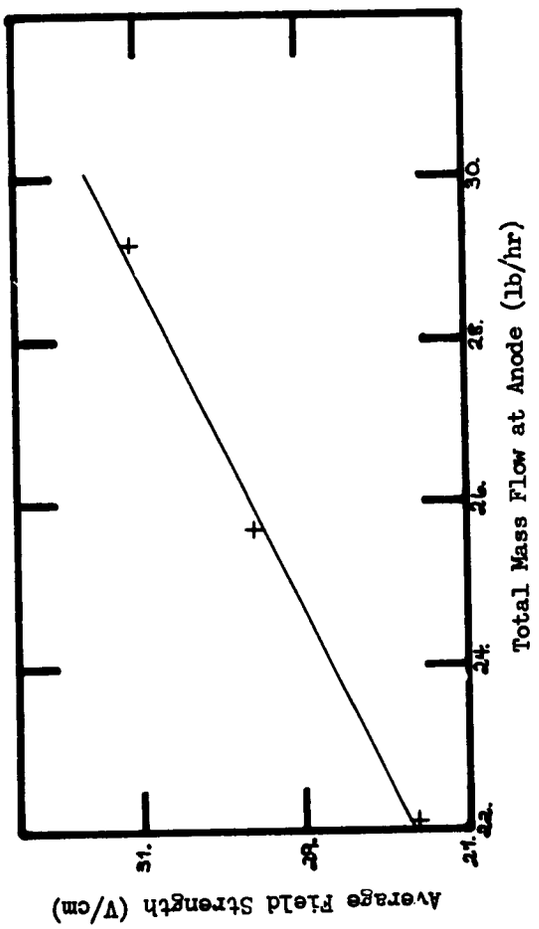

Fig. 25

Average, for Each Mass Flow, of Electric Field Strength, Segment 12 to Anode, as a Function of Mass Flow at Anode

nearly linearly with current at constant mass flow. (See Fig. 18, p. 40.) And, while the anode of the transpiration-cooled arc was not transpiration cooled, there was no evidence of an anode spot, either by visual observation of the arc through a filter, or by inspection of the inner surface of the copper anode. Schoeck also made this observation (Ref 15:93).

Moreover, when the arc was observed through a filter, there was a region about 1-mm thick of relatively low luminescence between the exhaust jet and the anode surface. The flame was about 2- or 3-cm high, and had a rounded rather than pointed appearance. On the basis of work done by Winter, it was concluded that the anode exhaust jet of the wall-stabilized, transpiration-cooled arc was turbulent (Ref 18:51). Calculation of Reynolds numbers for the experimental mass flows in a duct 0.25-in. in diameter also indicated a turbulent flow situation, at least next to the anode. (See Fig. 26, p. 56.)

The non-existence of an anode spot means that the gas temperature next to the anode is relatively low in comparison to that of the arc core. Since the electrical conductivity of argon is sensibly zero below 6,000°K, thermal ionization is not likely as a method of charge transfer from the arc to the anode. However, if the larger portion of the electric field observed in the anode region existed across a thin layer of cold gas, then a sufficient number of electrons from the core could penetrate this cold layer to carry the arc current to the anode. The available surface of the anode is 10.1 sq cm, and low current densities are possible. Anode spots require current densities on the order of 10^4 amp/sq cm, but current densities of about 10 amp/sq cm may occur for the case with no anode spot (Ref 9:13).

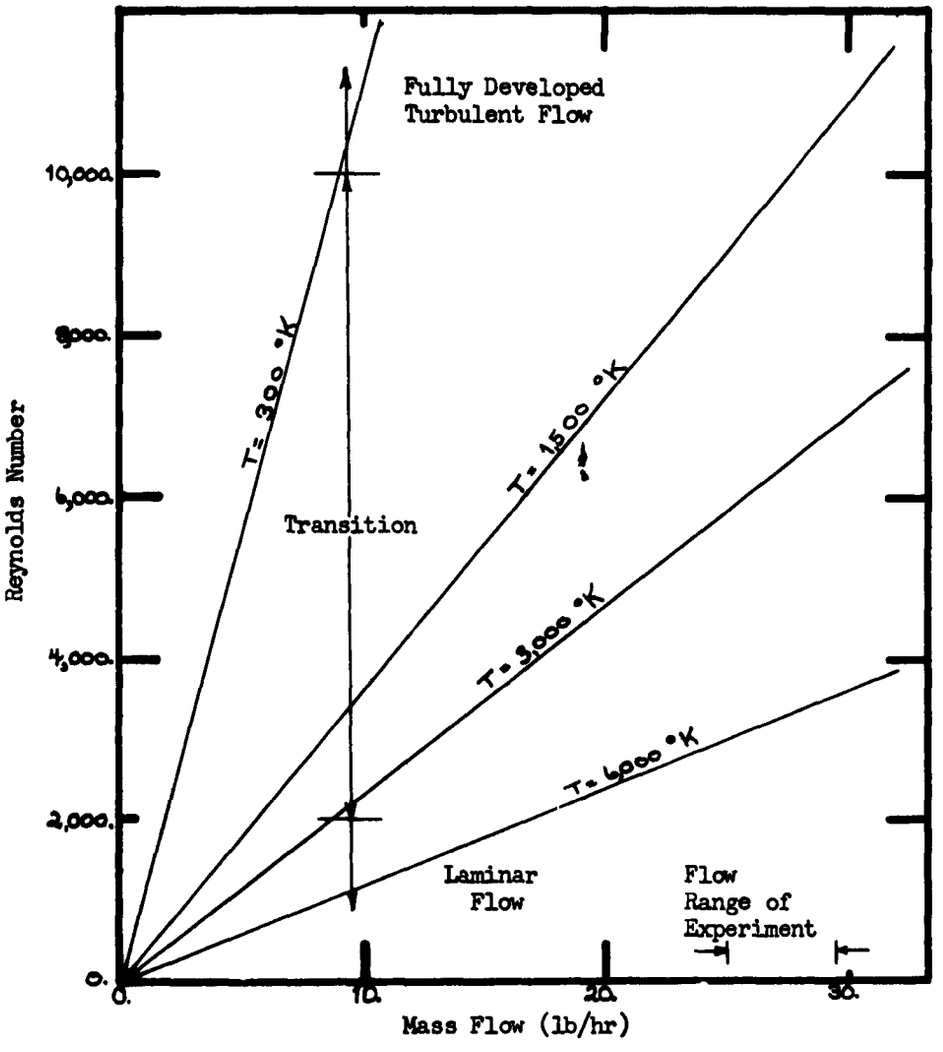

Fig. 26

Reynolds Number for Argon in
a 0.25-in. Diameter Tube

Power Losses and Device Performance

Figs. 27, 28, and 29, pp. 58-60, present the power losses to the various components of the wall-stabilised, transpiration-cooled arc as functions of arc power at constant mass flow. The cathode losses were about 1% of the arc power, but are not shown for clarity of presentation. Fig. 30, p. 61, presents the overall power loss (including cathode losses) to the device vs input power over these same ranges. For each component, as well as the total device, the fractional power loss seems to be approximately independent of the mass flow or the arc power. The total loss seems constant at about 50%. As mentioned previously in this chapter, this tends to support the hypothesis that the cooling effectiveness of the gas is constant at constant mass flow. In the preliminary investigation of this device at ARL, Tannen reported that the overall efficiency seemed to approach a limiting value of about 50% for the longest configuration he considered which was half the length used in this experiment (Ref 16:23). The physical reasons for this behavior are not known at this time, and no explanation can be offered here.

However, it is felt that the primary loss which occurs in the system may be radiation from the core. The gas flow at the wall is radially inward, and conduction and convection losses to the walls should be small. Radiation losses from argon arcs do become significant at higher temperatures (and hence higher powers), as seen in Fig. 4, p. 13, but the counter flow through the walls reduces the net loss to this system. Radiation could account for the higher losses to the wall sections as one proceeds up the arc channel from the cathode and the arc power per unit length increases. Also, the gas in the channel becomes hotter, and this does

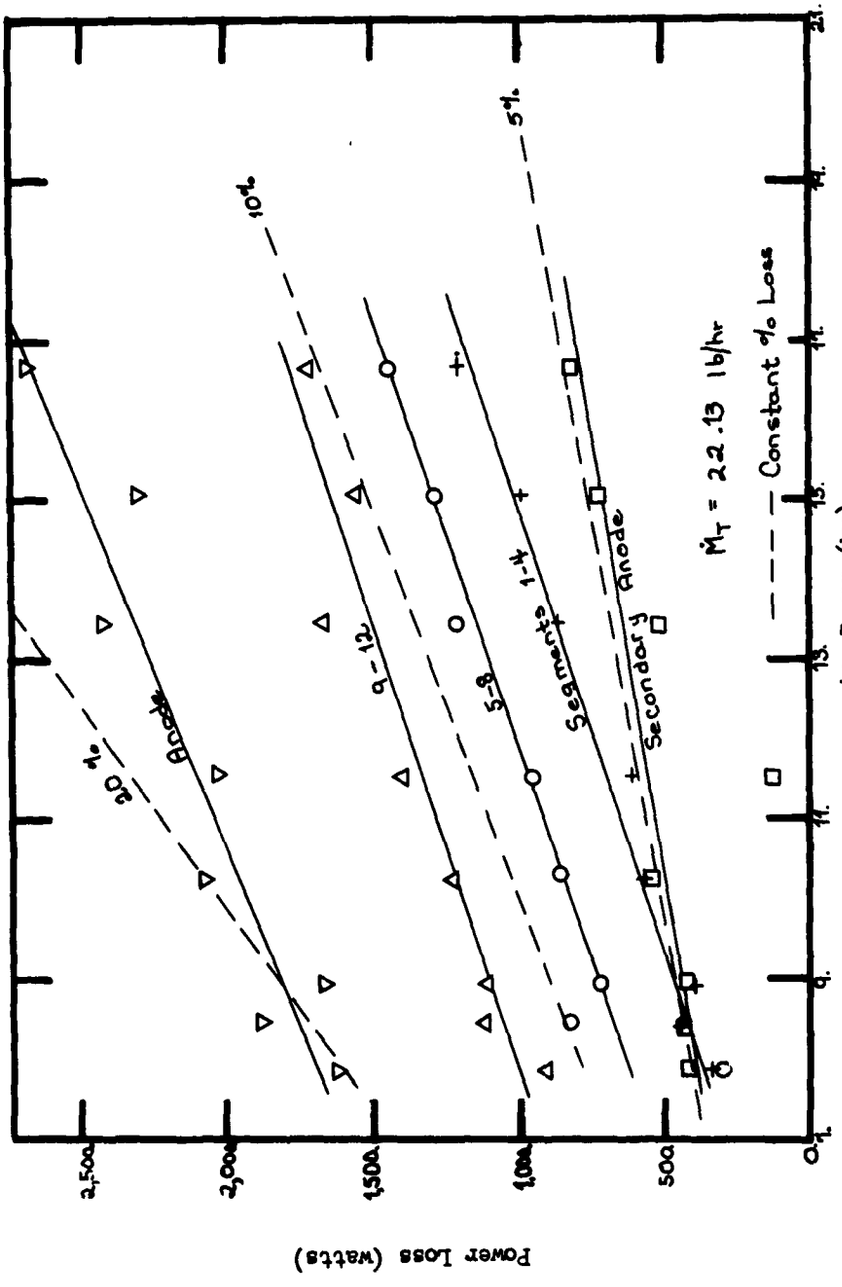

Fig. 27

Power Losses to Arc Components vs
Arc Power for $\dot{M}_t$ = 22.13 lb/hr

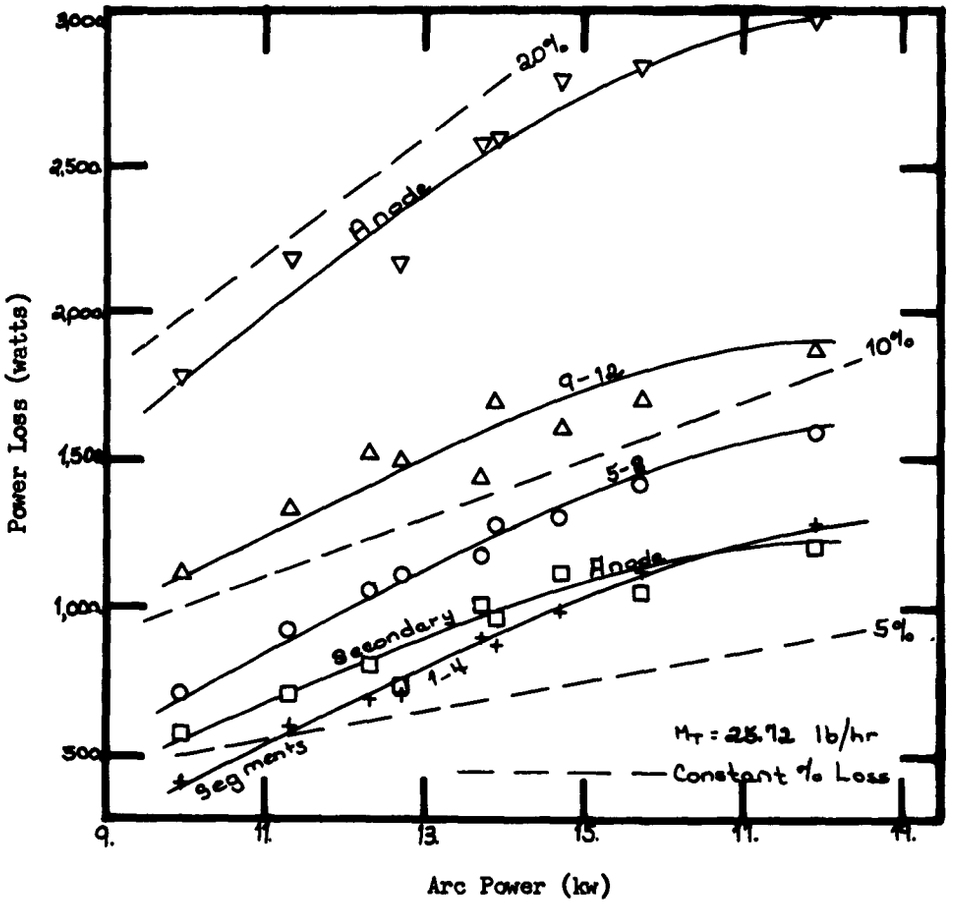

Fig. 28

Power Losses to Arc Components vs
Arc Power for $\dot{M}_t$ = 25.72 lb/hr

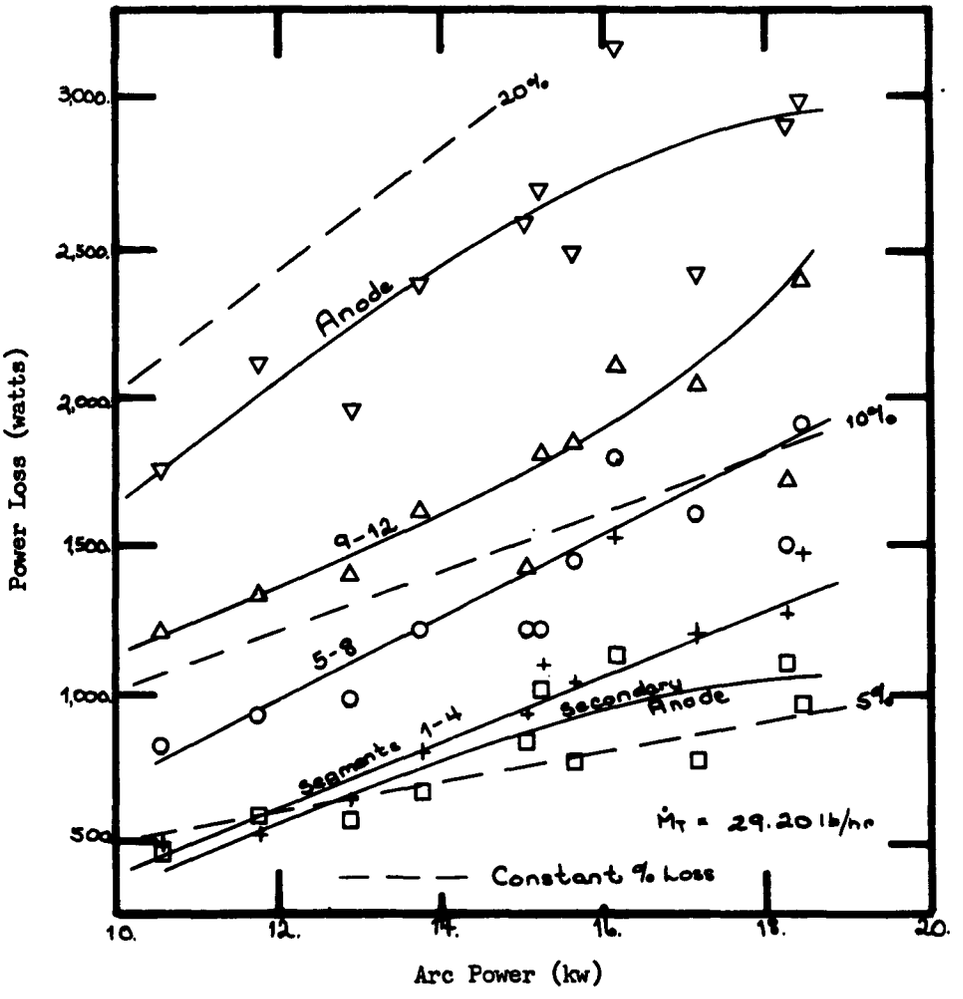

Fig. 29

Power Losses to Arc Components vs
Arc Power for M_t = 29.20 lb/hr

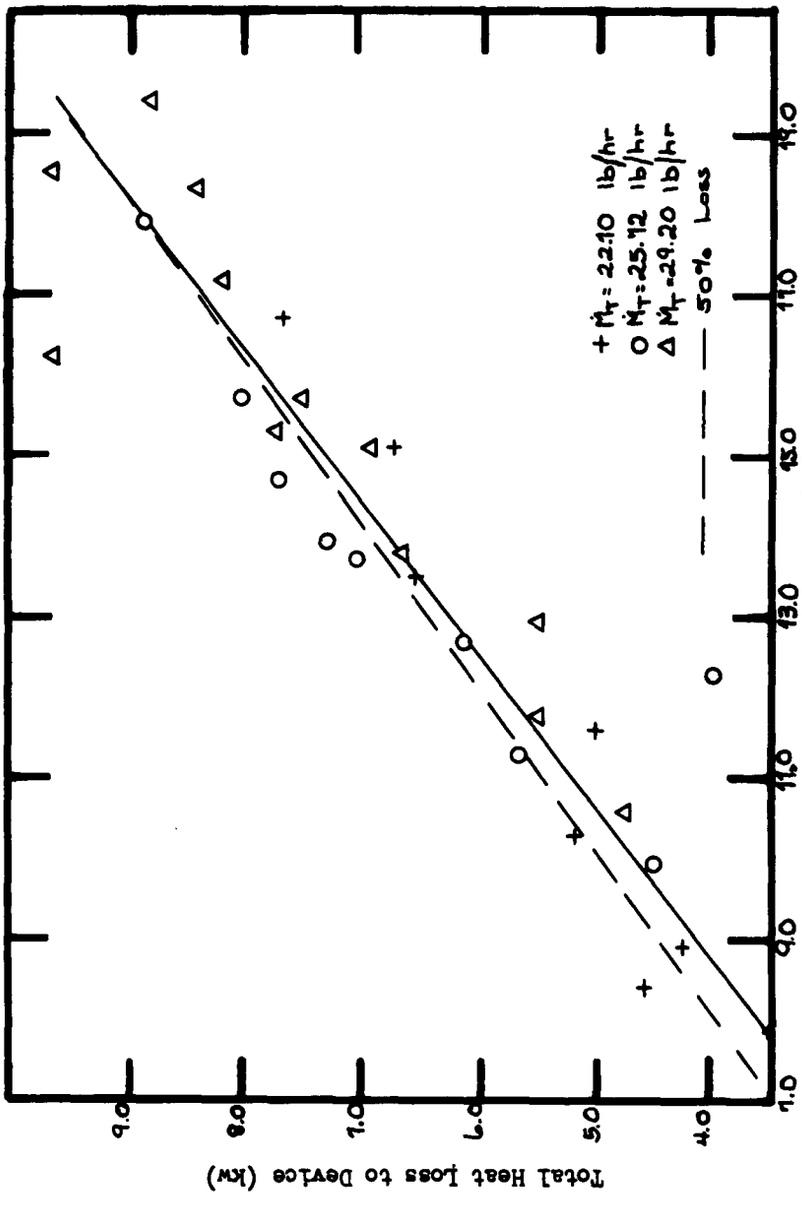

Fig. 30

Total Power Loss to Arc Device

tend to increase any conduction and convection losses to the wall sections. The 20% loss to the anode is lower than for the conventional anode, and is approximately as reported by Schoeck for the transpiration-cooled anode (Ref 15:100).

Fig. 31, p. 63, presents the specific enthalpy rise of the argon for the total range of arc powers and argon flow rates. The specific enthalpy is seen to depend on the arc power at constant mass flow in approximately a linear manner. This could arise because of the constant cooling of the arc and the independence of the efficiency of the device on mass flow or power in the experimental range. The specific enthalpy is not as high as some attained by Tannen in his work with this device, but the overall efficiency is greater as are the total arc power and mass flow (Ref 16:22). While this device was not primarily designed as a high-enthalpy gas heater, the efficiencies and enthalpies attained in this experiment are comparable to those of some of the larger commercial heaters (Ref 9:9).

Fig. 32, p. 64, presents a sample of the wall temperatures observed in each of the four positions (segments 1, 5, 9, and 12) for four powers at each mass flow. The abscissa is arbitrary, and the lines connecting the data points are not intended to represent the wall-temperature variations between the points. The purpose of the figure is merely to present graphically the behavior of the wall temperatures as functions of position, power, and mass flow.

As is readily seen in Fig. 32, the behavior of the wall temperatures seems to resemble that of the voltage gradient as presented in Fig. 22, p. 47. On the basis of previous discussion, the occurrence of the peaks in the temperatures at the locations shown is physically compatible with

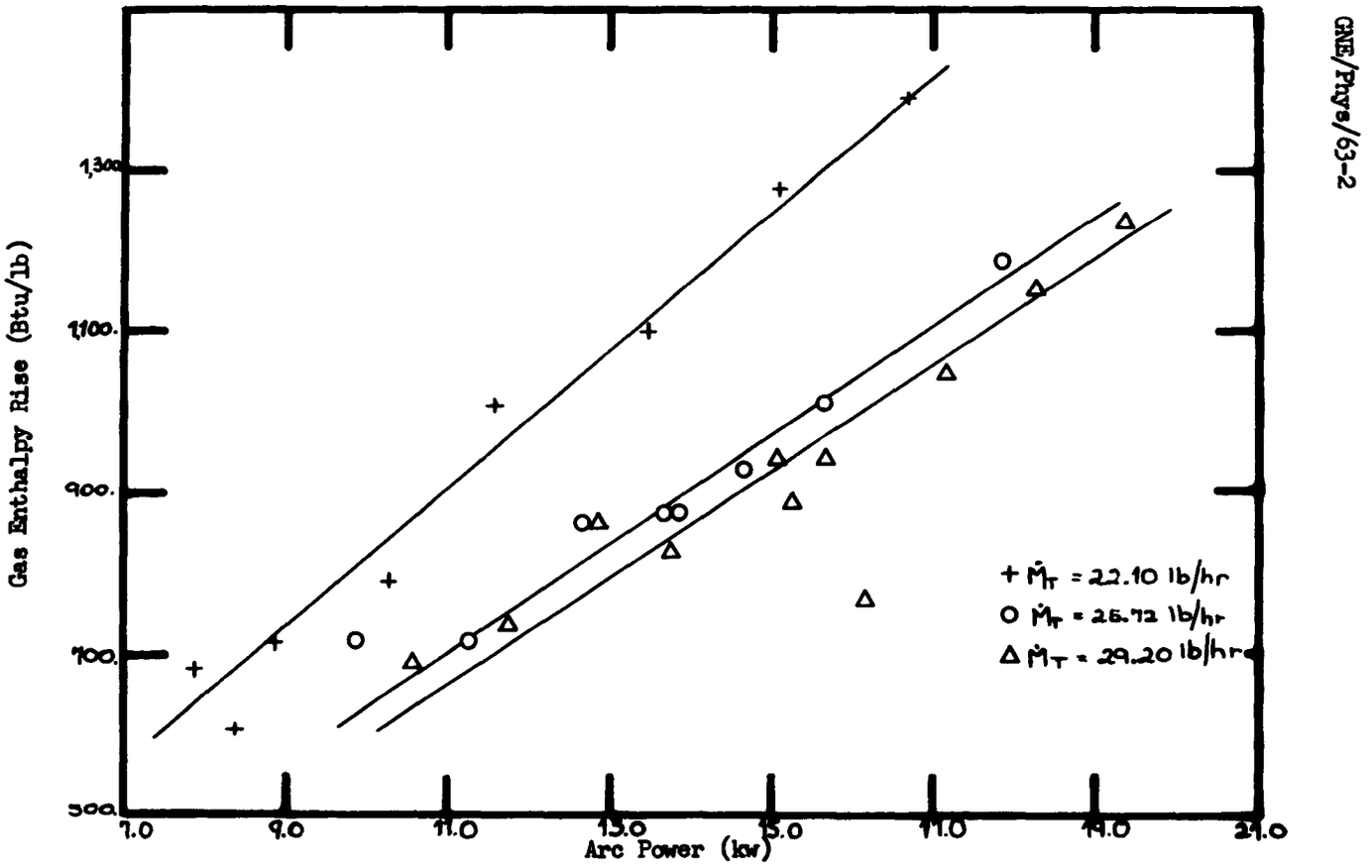

Fig. 31

Gas Enthalpy Rise for All Mass Flows

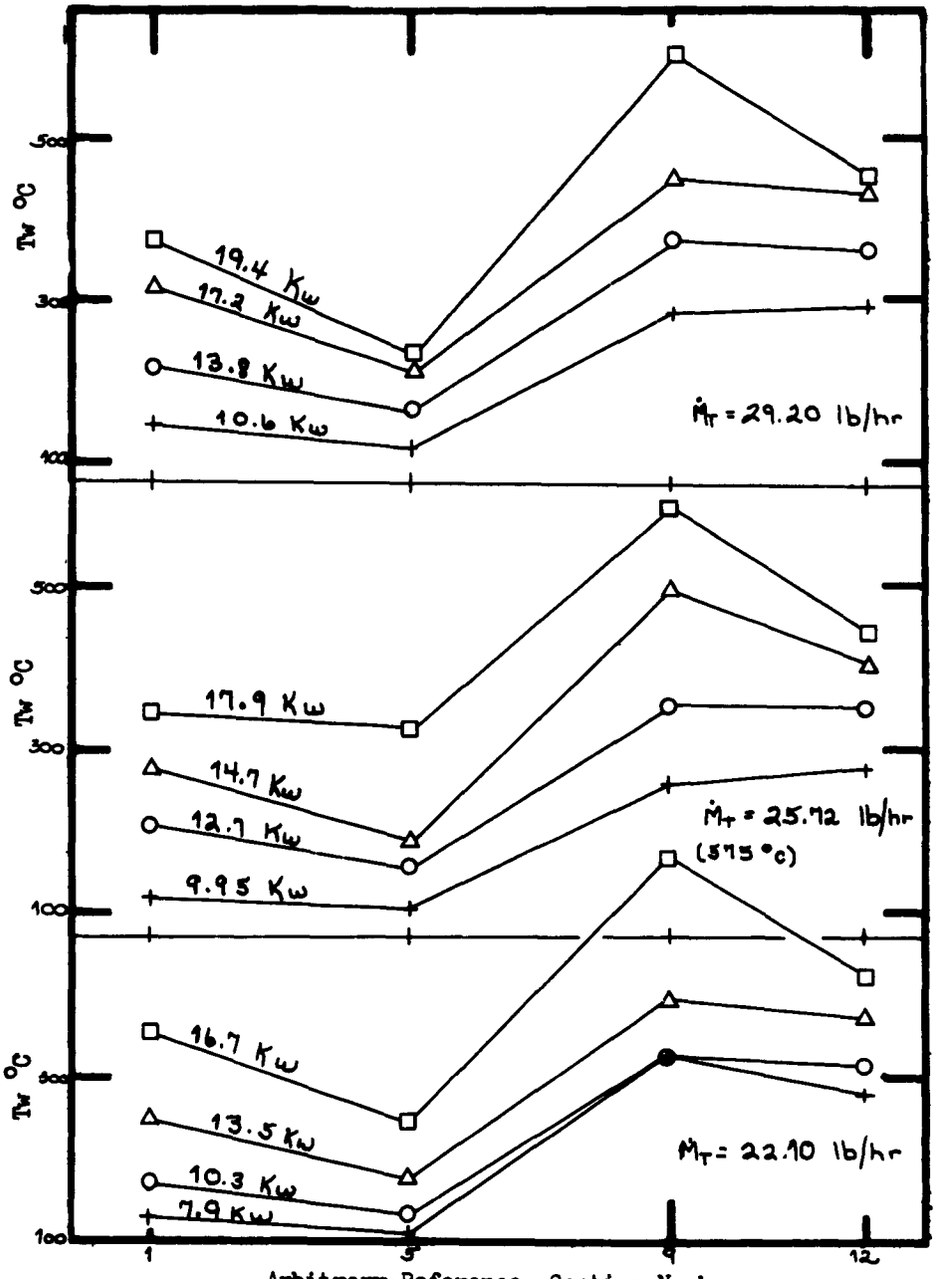

Fig. 32
Arc-Channel Wall Temperatures

the behavior of the voltage gradient at these points. If the arc power generated per unit length is increased, the radiation, conduction, and convection losses will also be increased. Hence, the power loss to the walls will be greater and the temperatures will respond accordingly.

Arc Radius Measurements and Comparison with Theory

Fig. 33, p. 66, presents the observed arc radii and the theoretical predictions of arc radius as a function of power per unit length with electric field strength as a parameter. The solid curves are for the data of Cann, the broken lines, the data of AVCO.

Six radius measurements were obtained for two different sets of arc parameters. An unexpected variation occurred in arc radius as the arc passed the window. This change was caused by the decrease in cooling of the arc in the vicinity of the window since no gas was injected at this point. Fig. 34, p. 67, shows the variation of the electric field in the region of the window as well as the method of interpolation used to calculate the potential gradient at the three positions of radius measurement. The gradient was assumed to vary linearly in this region, but the exact variation is unknown. Also, this variation in potential gradient produces such a small change in centerline temperature that axial heat flow is still negligible in comparison to that in the radial direction. This occurs because of the relative insensitivity of centerline temperature to arc power per unit length (Fig. 5, p. 15).

In general, agreement to well within the 10% experimental limit of error was obtained, and in most instances, the experimental and predicted values of arc radius agreed to within 5%. The experimental error is felt

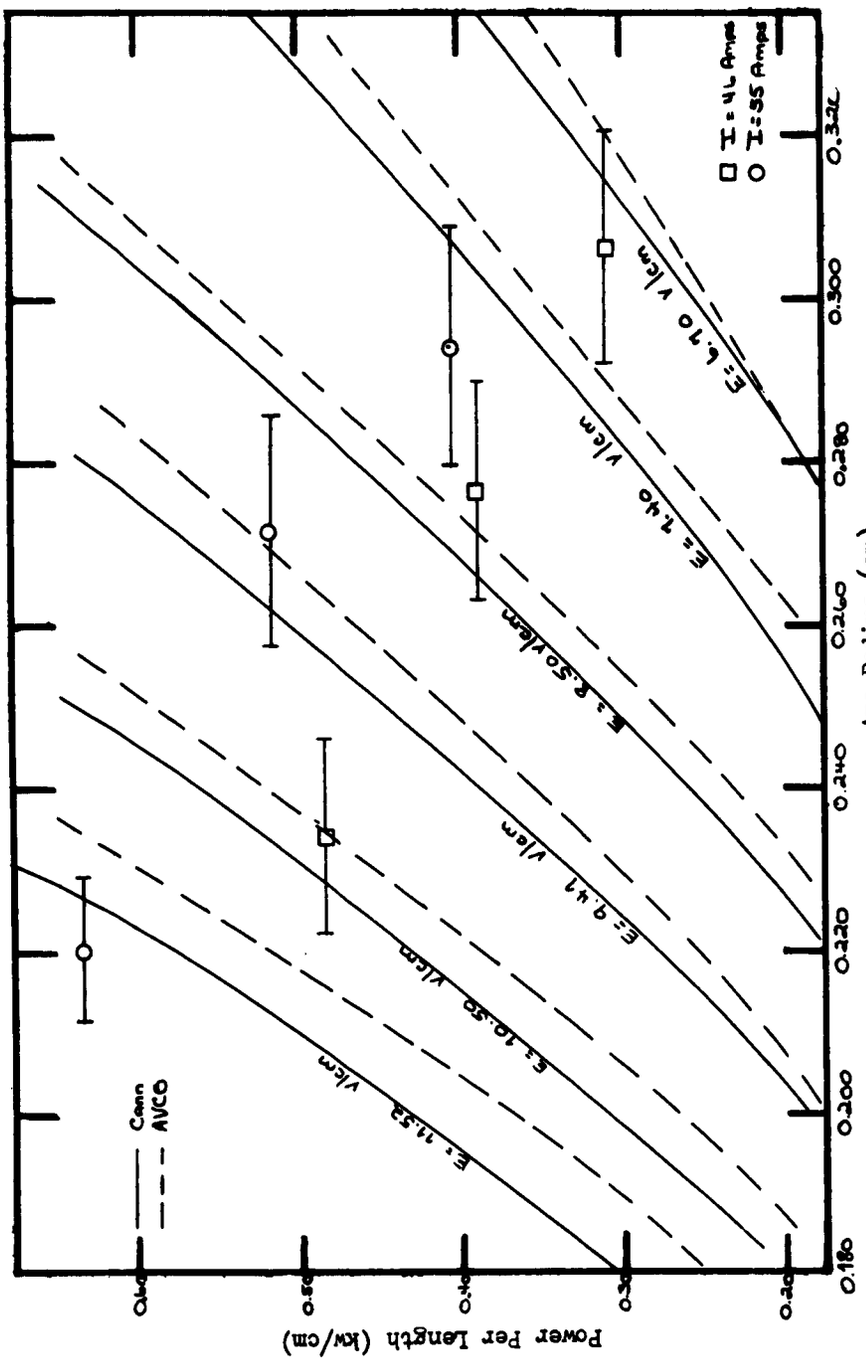

Fig. 33
Comparison Between Theoretical and Observed Arc Radii

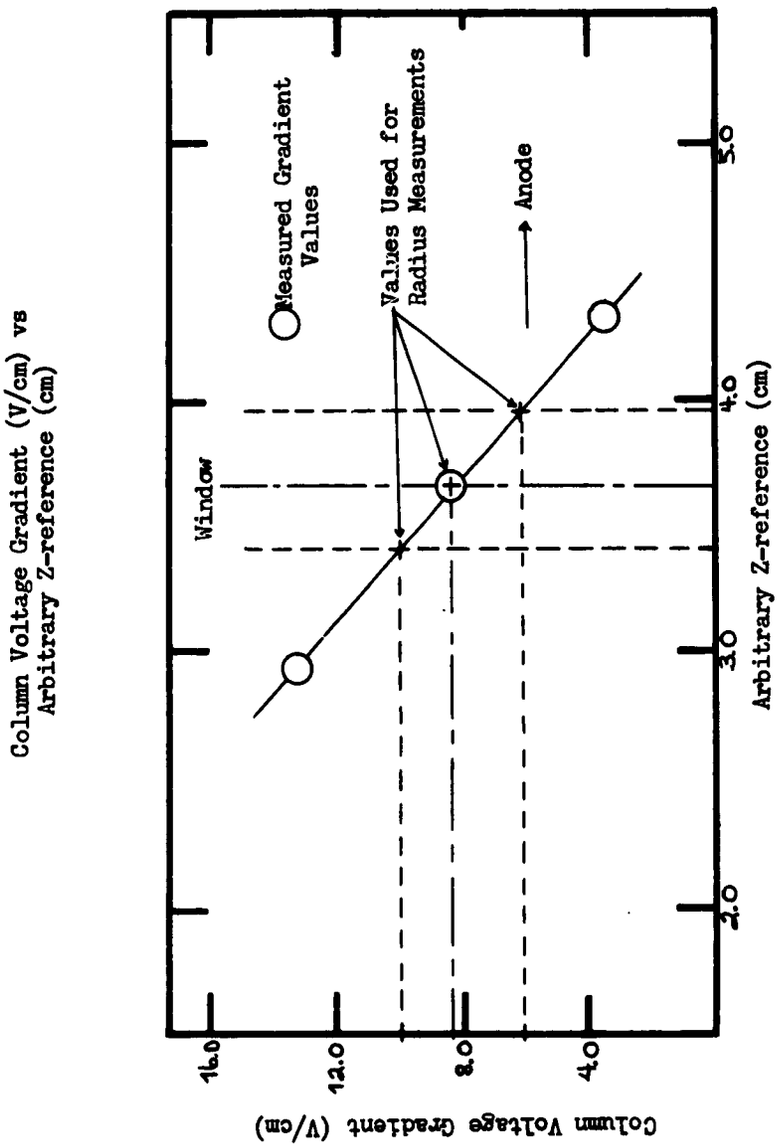
Column Voltage Gradient (V/cm) vs
Arbitrary Z-reference (cm)
Measured Gradient Values
Values Used for Radius Measurements
Anode
Window
16.0
12.0
8.0
4.0
2.0
3.0
4.0
5.0
Column Voltage Gradient (V/cm)
Arbitrary Z-reference (cm)

Fig. 34

to lie between 5 and 10%, but 10% is the upper limit and is a result of the fringe surrounding the core. Also, no systematic error is shown by these results for either set of transport data for argon.

It appears at this time that Cann has included the volumetric radiation loss in the values of thermal conductivity. This would account for the disagreement between Cann's and AVCO's data for thermal conductivity as well as the relatively close agreement in the two sets of curves for prediction of arc radii. (See Figs. 3 and 33, pp. 12 and 66.)

Accuracy of Results

Arc voltage could be read to ±5 volts, and arc current to ±1 amp. These were the largest errors associated with the system as they amounted to about 2% of normal operating voltages and currents. The water temperatures could be determined to ±0.5°F, and this was a 2% maximum uncertainty. The water flow rates were accurate to ±0.5% of the flow indicated. Argon flow was monitored to a maximum error of ±1%. In general, individual runs could be reproduced to about ±5%.

However, there were a great number of adjustments and variations which would be made with the device. For any one individual run, 6 water flows, 13 gas flows, and arc voltage and current had to be established, not to mention the numerous temperatures and voltage differences which had to be read and recorded. Obviously, the possibility for error is large. Care was taken to avoid these errors, but from the scatter of some of the data, it is evident that more than one or two were made.

VI. Conclusions

1. The device was stable and easy to operate. Except for the carbon injectors which may have been eroded in early start-up attempts, no wear was visible on either of the electrodes after twenty hours of operation. These same electrodes were also used by Capt. Tannen for approximately ten hours, for a total of thirty hours. The absence of an anode spot is probably the significant factor in the apparent longevity of the anode surface.

2. The cooling effect the gas has on the arc is approximately constant at constant mass flow, and is the primary cause of the early minimum in the voltage-current characteristic. This conclusion is based on the behavior of the voltage-current curves and the constant total fractional power loss to the device for all mass flows and arc powers. (See Figs. 18 and 30, pp. 40 and 61, and pp. 39-42.)

3. Increasing the mass flow increases the cooling of the arc and causes an increase in total voltage and voltage gradient at constant current. However, the increased cooling is offset by the higher power generation in the arc, and the device efficiency remains constant at 50% for argon. This, too, is supported by the data in Figs. 18 and 30.

4. The saw-tooth behavior of the column voltage gradient and the wall temperatures as functions of distance from the cathode may be the results of the highly complex gas flow around the arc, and the interaction with and cooling of the arc by this gas flow. Further work is necessary

to bear this out, as another possibility is a distortion of the electric field by variations in channel diameter. However, the overall increase in voltage gradient with distance from the cathode was expected as a result of the increased cooling of the arc as it proceeded up the channel.

5. The flow of the gas next to the anode is turbulent. This is indicated by the shape of the plasma flame at the anode, and by the value of the Reynolds number for the range of mass flows used in this experiment. (See Fig. 26, p. 56.) The turbulent flow maintains a cool layer of gas next to the anode, prevents formation of an anode spot, and keeps the power loss to the anode at about 20%.

6. More data is required to determine the mechanism of primary heat loss to the walls of the arc channel. At present, it is felt to be radiation from the arc core as argon does have a significant radiation loss at higher centerline temperatures (above 13,000°K). No data is available to estimate the magnitude of these radiation losses for the wall-stabilized, transpiration-cooled arc at the present time.

7. Operation over a wide range of gas flows and arc powers is possible, and high enthalpies may be attained at high device efficiency. The constant efficiency with mass flow and power is indicated in Fig. 30, p. 61. This characteristic enables one to produce gas of any desired enthalpy from about 600 to 1,400 Btu/lb, within the operational limits of the device.

8. The predictions of the Ellenbaas-Heller equation are in excellent qualitative agreement with the experimental observations. An increase in

field strength at constant current results in an increase in power generation and a decrease in arc radius. This is also supported quantitatively by the arc radius measurements as seen in Fig. 33, p. 66.

9. The assumptions of negligible radial mixing and axial heat flow within the arc core for the Ellenbaas-Heller equation appear valid in that agreement to ±5% was obtained between experimental measurements and theoretical predictions of arc radius as functions of arc power per unit length and electric field strength.

VII. Recommendations

Equipment Changes and Experimental Extensions

1. Install new porous injectors, preferably of alumina, zirconia, or cercor. Zirconia injectors had been ordered in October, 1962, but as of this writing, they had not been received. Use of another material besides porous graphite would permit use of nitrogen or other gases. Since the radiation losses from nitrogen are small in comparison to those from argon, it might be possible to obtain a reduction in the power losses to the walls and increase the device efficiency past 50%.

2. Also, install new boron nitride liners between the segments in place of any liners which may now be damaged. A smooth-bore channel may eliminate some of the fluctuations which were observed in the voltage gradient. This would then show that the saw-tooth behavior of the gradient was only a coincidence of no real physical significance.

3. Install a thermocouple in each porous injector in order to obtain a clearer picture of the channel-wall temperature behavior. It might be possible to correlate the losses to the walls to the power generation in the arc core by use of (4), below.

4. Use the existing calorimeter disks to measure the radiation from the arc core. Increasing the mass injection immediately upstream of the calorimeter should produce a decreasing loss to the calorimeter disk until a certain minimum or constant loss is obtained. The mechanism by which this heat gets through the boundary layer to the calorimeter disk must be radiation.

5. Install pressure taps between the sections of the column. The longitudinal pressure profile, combined with a theoretical analysis of the gas flow in the channel, could indicate the nature of the flow of gas around the arc, i.e., laminar or turbulent, sonic or sub-sonic. This may also explain the phenomenon of the saw-tooth voltage gradient as well as the constant efficiency of the device.

6. Use a calorimeter at the anode to measure the bulk enthalpy of the plasma jet. This would serve as a check on the accuracy of the measurements of power losses to the system which are presently used to compute the bulk enthalpy.

7. Reduce to as near zero as possible the mass flow to the first injector in order to see if the first peak in voltage gradient is related to the cooling of the arc. If it is, this procedure should shift it away from the cathode. A similar procedure could be used at the eighth or ninth injectors where the second peak occurs.

8. Vary the mass injection rate to each component in a regular manner, eg., as the first power of the distance from the cathode, etc. The resultant variations in the arc voltage and voltage gradient may indicate the nature of the relationship between the gas flow around the arc and the characteristics of the arc. Similarly, varying the ratio of transpiration flow to axial flow from the cathode chamber may also explain some of the phenomena which have been observed. Other variations in the mass flow might include a determination of the minimum mass injection rate and transpiration-longitudinal flow ratio at a given arc power for

which the efficiency of the device was still constant (50% for argon). This would yield gas of maximum enthalpy for that power and mass flow, as well as the optimal performance for this device.

9. Attempt to reduce the limit of error on arc radius measurements. This would require modification of the present window holder to permit water cooling. The interior surface of the holder could then be lamp-blacked to reduce the reflection from that surface, and thus sharpen the image of the arc. Also, a new quarty window should be installed as the present one is scratched sufficiently to interfere somewhat with the image of the arc. Improvement in the technique of measuring arc radius as well as in the accuracy of results will check further the validity of the assumptions used in the Ellenbaas-Heller equation as they apply to the wall-stabilized, transpiration-cooled arc.

Theoretical Extensions

1. Include an integration of the volumetric radiation power loss in the Ellenbaas-Heller program to obtain a theoretical prediction of radiated power per unit length using the data from AVCO. This could readily be checked against the observed losses, as in (4) of the previous section, p. 72.

2. Attempt to set up a simple model of the gas flow around the arc. Certain assumptions concerning velocity and temperature profiles will be necessary. These might include the assumption that the maximum longitudinal gas velocity occurs in the arc core, and that this velocity is constant across the diameter of the core. Also, a first approximation to

the temperature variation from the arc core to the channel wall might be made by assuming a polynomial variation of the second or third order. The temperature within the arc core as well as the gradient of the temperature at the arc surface may be obtained from the Ellenbaas-Heller program. A further assumption which may be necessary is that the arc core is an extremely hot rod with no radial velocity moving up through the arc channel. In any event, extensive use of a digital computer will probably be necessary. Results of this analytic effort should be directed towards explaining the cooling of the arc by the gas, as well as predicting, if possible, gas enthalpies, and conductive and convective heat losses to the walls of the device as functions of mass flow and arc power. These could then be compared with experimental values.

Bibliography

1. Baker, Mack E. Development of a Linear Flow Meter for Low Flow Rates. Unpublished Thesis. Wright-Patterson Air Force Base, Ohio Air Force Institute of Technology, August 1957.

2. Cambel, Ali Bulent, "Compressible Flow," in Handbook of Fluid Dynamics, edited by V. L. Streeter. New York: McGraw-Hill Book Company, Inc., 1961, pp. 8-42 to 8-62.

3. Cann, Gordon L. Energy Transfer Process in a Partially Ionized Gas. Memorandum No. 61, Hypersonic Research Project. Pasadena, California: Guggenheim Aeronautical Laboratory, California Institute of Technology, June 15, 1961. AD 263784.

4. Champion, K. S. W. "The Energy Balance Equations for the Positive Columns of High Pressure Arcs." Proceedings of the Physical Society, B66: 169-174 (1955).

5. Cobine, James Dillon. Gaseous Conductors (Second Edition). New York: Dover Publications, Inc., 1958.

6. Emmons, H. W. and R. I. Land. The Poiseuille Plasma Experiment. Cambridge, Massachusetts: Harvard University, n.d.

7. Etherington, Harold. (Editor) Nuclear Engineering Handbook (First Edition). New York: McGraw-Hill Book Company, Inc., 1958.

8. Howe, John T. Some Finite Difference Solutions of the Laminar Compressible Boundary Layer Showing the Effects of Upstream Transpiration Cooling. Memorandum No. 2-26-59A, NASA, n.d.

9. John, Richard R. and William L. Bade. "Recent Advances in Electric Arc Plasma Generation Technology." ARS Journal, 31:4-17 (January 1961).

10. Lin, Chia-Ch'iao. (Editor) "High Speed Aerodynamics and Jet Propulsion." Turbulent Flows and Heat Transfer. Volume V. Princeton, New Jersey: Princeton University Press, 1959.

11. McGinn, John Holton. A New Type Arc for Producing High Temperature, High Purity Plasma Jets. Report under Air Force Contract 04(647)269. Philadelphia, Pennsylvania: Space Sciences Laboratory, General Electric Company, n.d.

12. Powell, H. N. and W. G. Browne. "Use of Coiled Capillaries in a Convenient Laboratory Flowmeter." The Review of Scientific Instruments, 28:138-141 (February 1957).

13. Ragent, Boris and Charles E. Noble, Jr. High-Temperature Transport Coefficients of Selected Gases. Technical Report No. ARL 62-328. Palo Alto, California: Vidya, Inc., April 1962.

14. Schmitz, G. The Profile of the Arc Column, edited by J. Birkeland, Plasma Physics Research Laboratory, ANL. Technical Report No. ARL 62-401. Wright-Patterson Air Force Base, Ohio: Aeronautical Research Laboratories, Office of Aerospace Research, USAF, August 1962.

15. Schroeck, Peter A., et al. An Investigation of the Anode Losses in Argon Arcs and Their Reduction by Transpiration Cooling. Technical Report No. ARL 62-341. Minneapolis, Minnesota: University of Minneapolis, April 1962.

16. Tannen, Peter D. Experimental Study of a Transpiration-Cooled, Wall-Stabilized D-C Arc. Unpublished Thesis. Wright-Patterson Air Force Base, Ohio: Air Force Institute of Technology, August 1962.

17. Theoretical and Experimental Investigation of Arc Plasma Generation Techniques. A computer program for the evaluation of the transport properties and radiation losses for an argon arc. Wilmington, Massachusetts: R. A. D. Division, AVCO Corporation, ASD TDR 62-729, n.d.

18. Winter, E. R. F. and C. J. Cremers. Temperature Distribution in a Low Mass Flux Argon Plasma Jet. Technical Report No. ARL 62-388. Minneapolis, Minnesota: University of Minnesota, July 1962.

19. Yuan, S. W. and L. S. Galowin. Transpiration Cooling in the Turbulent Flow Through a Porous-Wall Pipe. Technical Report for NR-089-038. Brooklyn, New York: Polytechnic Institute of Brooklyn, July 1956.

General Bibliography

Abramovich, G. N. Homogeneous Gas Flows. A translation from Russian by Technical Information and Library Services, Ministry of Aviation. U. S. S. R.: Technical Information and Library Services, Ministry of Aviation, October 1961.

Bartle, E. Roy and Bernard M. Leadon. The Compressible Turbulent Boundary Layer on a Flat Plate with Transpiration Cooling. Technical Report No. 11. Convair Scientific Research Laboratory, May 1961.

Beckmann, Herbert, and Alan J. Chapman. "Thrust from Partly Ionized Monatomic Gases." ARS Journal, 32:1369-73 (September 1962).

Brown, W. Byron and Patrick L. Donoughe. Tables of Exact Laminar-Boundary-Layer Solutions when the Wall is Porous and Fluid Properties Are Variable. Technical Note 2479. Cleveland, Ohio: Lewis Flight Propulsion Laboratory, NACA, September 1951.

Cann, Gordon L. Basic Research on Gas Flows Through Electric Arcs. Progress Report on Contract No. AF33(657)-7940, Task No. 70192. Pasadena, California: Electro-Optical Systems, Inc., December 1962.

Cassie, A. M. Some Theoretical Aspects of Arcs in Nozzles Under Forced Convection. Leatherhead, Surrey, England: The British Electrical and Allied Industries Research Association, 1962.

Chen, Michael Ming, and Jerrold Yos. Theory for the Arc Column in High Pressure Discharges in the Absence of Convection. Wilmington, Massachusetts: Senior Staff Scientists, Research and Advanced Development Division, AVCO Corporation, n.d.

Dean, Robert C. Jr. Research Study of the Interactions Between Electric Arcs and Gas Flows in the Anode Sheath Region. Progress Report No. AF33(657)-8179. Hanover, New Hampshire: Thayer School of Engineering, Dartmouth College, October 1962.

---------- Research Study of the Interactions Between Electric Arcs and Gas Flows in the Anode Sheath Region. Progress Report No. AF33(657)-8179. Hanover, New Hampshire: Thayer School of Engineering, Dartmouth College, December 1962.

Delcroix, J. L. Introduction to the Theory of Ionized Gases. (Translated from the French by Melville Clark, Jr., David J. BenDaniel, and Judith M. BenDaniel.) New York: Interscience Publishers, Inc., 1960.

Eckert, Ernst R. G. Survey of Boundary Layer Heat Transfer at High Velocities and High Temperatures. Technical Report WADC 59-624. Wright-Patterson Air Force Base, Ohio: Wright Air Development Center, April 1960.

Eckert, Hans Ulrich. "Characteristics of the Turbulent Boundary Layer on a Flat Plate in Compressible Flow from Measurements of Friction in Pipes." Journal of the Aeronautical Sciences, 17:573-84 (September 1950).

---------- "Simplified Analysis of Turbulent Boundary-Layer Development Along Cylindrical Surfaces with Variable Free-Stream Mach Number." Journal of the Aeronautical Sciences, 21:695-706 (October 1954).

Emmons, Howard W. (Editor) "One-Dimensional Treatment of Steady Gas Dynamics." Fundamentals of Gas Dynamics. Princeton, New Jersey: Princeton University Press, 1958.

Green, L. Jr. Gas Cooling of a Porous Heat Source. Technical Report under Contract AT-1-GEN-8. Downey, California: Atomic Energy Research Department, North American Aviation, Inc., December 13, 1951.

Green, L. Jr. and K. L. Nall. Experiments on Porous-Wall Cooling and Flow-Separation Control in a Supersonic Nozzle. Aerojet Technical Report No. 1490 under Contract AF33(616)-5552. Azusa, California: Aerojet-General Corporation, December 1958.

Kreith, Frank. Principles of Heat Transfer. Scranton, Pennsylvania: International Textbook Company, 1958.

Landshoff, Rolf K. M. (Editor) The Plasma in a Magnetic Field. A symposium on magnetohydrodynamics. Stanford, California: Stanford University Press, 1958.

Lochte-Holtgreven, W. Production and Measurement of High Temperatures. Kiel, Germany: Kiel University, n.d.

Shapiro, Ascher H. The Dynamics and Thermodynamics of Compressible Fluid Flow. New York: Ronald Press Company, 1953.

Sherman, Christopher and J. M. Yos. "Scaling Laws for Electric Arcs Subject to Forced Convection." Journal of Applied Physics, 32:744 (November 1960).

Skifstad, J. G. A Study of Thermal Arc-Jet Propulsion. Technical Report No. I-61-2. Lafayette, Indiana: Purdue University and Purdue Research Foundation, August 1961.

Somerville, J. M. The Electric Arc. New York: John Wiley & Sons Inc., 1959.

Spitzer, Lyman, Jr. Physics of Fully Ionized Gases. New York: Interscience Publishers, Inc., 1956.

Stine, Howard A. and Velvine R. Watson. The Theoretical Enthalpy Distribution of Air in Steady Flow Along the Axis of a Direct-Current Electric Arc. Technical Note D-1331. Moffett Field, California: Ames Research Center, NASA, August 1962.

Treham, S. K. Plasma Physics. Notes from a course given by S. Chandrasekhar at the University of Chicago. Chicago, Illinois: University of Chicago Press, 1960.

Yuan, S. W., et al. Heat Transfer in Turbulent Pipe Flow with Coolant Injection. Austin, Texas: University of Texas, n.d.

Table I

Sample of Raw Data

Item \ Run No. / Date	1 28 Mar	2 28 Mar	3 28 Mar	1 29 Mar
Argon Flow (cmHg)*	0.8	1.2	1.2	1.0
Water Flows (gpm)				
Cathode	1.31	1.31	1.31	1.18
Secondary Anode	1.31	1.31	1.31	1.18
Sections 1-4	0.26	0.26	0.26	0.24
Sections 5-8	0.26	0.26	0.26	0.24
Sections 9-12	0.26	0.26	0.26	0.24
Anode	1.40	1.40	1.40	1.35
Water Temperatures (°F)				
Cathode, out	52.7	53.0	53.0	54.5
Secondary Anode, out	55.0	55.0	55.5	56.2
Sections 1-4, out	67.0	65.5	69.0	64.0
Sections 5-8, out	75.0	74.0	78.0	72.5
Sections 9-12, out	84.2	84.2	89.0	84.0
Anode, out	61.7	61.0	62.0	62.0
Anode, in	52.3	52.5	52.5	53.0
Argon Temperature, in (°F)	78.0	80.8	82.2	75.5
Wall Temperatures, °C				
Section 1	170.0	150.0	180.0	120.0
Section 5	135.0	125.0	140.0	110.0
Section 9	330.0	290.0	330.0	265.0
Section 12	320.0	300.0	340.0	285.0
Arc Current (DC amps)	45.0	41.0	49.0	39.0
Arc Voltage (DC volts)	229.0	259.0	260.0	255.0
Potential Differences				
Cathode-Secondary Anode	5.8	5.2	5.9	4.0
Secondary Anode-Sec. 1	17.0	19.5	19.0	18.9
Section 1-2	14.7	15.5	15.9	14.8
Section 2-3	13.0	13.8	14.2	18.0
Section 3-4	16.0	17.5	17.9	16.9
Section 4-5	15.0	16.9	17.1	16.2
Section 5-6	15.3	18.2	18.0	17.7
Section 6-7	15.0	17.5	17.5	17.1
Section 7-8	15.2	18.5	18.1	18.3
Section 8-9	17.2	20.2	19.8	20.2
Section 9-10	15.7	18.6	18.3	19.0
Section 10-11	17.0	19.7	19.6	19.1
Section 11-12	19.0	21.3	21.4	21.6
Section 12-Anode	26.9	29.1	29.1	29.3

* See Table II, p. 82.

Table II

Argon Mass Flow Rates to Components

Flowmeter	Component	Pressure Drop Across Flowmeter (cm Hg) / Mass Flow in lb/hr: 0.80	1.00	1.20
1	Cathode Chamber	1.70	2.00	2.24
2	Section 1	1.70	2.00	2.25
3	Section 2	1.70	2.00	2.30
4	Section 3	1.70	2.00	2.20
5	Section 4	1.75	1.85	2.10
6	Section 5	1.85	1.95	2.20
7	Section 6	1.65	2.00	2.25
8	Section 7	1.70	2.00	2.28
9	Section 8	1.63	1.90	2.22
10	Section 9	1.67	1.97	2.24
11	Section 10	1.75	2.05	2.35
12	Section 11	1.63	2.00	2.26
13	Section 12	1.70	2.00	2.30
Total Mass Flow		22.13	25.72	29.20

Table III

Center-to-Center Separations
Device Components

Components	Separation of Centers (cm)
Cathode-Secondary Anode	0.25
Secondary Anode--Segment 1	2.51
Segment 1 - Segment 2	1.79
Segment 2 - Segment 3	1.43
Segment 3 - Segment 4	1.47
Segment 4 - Segment 5	1.46
Segment 5 - Segment 6	1.45
Segment 6 - Segment 7	1.46
Segment 7 - Segment 8	1.45
Segment 8 - Segment 9	1.41
Segment 9 - Segment 10	1.44
Segment 10 - Segment 11	1.44
Segment 11 - Segment 12	1.46
Segment 12 - Anode (bottom)	1.48

Appendix A

Numerical Form of Solution for the Ellenbaas-Heller Equation

Eq (7), p. 9, is as follows:

$$-\frac{1}{r}\frac{d}{dr}\left(r k \frac{dT}{dr}\right) + U(T) = \sigma E^2 \tag{7}$$

If we let $S = \sigma E^2 - U(T)$, we have:

$$-\frac{1}{r}\frac{d}{dr}\left(r k \frac{dT}{dr}\right) = S \tag{8}$$

Or, upon integration from r_{n-1} to r_n :

$$r k \frac{dT}{dr}\Big|_{r_n} - r k \frac{dT}{dr}\Big|_{r_{n-1}} = -\int_{r_{n-1}}^{r_n} S(r)\, r\, dr \tag{9}$$

Assuming S is locally linear in r :

$$S = A + Br \tag{10}$$

and

$$S_n = S_{n-1} + \Delta S \tag{11}$$

$$\Delta S = S_{n-1} - S_{n-2} \tag{12}$$

Eq (9) becomes, upon integration of the right-hand side:

$$r k \frac{dT}{dr}\Big|_{r_n} = r k \frac{dT}{dr}\Big|_{r_{n-1}} - \left(\frac{Ar^2}{2} + \frac{Br^3}{3}\right)\Big|_{r_{n-1}}^{r_n} \tag{13}$$

$$= r k \frac{dT}{dr}\Big|_{r_{n-1}} - \frac{\Delta r}{6}\left[3A(r_n + r_{n-1}) + 2B(r_n^2 + r_n r_{n-1} + r_{n-1}^2)\right] \tag{14}$$

This last equation reduces to:

$$r k \frac{dT}{dr}\Big|_{r_n} = r k \frac{dT}{dr}\Big|_{r_{n-1}} - \frac{\Delta r}{6}\left[S_n r_n + S_{n-1} r_{n-1} + (S_n + S_{n-1})(r_n + r_{n-1})\right] \quad (15)$$

Substituting for terms containing S_n with terms in S_{n-1} and S_{n-2}, (15) reduces to:

$$r k \frac{dT}{dr}\Big|_{r_n} = r k \frac{dT}{dr}\Big|_{r_{n-1}} - \frac{\Delta r}{6}\left[S_{n-1}(5 r_{n-1} + 4 r_{n-1}) - S_{n-2}(2 r_n + r_{n-1})\right] \quad (16)$$

Eq (16) gives the value of $rk\frac{dT}{dr}$ at a point, r_n, based on a linear forward extrapolation to r_n of the function S, from r_{n-1} and r_{n-2}.

Assuming k, the thermal conductivity, behaves similarly to S, the temperature gradient, $\frac{dT}{dr}$, at r_n becomes:

$$\frac{dT}{dr}\Big|_{r_n} = r k \frac{dT}{dr}\Big|_{r_n} \Big/ \left[r_n(2 k_{n-1} - k_{n-2})\right] \quad (17)$$

Similarly, the temperature, T, at r_n is:

$$T_n = T_{n-1} + \frac{1}{2}\left(\frac{dT}{dr}\Big|_{r_n} + \frac{dT}{dr}\Big|_{r_{n-1}}\right)\Delta r \quad (18)$$

Eqs (16), (17), and (18) are the heart of the Fortran program which was used to compute the arc radius as a function of centerline temperature and electric field strength. These three equations are located in section I of the Fortran program as indicated on p. 93, following.

The increment of r, Δr, was varied at first in order to determine the step size required for optimal accuracy and minimum computing time. A value of 0.005 cm for Δr was found to be satisfactory. However, for centerline temperatures and electric field strengths above 12,000°K,

and 16 volts/cm, respectively, an increment of 0.0025 cm was used.

After each value of T was computed, new values of σ, k, and u would be interpolated parabolically, and the power generation, σE^2, added to the appropriate term of the Simpson's Rule integration used to compute the power per unit length.

Operating Instructions for Fortran Computer Program

1. A request for the numbers of values in each of the tables of electrical and thermal conductivities, and volumetric radiation loss as functions of temperature will be printed on the console typewriter. Enter the numbers in fixed point format at the typewriter.

2. Read in the tables of electrical conductivity (ohm^{-1} cm^{-1}), thermal conductivity (watt/m-deg K), and radiation loss ($watt/cm^3$) as functions of temperature (deg K), one value and one temperature per card.

3. A request for a starting radius (cm), an increment (cm) in radius, the square of the electric field strength ($volt^2/cm^2$), centerline temperature (deg K), and temperature gradient (deg K/cm) will be made on the typewriter. The first and last items are generally 0 at the centerline of a cylindrically symmetric arc.

4. If a complete arc profile is desired, turn Switch 2 OFF. If the arc radius is what is primarily desired, turn Switch 2 ON. In either event, the output will be, from left to right, radius, temperature, temperature gradient, electrical conductivity, and thermal conductivity. However, if Switch 2 is OFF, print-out will occur for each radius, starting at the centerline temperature (radius = 0), and continuing until

the temperature is less than 6,000°K. If Switch 2 is ON, print-out will occur only after the temperature is below 8,500°K, again continuing until the temperature is less than 6,000°K.

5. After the temperature falls below 6,000°K, and the power per unit length is printed, the operator may either enter a new set of starting values for another solution (Switch 1 OFF), or the operator may enter new tables of conductivities and radiation loss and start the program over for a new medium (Switch 1 ON).

Dictionary of Variables

N : Number of values in table of electrical conductivity.

M : Number of values in table of thermal conductivity.

L : Number of values in table of volumetric radiation power loss.

TSIG(I) : Reference temperature for value of electrical conductivity in table; deg K.

SIG(I) : A value of electrical conductivity, σ, in the table, corresponding to TSIG(I); mho/cm.

Similar remarks apply to TCON(I), CON(I) (thermal conductivity, k, w/m-deg K), and TRAD(I), RAD(I) (volumetric radiation power loss, u, w/cm^3).

R : Radius (cm) at any point in the arc core; r_n.

DR : Increment or step in R.

ESQ : The square of the electric field strength ($volt^2/cm^2$).

T : Temperature (deg K).

TPR : Temperature gradient (deg K/cm).

POWER : Power per unit length (watts/cm).

CNST1 : Dummy for Simpson's Rule Integration for power per unit length; 4(DR)/3; see IV of program, p. 92.

CNST2 : 2(DR)/3; see IV of program, p. 92.

II : Control index for Simpson's Rule Integration; II = 1, 2, or 3 for first, even, or odd terms, respectively.

U, DELY1, DELY0 : Dummy variables used only in interpolation of SIGMA, COND, and PRAD.

SIGMA : Interpolated value of electrical conductivity; applied at r_n.

COND : Interpolated value of thermal conductivity, corrected to w/cm-deg K; applied at r_n.

PRAD : Interpolated value of volumetric radiation loss; applied at r_n.

S1 : Conduction loss at r_{n-1}; equals power generated - radiation loss.

R1 : $r_{n-1} = R - DR$ unless $R = 0$; then $R1 = r_{n-1} = R$.

S2 : Conduction loss at r_{n-2}.

COND1 : Thermal conductivity at r_{n-2}.

TPR1 : Temperature gradient at r_{n-2}.

RKTPR : $r k \frac{dT}{dr}$ at r_n and r_{n-1}.

Fortran Flow Chart

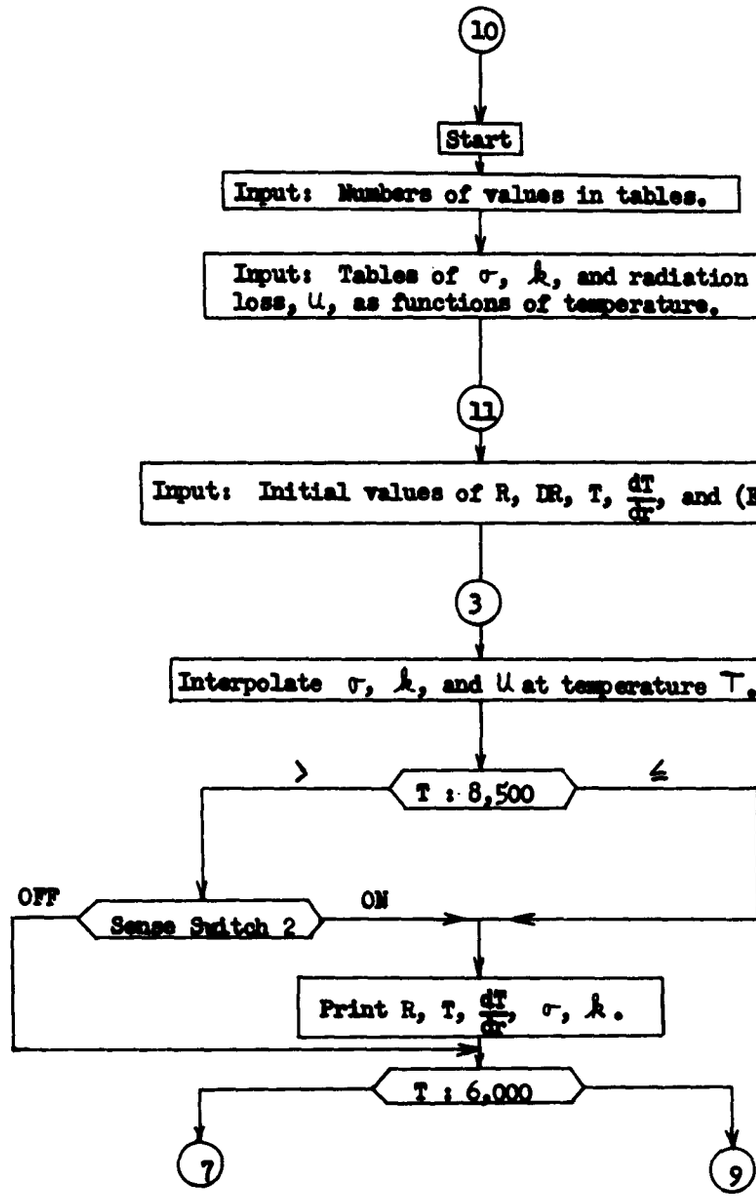

Note: Roman Numerals correspond to those on Fortran Computer Program, pp. 92-93, following.

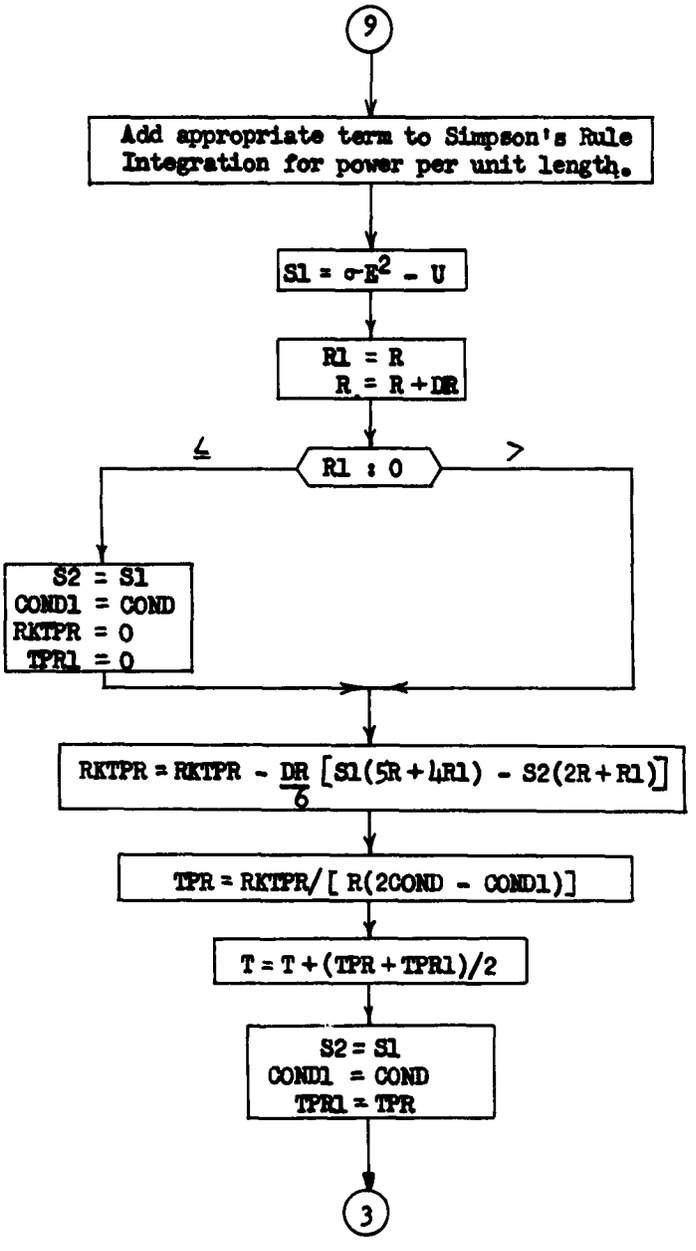
9
Add appropriate term to Simpson's Rule Integration for power per unit length.
VII
S1 = σE² - U
VIII
R1 = R
R = R + DR
≤
R1 : 0
>
S2 = S1
COND1 = COND
RKTPR = 0
TPR1 = 0
IX
RKTPR = RKTPR - DR/6 [S1(5R + 4R1) - S2(2R + R1)]
TPR = RKTPR/[R(2COND - COND1)]
X
T = T + (TPR + TPR1)/2
S2 = S1
COND1 = COND
TPR1 = TPR
3

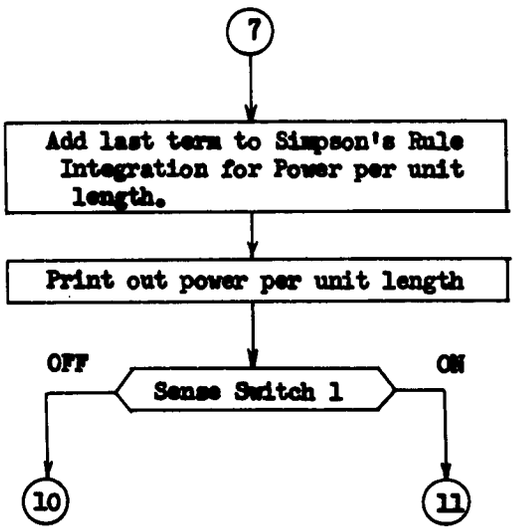
7
Add last term to Simpson's Rule Integration for Power per unit length.
Print out power per unit length
OFF
Sense Switch 1
ON
10
11

XI

Fortran Computer Program

```
   DIMENSION TSIG(100),SIG(100),TCON(100),CON(100),TRAD(100),RAD(100)
10 PRINT 100
   ACCEPT,N
   PRINT 101
   ACCEPT,M
   PRINT 107
   ACCEPT,L
   PRINT 102
   PRINT 109
   DO 1 I=1,N
 1 READ,TSIG(I),SIG(I)
   DO 2 I=1,M
 2 READ,TCON(I),CON(I)
   DO 13 I=1,L
13 READ,TRAD(I),RAD(I)
11 PRINT 103
   ACCEPT,R,DR,ESQ,T,TPR
   PRINT 200
   POWER=0.
   CNST1=DR*4./3.
   CNST2=DR*2./3.
   II=1
 3 DO 4 I=1,N
   IF(T-TSIG(I))41,42,4
 4 CONTINUE
42 SIGMA=SIG(I)
   GO TO 50
41 U=(T-TSIG(I-1))/(TSIG(I)-TSIG(I-1))
   DELY1=SIG(I-1)-SIG(I-2)
   DELYO=SIG(I)-SIG(I-1)
   SIGMA=SIG(I-1)+(U*(DELY1+DELYO)+(U**2)*(DELYO-DELY1))/2.
50 DO 5 I=1,M
   IF(T-TCON(I))51,52,5
 5 CONTINUE
52 COND=CON(I)
   GO TO 59
51 U=(T-TCON(I-1))/(TCON(I)-TCON(I-1))
   DELY1=CON(I-1)-CON(I-2)
   DELYO=CON(I)-CON(I-1)
   COND=CON(I-1)+(U*(DELY1+DELYO)+(U**2)*(DELYO-DELY1))/2.
59 COND=COND*.01
   DO 60 I=1,L
   IF(T-TRAD(I))61,62,60
60 CONTINUE
62 PRAD=RAD(I)
   GO TO 29
61 U=(T-TRAD(I-1))/(TRAD(I)-TRAD(I-1))
   DELY1=RAD(I-1)-RAD(I-2)
   DELYO=RAD(I)-RAD(I-1)
   PRAD=RAD(I-1)+(U*(DELY1+DELYO)+(U**2)*(DELYO-DELY1))/2.
```

```
 29 IF(T-8500.)31,31,30                                                    VI
 30 IF(SENSE SWITCH 2)31,32
 31 PRINT 104,R,T,TPR,SIGMA,CØND
 32 IF(T-6000.)7,7,9
  9 GØ TØ(20,21,22),II
 20 PØWER=PØWER+SIGMA*R*DR/3.                                              VII
    II=2
    GØ TØ 16
 21 PØWER=PØWER+SIGMA*R*CNST1
    II=3
    GØ TØ 16
 22 PØWER =PØWER+SIGMA*R*CNST2
    II=2
 16 S1=SIGMA*ESQ-PRAD                                                      VIII
    R1=R
    R=R+DR
    IF(R1)8,8,6
  8 S2=S1                                                                   IX
    CØND1=CØND
    RKTPR=0.
    TPR1=0.
  6 RKTPR=RKTPR-(DR/6.)*(S1*(5.*R+4.*R1)-S2*(2.*R+R1))
    TPR=RKTPR/(R*(2.*CØND-CØND1))
    T=T+(TPR+TPR1)*DR/2.                                                     X
    S2=S1
    CØND1=CØND
    TPR1=TPR
    GØ TØ 3
  7 PØWER=(PØWER+SIGMA*R*DR/3.)*6.2832*ESQ
    PRINT 108,PØWER                                                         XI
    PRINT 105
    PAUSE
    IF(SENSE SWITCH 1)10,11
100 FØRMAT(//44HENTER NUMBER ØF VALUES ØF TSIG(I) AND SIG(I))
101 FØRMAT(//44HENTER NUMBER ØF VALUES ØF TCØN(I) AND CØN(I))
102 FØRMAT(//55HREAD IN TABLES ØF TSIG(I), SIG(I), TCØN(I), CØN(I), AND)
103 FØRMAT(//35HENTER R, DR, E**2, T(0), AND TPR(0))
104 FØRMAT(/5E16.7)
105 FØRMAT(//55HTØ START ØVER, TURN SW 1 ØN. TØ CØNTINUE, TURN SW 1 ØFF)
107 FØRMAT(//44HENTER NUMBER ØF VALUES ØF TRAD(I) AND RAD(I))
108 FØRMAT(//14HPØWER/LENGTH =E16.7,9H WATTS/CM)
109 FØRMAT(16H TRAD(I), RAD(I))
200 FØRMAT(/)
    END
```

Appendix B

Instrumentation and Support Equipment

Electrical Equipment

The electrical schematic of the arc is shown in Fig. 35, p. 95. Electrical power was supplied by two A. O. Smith rectifiers, model A2500-10SP. Each unit had a maximum continuous output of 250 amps at 500 volts, DC, or 125 kw. Both rectifiers were used for starting, but only one was needed for operation. Since the arc device did not offer enough of a load to the rectifier, a series load resistor was used. While smaller power supplies would have been desirable, the above units were the only ones available.

The load resistor consisted of a 0.50-in.-diameter stainless steel tube, 100-ft long, which provided a 1-ohm load, and two water resistors, each of which provided an 8-ohm load. The water resistors were stainless steel drums filled with water, open on one end, 17-in. in diameter, each with an inner cylinder of stainless steel, 12-in. in diameter. The inner cylinders were supported by 3-in. phenolic blocks and were separated radially from the outer cylinders by fiberglass cylinders, 15.3-in. in diameter. Each component was 28-in. high.

The power level of the arc could be increased by raising the output of the rectifier, or by raising one of the fiberglass separators in the water resistors. The entire load bank was capable of absorbing up to 30 kw for as long as one hour. Cooling was provided by circulating water through the stainless steel tube load bank, and by copper cooling coils suspended in the center of the two water resistors. The available power

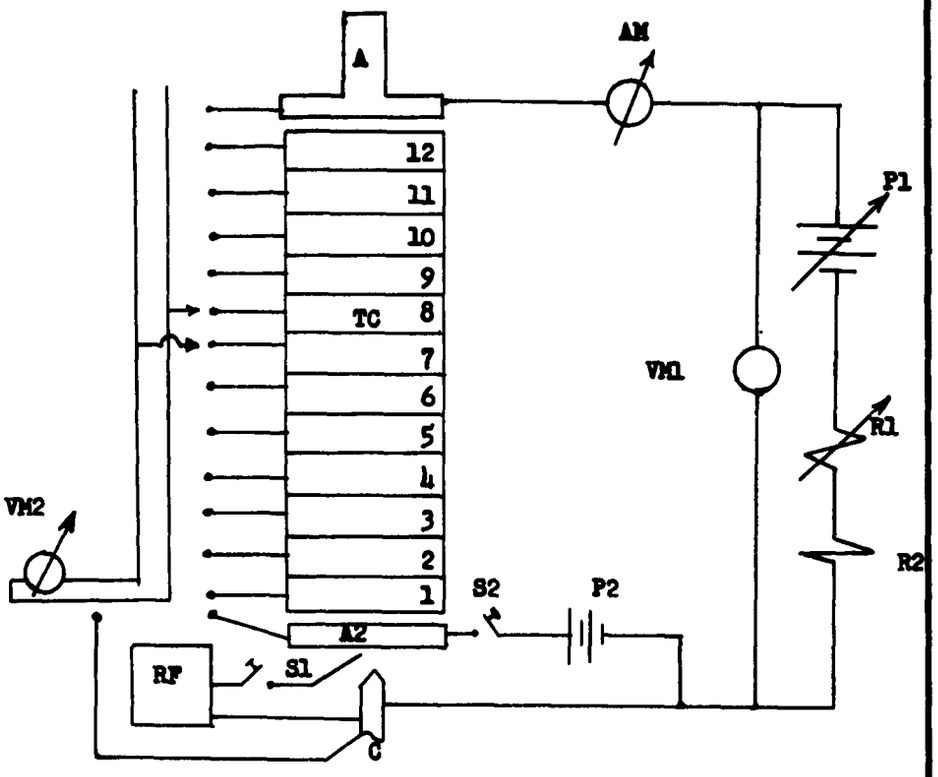

A: Primary anode
C: Cathode
A2: Secondary anode
TC: Transpiration column; segmented
AM: Ammeter for arc current
VM1: Voltmeter for arc voltage
P1: Operating power supply, variable
R1: Variable load resistor
R2: Fixed load resistor
VM2: Voltmeter for disk potential differences
P2: Starting power supply
RF: Radio-frequency-spark generator and battery
S1, S2: Switches; closed only for starting

Fig. 35

Electrical Schematic of Arc Device

range was from about 8 kw to beyond the 25 kw limit of the arc device.

A radio-frequency generator, manufacturer unknown, was used to provide the starting spark. Power for this unit was supplied by a twenty-four volt aircraft battery of the lead-acid type.

The arc voltage and current were measured by Assembly Products Model 4 voltmeter and ammeter. The voltmeter had a double scale setting of 0 to 1,000 volts, DC, in 20 volt increments, and 0 to 500 volts, DC, in 10 volt increments. The range was controlled by a toggle switch. The ammeter had a full scale deflection of 100 amps, DC, in 1 amp increments.

The voltage differences between the wall segments were measured by an RCA Senior Volt-Ohmyst vacuum-tube voltmeter, model WV97A, with an input impedance of one million ohms. This instrument was also used for measuring the operating ripple voltage of the rectifier.

This ripple voltage was determined by short-circuiting the arc and measuring the AC ripple in the voltage drop across the load resistance. At a rectifier output of 58 amps at 610 volts, DC, the ripple voltage was observed to be 19.4 volts, AC, RMS. This is about 3% of the DC voltage and is as specified by the manufacturer.

Thermocouples and Read-Outs. The temperature monitoring system is sketched in Fig. 36, p. 97. Two sets of temperature measurements were of importance in this experiment. The first set included the temperature changes in the cooling water to the different components and the argon temperature as it entered the injectors; and the second, the wall temperatures. The former were monitored by eight Harco Laboratories, Inc., Thrift-therm iron-constantan thermocouples which were read out on a Brown-Honeywell Pyrometer, model Y156X63P48-X-(L). This instrument had

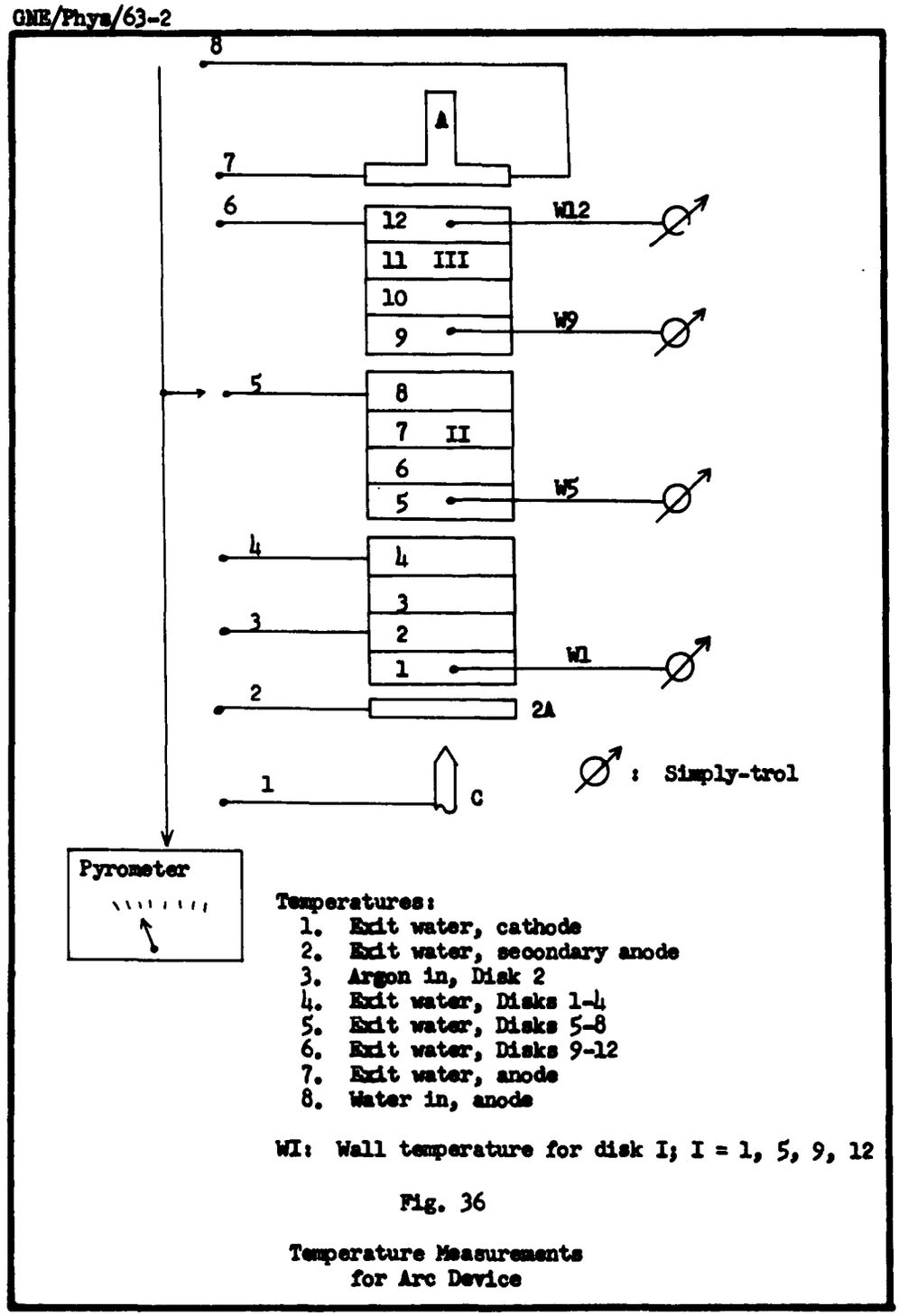

Temperatures:

1. Exit water, cathode
2. Exit water, secondary anode
3. Argon in, Disk 2
4. Exit water, Disks 1-4
5. Exit water, Disks 5-8
6. Exit water, Disks 9-12
7. Exit water, anode
8. Water in, anode

WI: Wall temperature for disk I; I = 1, 5, 9, 12

Fig. 36

Temperature Measurements
for Arc Device

a range of -100 to 700°F in 2°F increments for iron-constantan thermocouples. The high conductivity of the cooling water necessitated the use of Alphex shrinkable tubing to insulate the thermocouples from the arc voltages. Use of this material increased the response time of the thermocouples by a slight, but insignificant, amount.

The eight temperatures which were measured were the outlet water temperatures from the cathode, secondary anode, each of the three sets of 4 disks, and the primary anode; the inlet water temperature at the primary anode; and the inlet gas temperature to the second gas injector from the cathode.

The wall temperatures were monitored in the first, fifth, ninth, and twelfth disks from the cathode. The thermocouples used here were Leeds and Northrup Super Temp, model 600-J-A, and had a length of 18-in. and a diameter of 0.025-in. Since it was not feasible to insulate these thermocouples from the system, independent read-outs were used. These were four model 421-866 Simply-trols, manufactured by Assembly Products, Inc., of Chesterland, Ohio, with a range of 0 to 1,500°F in increments of 20°F.

Water Control and Monitoring. A sketch of the water flow system for the arc device is presented in Fig. 37, p. 99. Water flow rates were measured by six Fischer and Porter Flowrators, tube number B5-21-10/27, rated at 1.96 gpm at 100% flow. However, a calibration check showed the maximum flow rate to be 1.87 gpm. The flows were controlled individually by Lunkenheimer bronze globe valves, model 408. The calibration curve for the Flowrators is presented in Fig. 38, p. 100.

Argon Gas Flow Control and Monitoring. Fig. 39, p. 101, is a diagram of the argon gas flow control system. The high-pressure manifold permitted

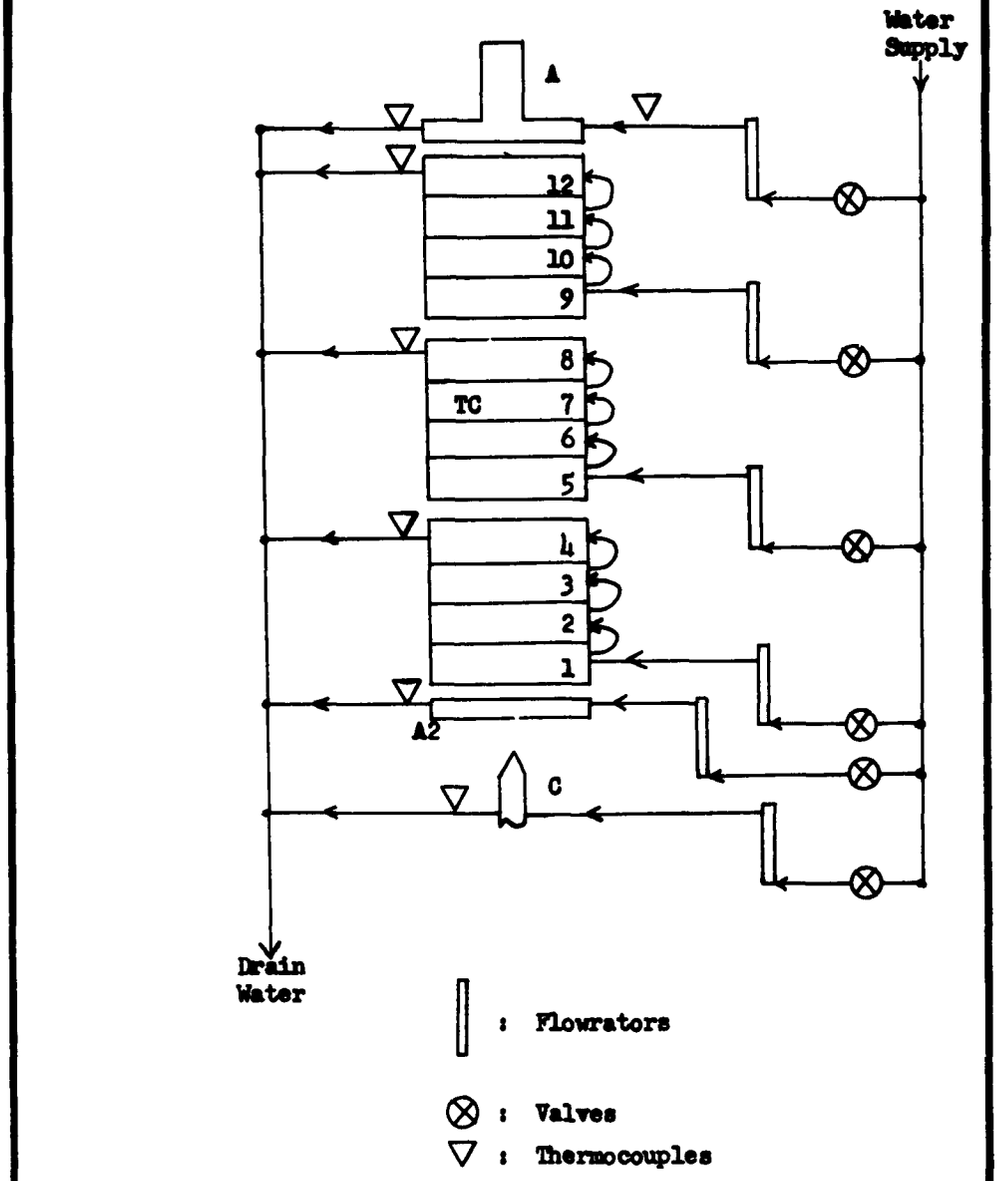

Fig. 37

Schematic of Cooling Water System

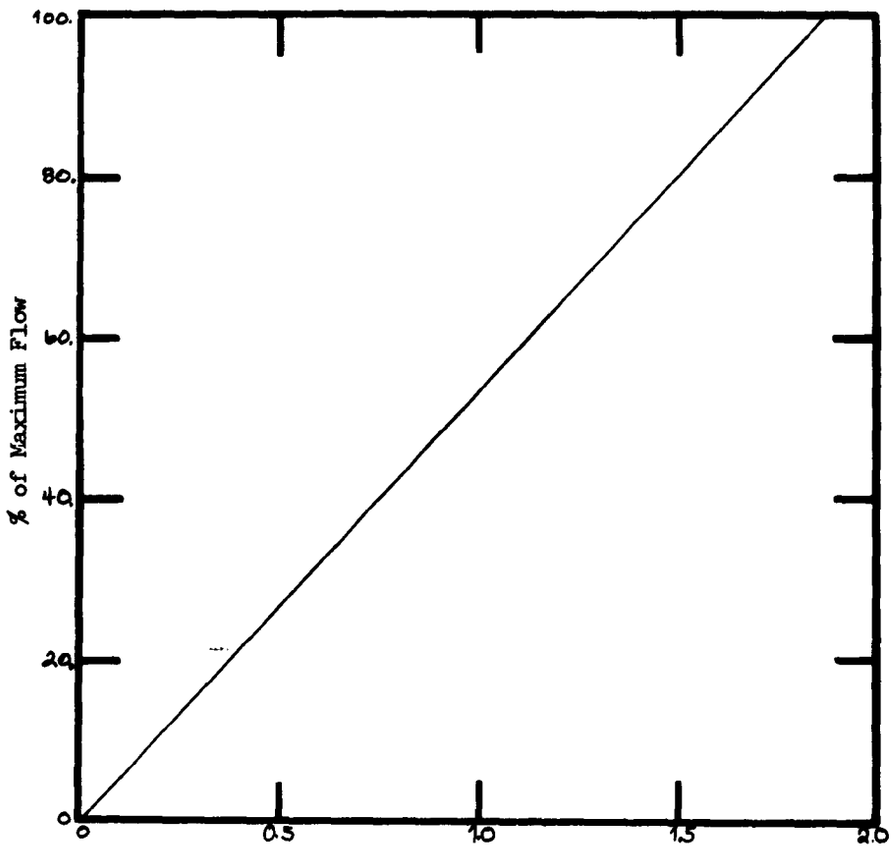

Fig. 38

Water Flowmeter Calibration

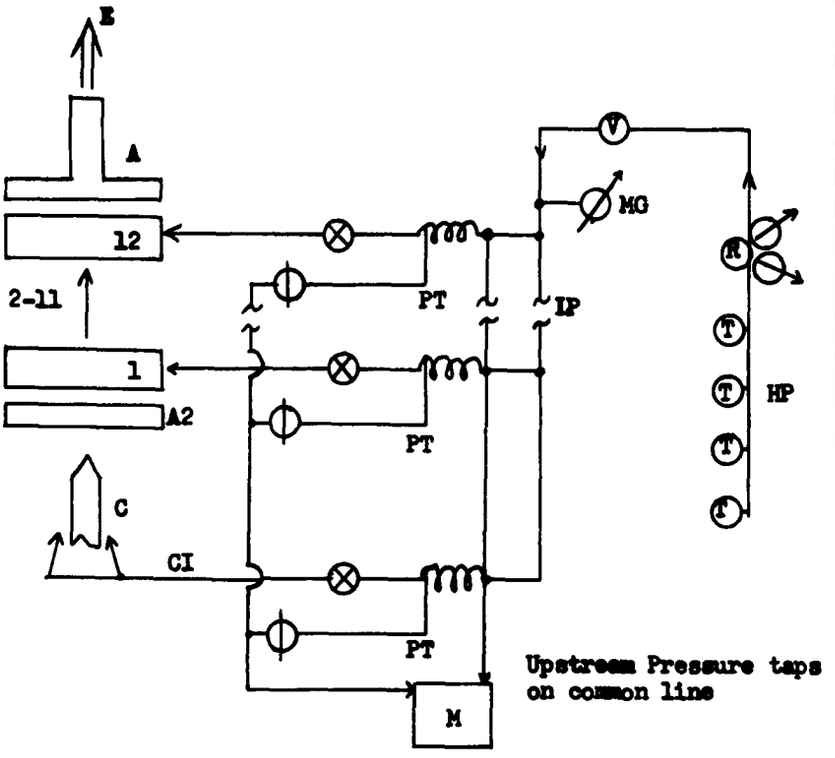

E: Anode exhaust jet
⊗: Needle valves
: Coiled-capillary flowmeters
CI: Cathode chamber gas feed
M: Hg manometer for determining flow rate through flowmeters
V: Secondary gas shut-off
R: Pressure regulator
HP: High-pressure manifold
LP: Low-pressure manifold
MG: Low-pressure manifold gauge
T: High-pressure argon cylinder
PT: Down-stream pressure taps on flowmeters
ϕ: Valves for selection of flowmeter to be read.

Fig. 39

Gas Flow Measurement
and Control Schematic

use of four tanks of water-pumped argon to obtain longer running times before depletion of the gas supply occured. The gas flow to the low pressure manifold was regulated by a Hoke-Phoenix Regulator, model 901.

A stainless steel tank, 4-ft. long, and 10-in. in diameter, was used as the low-pressure manifold. From each of the 16 hose fittings attached to the tank, the argon passed to the coiled capillary flowmeters. A Duragauge Bronse Tube pressure gauge, model AMP 6319, was used to monitor the pressure in this manifold. Adjustment of the regulator at the high-pressure manifold kept the pressure in this tank constant at 30 psig for all flow rates.

The coiled capillary flowmeters were constructed from 0.25-in. diameter soft-drawn copper tubing, wrapped in 13-ft. lengths around a piece of 1.625-in. pipe. Fig. 40, p. 103, shows a typical flowmeter with the upstream pressure tap on the left of the photograph. Pressure taps were located on the coils 30 turns, or 12-ft., apart. The calibration curves of each of the 16 coils agreed with each other to ±5%. A typical curve is shown in Fig. 41, p. 104, and presents corrected pressure drop in cm Hg vs argon mass flow in lb/hr. The coils were immersed in a constant temperature bath. The control unit for the bath was an Arthur M. Thomas Company, Model 9934 Constant Temperature Bath with Electric Circulating Pump. The bath temperature was held at 25.5°C, ± 0.2°C. The details of the design and calibration of these flowmeters are given in Appendix C, p. 106.

The flow to each wall segment and the cathode chamber was controlled by a Hoke needle valve, model 4RB281. The pressure drop across these valves reduced the argon pressure at the arc device to about 30 mm Hg

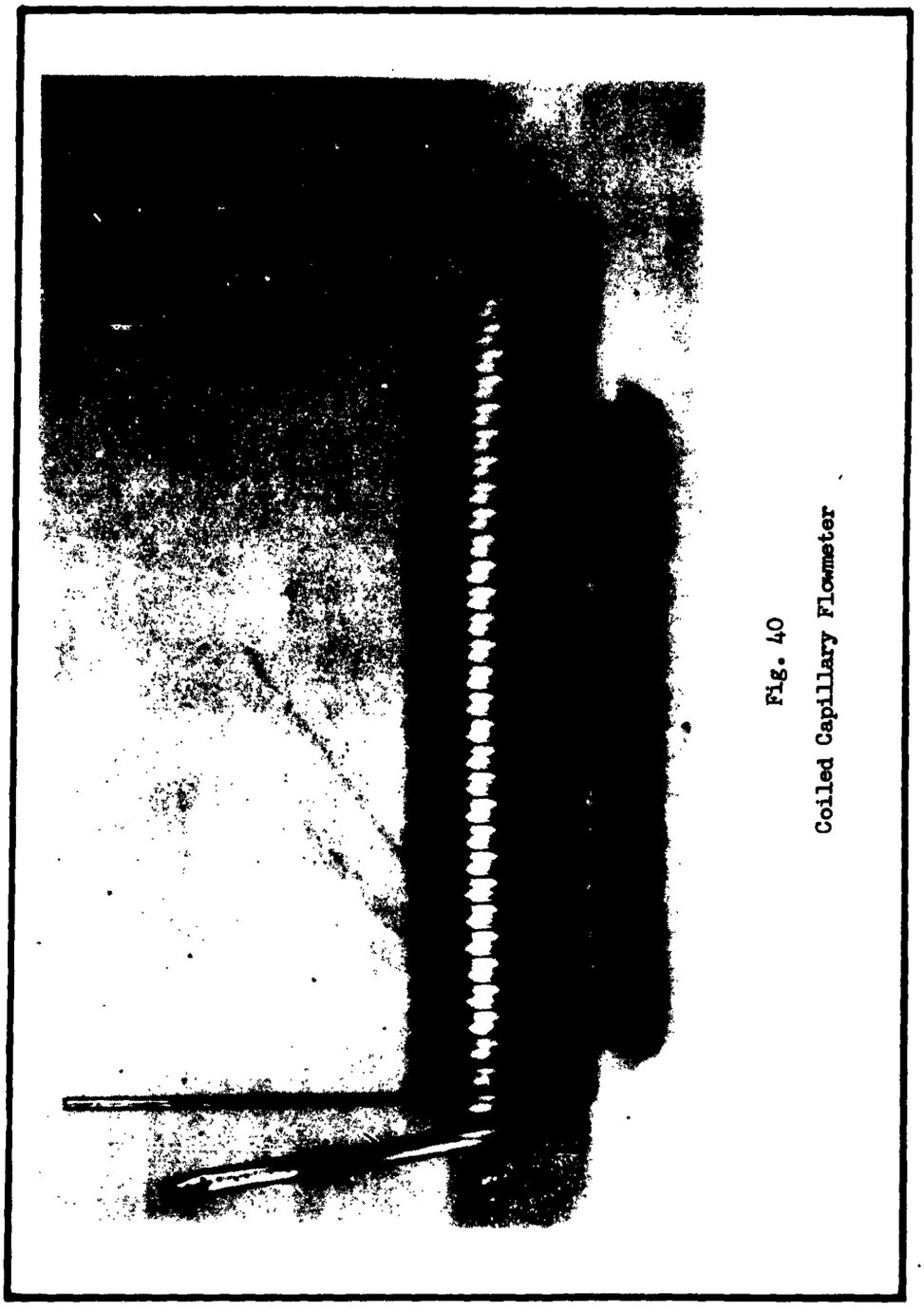

Fig. 40
Coiled Capillary Flowmeter

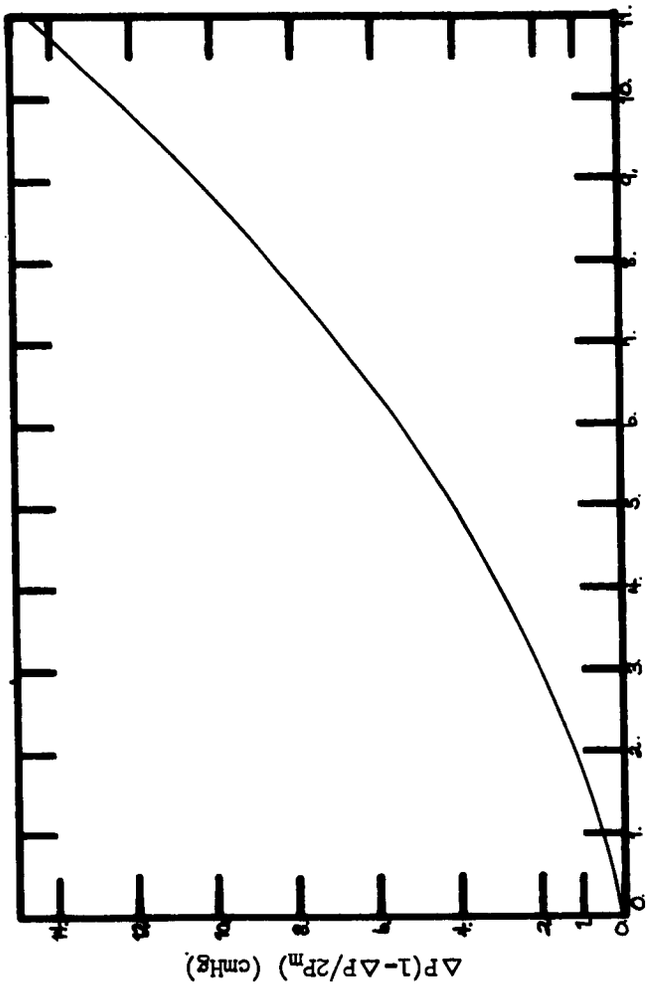

Fig. 41

Coiled Capillary Flowmeter Calibration

above one atmosphere. This was determined from cold flow measurement of static wall pressures in the arc channel.

Miscellaneous. Other equipment used in this experiment included that necessary for the measurement of the arc radius. The camera and stops were fabricated at ARL. The optical bench was by Cenco, with a calibrated length of 110 cm. The densitometer was manufactured by National Scientific Laboratories, but no modal or serial number was known as this item was obtained from surplus stock.

The read-out equipment for the densitometer included a Multiflex Galvanometer and a Mauchlaufschrieber 2. The latter is the chart recorder which drew the trace of the density of the negative being scanned by the densitometer. Both these items were credited to Dr. B. Lange of West Berlin, Germany.

The window used for viewing the arc was an annular piece of brass, 1.25-in. in inside diameter, 2.0-in. in outside diameter, and 0.50-in. thick. A rectangular hole machined in one side received the quarts window, which was 1.50 cm by 0.53 cm. A sketch of the window assembly in the arc device is presented in Fig. 14, p. 30.

Appendix C

Design of the Coiled Capillary Flowmeters

The requirement that the mass flow to each of the thirteen gas injection components of the transpiration-cooled arc be monitored and controlled posed a significant problem in the early stages of the experimental study. The range of mass flows which was desired was from about 1.0 lb/hr to 10.0 lb/hr of argon at any convenient pressure at or above 1 atm. While commercial flowmeters were avaliable for this flow range, their expense and complex support equipment made it advisable to seek another means of measuring these mass flows.

The capabilities of the capillary flowmeter in a linear configuration were considered in detail by Capt. Mack E. Baker of the Graduate Aeronautical Engineering Class of 1957 at AFIT in his thesis, Development of a Linear Flowmeter for Low Flow Rates (Ref 1). However, in order to obtain pressure drops on the order of 1.0 to 10.0 cm Hg from these flowmeters at the required flow rates for this experiment, excessively long flowmeters of rather large diameter were necessary to maintain the laminar flow of gas within them. The requirement that the flowmeter response be nearly linear with mass flow demands laminar or Poiseuille pipe flow and insures that the error in reading the calibration curve will be nearly constant with mass flow (Ref 12:1-14).

For the above reasons, the coiled capillary flowmeters were selected as meeting the criteria of simplicity, linearity of response, and nominal expense. Thanks are due Mr. Erich Soehngen of the Thermomechanics Branch of ARL for his assistance in obtaining the critical information concerning

the design and construction of these flowmeters.

The complete derivation of the theory for the coiled capillary flowmeter may be found in an article by H. N. Powell and W. G. Browne in The Review of Scientific Instruments, Vol. 28, No.2, February, 1957, entitled "Use of Coiled Capillaries in a Convenient Laboratory Flowmeter." The remarkable thing about these flowmeters is that laminar flow may be maintained at Reynolds numbers as high as 15,000. For the linear flowmeters, transition from laminar to turbulent begins at a Reynolds number of about 2,000. Thus, mass flows as much as 7 times as high as those in linear meters may be monitored with the coiled capillaries, yielding the desired range of use. Fig. 42, p. 108, shows the dependence of the critical Reynolds number on the ratio of capillary diameter to the center-to-center coil diameter. The maximum allowable Reynolds number of 15,000 occurs at a ratio of about 0.11 (Ref 12:139).

Hand computations were performed for a mass flow of 10.0 lb/hr of argon at an upstream pressure of 226.0 cm hg, and a pressure drop of 12.0 cm Hg for a coil with 12-ft. of tube between pressure taps and a total length of 13-ft. The results indicated a need for the use of the optimal capillary-diameter-to-coil-diameter ratio of 0.11. Fortunately, 0.25-in. OD soft-drawn copper refrigeration tubing with an inside diameter of 0.172-in. provided this ratio when wrapped around a 1.312-in. diameter pipe:

$$D = 0.172 \text{ in.}$$

$$D_c = 1.312 + 0.250 = 1.562 \text{ in.}$$

$$\frac{D}{D_c} = \frac{0.172}{1.562} = 0.110$$

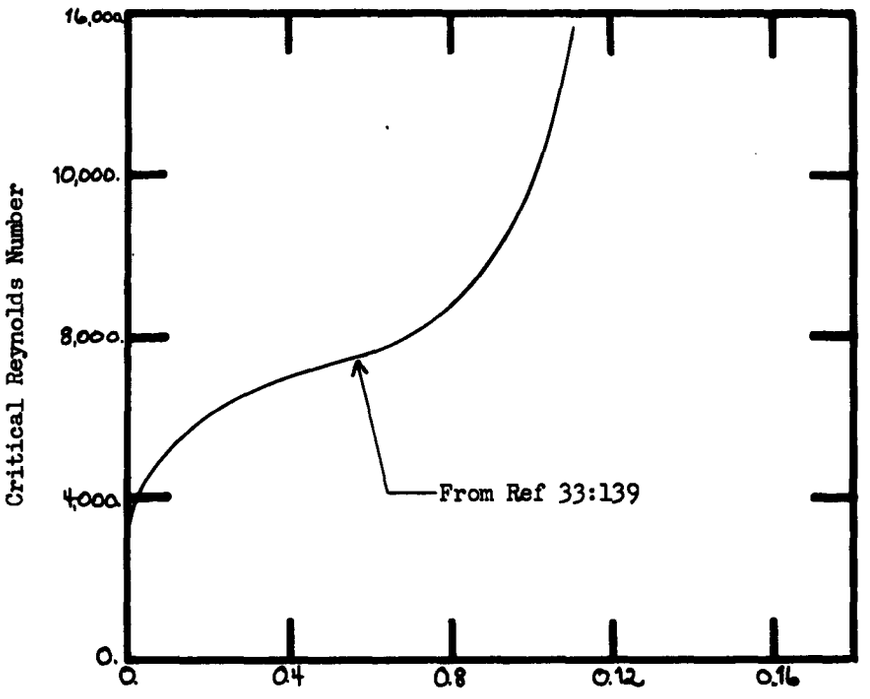

Fig. 42

Dependence of Critical Reynolds Number
(for Transition to Turbulent Flow)
on Diameter Ratio, D/D_c

The 0.25-in. copper tube was selected as this is a readily available item. The pipe for winding the coils was found in the laboratory.

While the authors of the article on the flowmeters suggested a combination of empirical and theoretical calibration, the non-uniformity in the diameter of the copper tubing made it just as easy to calibrate the coils by empirical means. The procedure employed was as follows:

1. The number of cubic feet of argon at known temperature and pressure which passed through the flowmeter in a time somewhat greater than 200 sec was recorded. The calibrating gas meter was an American Meter Co. Model 176, with a range of 20.0 to 450.0 cu ft/hr at STP, and a scale calibration of 0.01 cu ft. Pressure on the upstream side of this meter was measured with a mercury manometer; the temperature, with a Harco Laboratories, Inc., Thrift-therm iron-constantan thermocouple. The time was monitored with a stopwatch. Use of 200 sec as a monitoring period allowed sufficient gas to pass through the system to reduce the experimental error. Also, an error ±1 sec was only 0.5% of the total time.
2. The above data was converted to lb/hr by the conversion:

   $$\text{lb/hr} = [(\text{sec/cu ft}) \times (\text{hr/sec}) \times (\text{cu ft/lb})]^{-1}$$

   where the last or density term was corrected for temperature and pressure at the calibrating meter.
3. The observed drops, Δp, were then corrected.

$$\Delta p' = \Delta p (1 - \Delta p / 2 p_m) \qquad (19)$$

p_m = 224. cm Hg, the pressure at the upstream tap of the coiled capillary flowmeter. Variations in this pressure from atmospheric fluctuations were 1% or less, and produced less of an error in the value of $\Delta p'$. For low flows, (less than 4.0 lb/hr), the correction for the upstream pressure may be neglected.

4. The final results were plotted as corrected pressure drop in cm Hg vs argon mass flow in lb/hr as shown in Fig. 41, p. 104.

Empirical calibration eliminated the chance of large error from an erroneous or varying value of capillary diameter which must be raised to the fourth power in the analytic expressions for the coiled capillaries. The equations which follow are the key equations in the design of the coiled capillary flowmeters.

The pressure drop in cm Hg across the coil is given by (Ref 12:139):

$$\Delta p(1-\Delta p/2p_m) = \frac{9.61\times10^{-9}\,\dot{M}\,\nu\,L\,C\,k}{D^4} \qquad (20)$$

where $\dot{M}$ = mass flow, lb/hr

L = length of coil between pressure taps, ft.

D = coil diameter, ft.

ν = absolute viscosity, ft^2/hr

k = conversion factor, lb/ft^2 to cm Hg

C = coil factor.

The coil factor, C, has been determined for a wide range of capillary-coil ratios and is given by (Ref 12:139):

$$C = \left\{1-\left[1-\left(\frac{11.6}{Re\,(D/D_o)^{.5}}\right)^{.45}\right]^{2.22}\right\}^{-1} \qquad (21)$$

From Fig. 41, p. 104, we can see that for a flow of 10.0 lb/hr, a corrected pressure drop of 12.3 cm Hg is obtained. Applying the above formulas for the same mass flow, the pressure drop is 12.4 cm Hg at a Reynolds number of 16,000. The numerical data and this latter computation may be found in Appendix D, Sample Computations, pp. 116-117.

It is necessary to note that no corrections were applied for the capillary diameter as recommended by Powell and Browne (Ref 12:141). There was a degree of flattening suffered by the tube in the winding process, but this flattening apparently did not change the effective diameter by a significant amount. Other computations for various mass flows showed agreement to $\pm 5\%$ or less between the theoretical and observed pressure drops.

In general, the calibration of the flowmeters was carried to $\pm 1\%$ or less.

Appendix D

Sample Computations

The data used in the computations in this appendix was taken from the first or right-hand column of Table I, p. 81, except as noted.

Arc Power

Power = Voltage x Current

= 229.0 x 45.0

P = 10.3 kw

Voltage Gradient

$$E = \frac{V}{Z}$$

For sections 5-6:

V = 15.3 volts

Z = 1.45 cm (Table III, p. 82.)

$$E = \frac{15.3}{1.45}$$

E = 10.6 v/cm

Power Losses to Components

Constants for Water

Inlet temperature = 52.3°F

C_p = 1.00 Btu/lb °F for temperature range 50-150°F.

1 gpm = 501.0 lb/hr

Cathode Loss

Water outlet temperature = 52.7°F

$\Delta T = 52.7 - 52.3 = 0.4°F$

Water flow = 1.31 gpm x 501.0 lb-min/hr-gal

$\dot{m} = 656.3$ lb/hr

$Pc = \dot{m} C_p \Delta T$

$= (656.3)(1.00)(0.4)$

Pc = 263.0 Btu/hr

1 Btu/hr = 0.293 watts

Pc = 77.1 w

Secondary Anode Loss

$\dot{m} = 1.31$ gpm

= 656.3 lb/hr

Outlet water temperature = 55.0°F

$\Delta T = 55.0 - 52.3 = 2.7°F$

$P_2 = (656.3)(1.00)(2.7)$

$= 1772.0$ Btu/hr

$P_2 = 519.0$ w

Loss to Wall Segments 1-4

$\dot{m} = 0.26$ gpm

= 130.0 lb/hr

Outlet water temperature 67.0°F

$\Delta T = 67.0 - 52.3 = 14.7^{\circ}F$

$P_{1-4} = (130.0)(1.00)(14.7)$

$= 1911.0$ Btu/hr

$P_{1-4} = 560.0$ w

Loss to Wall Segments 5-8

$\dot{m} = 0.26$ gpm

$= 130.0$ lb/hr

Outlet water temperature = $75.0^{\circ}F$

$\Delta T = 75.0 - 52.3 = 22.7^{\circ}F$

$P_{5-8} = (130.0)(1.00)(22.7)$

$= 2951.0$ Btu/hr

$P_{5-8} = 765.0$ w

Loss to Wall Segments 9-12

$\dot{m} = 0.26$ gpm

$= 130.0$ lb/hr

Outlet water temperature = $84.2^{\circ}F$

$\Delta T = 84.2 - 52.3 = 31.9^{\circ}F$

$P_{9-12} = (130.0)(1.00)(31.9)$

$= 4147.0$ Btu/hr

$P_{9-12} = 1215.0$ w

Anode Loss

$\dot{m}$ = 1.40 gpm

= 701.0 lb/hr

Outlet water temperature = 61.7°F

ΔT = 61.7 - 52.3 = 9.4°F

P_a = (701.0)(1.00)(9.4)

= 6589.0 Btu/hr

P_a = 1930.0 w

Total Power Loss

$P_t = P_c + P_2 + P_{1-4} + P_{5-8} + P_{9-12} + P_a$

= 77.1 + 519.0 + 560.0 + 765.0 + 1215.0 + 1930.0

= 5066.1 w

P_t = 5.07 kw

Gas Enthalpy Rise

$P_g = P - P_t$

= 10.3 - 5.07

P_g = 5.23 kw

1 kw = 3413.0 Btu/hr

P_g = 17,850.0 Btu/hr

$H = P_g/\dot{M}_t$

$\dot{M}_t$ = 22.13 lb/hr

H = (17,850.0)/(22.13)

H = 807.0 Btu/lb

Calibration of Densitometer Distance Scale

The following data is available on request from the author. The recorder charts were far too long to be included in this work.

Width of window = 0.530 cm

Width of densitometer trace at half-maximum = 91.0 units

$$\text{Scale factor} = \frac{0.530}{91.0}$$

$$= 0.00580 \text{ cm/div}$$

Arc Radius Measurement

Extrapolated arc diameter = 94.2 units

Arc diameter = Scale factor x Extrapolated arc diameter

$$= (0.00580)(94.2)$$

$$D_a = 0.546 \text{ cm}$$

$$R_a = \frac{D_a}{2} = \frac{0.546}{2}$$

$$R_a = 0.273 \text{ cm}$$

Calculations for Coiled Capillary Flowmeters

Assuming the following values for the flowmeters and argon (at 298.5 C and 226.0 cm Hg):

$D = 0.172 \text{ in.} = 0.0143 \text{ ft}$

$\frac{D}{D_c} = 0.110$

$\dot{M} = 10.0 \text{ lb/hr}$

$L = 12.0 \text{ ft}$

$\mu = 0.0555 \text{ lb/hr-ft}$

$\nu = 0.167 \text{ ft}^2/\text{hr}$

$K = 0.0359 \text{ cm Hg}/(\text{lb}/\text{ft}^2)$

$$Re = \frac{4\dot{M}}{\pi D \mu} = \frac{4\ (10.0)}{(0.0143)(0.0955)}$$

$$Re = 1.60 \times 10^4 = 16{,}000.0$$

$$C = \left\{ 1 - \left[1 - \left(\frac{11.6}{Re\ (D/Dc)^{.5}} \right)^{.45} \right]^{2.22} \right\}^{-1}$$

$$C = \left\{ 1 - \left[1 - \left(\frac{11.6}{(1.6 \times 10^4)(0.11)^{.5}} \right)^{.45} \right]^{2.22} \right\}^{-1}$$

$$C = 7.51$$

$$\Delta p(1-\Delta p/2p_m) = \frac{(9.61 \times 10^{-8})\ M\ L\ C\ \nu\ K}{D^4}$$

$$= \frac{(9.61 \times 10^{-8})(10.0)(7.51)(0.167)(0.0359)}{(1.43 \times 10^{-2})^4}$$

$$\Delta p(1-\Delta p/2p_m) = 12.4 \text{ cm Hg}$$

Appendix E

List of Symbols

Symbol	
A	Dummy constant for numerical solution to Ellenbaas-Heller equation.
B	Dummy constant for numerical solution to Ellenbaas-Heller equation.
B	Empirical constant of radiation
C	Coil factor for coiled capillary flowmeter
C_p	Specific heat at constant pressure
D	Capillary diameter
D_c	Coil diameter
E	Electric field strength
H	Rise in specific gas enthalpy
k	Thermal conductivity
K	Boltzmann's constant
K	Conversion factor
$\mathcal{K}$	Total electron and ion mobility
L	Length of coil
$\dot{m}$	Mass flow rate
$\dot{M}$	Mass flow rate
n_e	Electron density
p	Pressure
P	Power
q	Electron charge
r	Instantaneous radius

Symbol

R	Fixed radius
Ra	At the arc radius
Re	Reynolds number
s	Specific heat at constant pressure
S	Heat loss by conduction
T	Temperature
U	Volumetric radiation loss
v	Velocity
V	Voltage
Vex	Excitation potential
Z	Axial distance parameter
Δ	Increment in a variable
Θ	Dimensionless temperature
λ	Dimensionless thermal conductivity
μ	Dynamic viscosity
ν	Absolute viscosity
ρ	Density
σ	Electrical conductivity
Σ	Dimensionless electrical conductivity
ϕ	Dimensionless temperature gradient
∇	Del operator

Subscripts

a	Pertaining to or at the anode
c	Pertaining to or at the cathode

Subscripts

g	Gas
L	Per unit length
m	Condition at reservoir
n	Present instantaneous value
n-1	Last previous instantaneous value
n-2	Second last previous instantaneous value
t	Total loss
T	Total flow
V	Per unit volume
W	Pertaining to or at the channel wall
2	Pertaining to or at the secondary anode
1-4	Pertaining to porous injector wall segments 1-4, inclusive
5-8	Pertaining to porous injector wall segments 5-8, inclusive
9-12	Pertaining to porous injector wall segments 9-12, inclusive